

RELIABILITY MODELING AND FAILURE ANALYSIS
OF A BIOTELEMETRY DATA-RECORDER TAG

JUNAID SHAFAT



Reliability Modeling and Failure Analysis
Of a Biotelemetry Data-Recorder Tag

By

© Junaid Shafaat

A thesis submitted to School of Graduate Studies

In partial fulfillment of requirement for the Degree of Masters of Engineering

Faculty of Engineering and Applied Sciences
Memorial University of Newfoundland

May 25, 2009

St. John's

Newfoundland

Canada

Abstract

Biotelemetry tags are used widely by biologists throughout the world to research animal behaviour and patterns to sustain healthy environment. These instruments are microelectronics encapsulated in plastic packages for environment protection and attached to the animal. Physiological data of animal body and environmental conditions in terms of temperature and pressure is recorded on the on-board memory of the data-recorder tags and can only be retrieved when the tag is retrieved back from the animal. These tags are usually deployed for long missions and usually contain information that is recorded over years, in some cases, is very valuable to scientists and thus makes it very important for these microelectronic devices to have high Reliability. There is a lot of information on consumer electronics product but little known about these microelectronic devices as they sustain harsh environments and conditions which is not required by consumer electronics. This thesis is an attempt to conduct Reliability analysis of such biotelemetry devices and provide methodology for other similar biotelemetry microelectronic devices.

This thesis comprises of two parts; first part of the thesis deals with the weibull analysis of the failure data obtained from field and also understanding of component based Reliability analysis. During this process Fault Tree Analysis, Weibull Analysis and component criticality analysis was conducted.

Second part of the thesis focused on design failures as pointed out by first part of the thesis. This led to the qualification of the components and the packaging reliability by comprehensive analysis, experiments and calculations to evaluate each critical component of the product which failed at early mortality stage as pointed out by bathtub curve. During these analysis actual environments were simulated which is these products are designed for.

This research brings in to focus the need for a better packaging design and extensive accelerated testing of product, considering this a non-repairable system, before qualifying moulding materials and electronic components to achieve high Reliability of the system

Keywords: Biotelemetry, microelectronics, Weibull analysis, Reliability engineering, Fault tree analysis, moisture diffusion, finite element analysis.

Acknowledgements

First of all I would like to Thank God Almighty for this accomplishment and making me strong and keeping me steadfast in the ways of trials and tribulations that has come during the completion of thesis.

I would like to extend my deepest gratitude toward my both supervisors Drs. Mahmoud Haddara and Andrew Fisher for providing me with this unique research opportunity. I would like to thank them for supporting me and guiding me through my Masters of Engineering Degree. Without their proper guidance and timely advice I would not have been able to accomplish the deadlines and quality in my work that was expected from me.

I also express my appreciation for the staff at the Lotek Wireless Inc. who has been very cooperative and supportive. I would like to thank my parents for their blessings. I would like to thank my sisters for the blessing and support they provided throughout the whole process.

Finally, I would like to express my respect, love and appreciation for my wife for her unconditional support, encouragement and appreciation.

Table of Contents

Abstract.....	ii
Acknowledgements.....	iv
Table of Contents.....	v
List of Tables.....	ix
List of Figures.....	xi
List of Symbols and Abbreviations.....	xv
Chapter 1 Introduction.....	1
1.1 Introduction to Microelectronics.....	1
1.2 Biotelemetry Devices and Components.....	2
1.3 Data Recorders – System Description.....	5
1.4 Scope and Purpose of Research.....	7
1.5 Outline of Thesis.....	9
Chapter 2 Literature Review.....	12
2.1 Introduction.....	12
2.2 Current Research.....	15
2.3 Hardware Design of Biotelemetry Electronic Devices.....	16
2.4 Specific Reliability Models for Electronics.....	17
2.5 Prediction Modeling and Assessment.....	18
2.6 Moisture Diffusion Problem.....	26
2.7 Significance of Current Research.....	33
Chapter 3 Failure Data Analysis.....	35

3.1	Introduction.....	35
3.2	Data Recorder Tag.....	35
3.3	Failure Data Analysis.....	42
3.4	Hazard Rate Plotting.....	43
3.4.1	Plotting Steps.....	46
3.5	Failure Mode 1: Power Failure.....	51
3.6	Failure Mode 2: Packaging Failure.....	53
3.7	Failure Mode 3: Communications Failure.....	54
3.8	Failure Mode 4: Pressure Sensor Failure.....	55
3.9	Failure Mode 5: Temperature Sensor Failure.....	56
3.10	Fault Tree Analysis.....	57
3.10.1	Temperature Sensor Failure.....	61
3.10.2	Pressure Sensor Failure.....	63
3.10.3	Communications Failure.....	65
3.10.4	Power Failure.....	67
3.11	Conclusion.....	69
Chapter 4 Failure Mode Analysis: Power Failure.....		71
4.1	Introduction.....	71
4.2	Battery Type and Specification.....	72
4.3	Battery Lifetime Analysis.....	73
4.4	Experiment 1: Battery Lifetime in Continuous Drain Condition at +25°C.....	74
4.5	Experiment 2: Battery Lifetime in Continuous Drain Condition at -16°C.....	76

4.5.1	Results.....	79
4.6	Experiment 3: Battery Lifetime in Intermittent Drain Conditions.....	82
4.6.1	Calculations.....	86
4.6.2	Results.....	89
4.7	Conclusion	90
Chapter 5 Failure Mode Analysis: Packaging Failure.....		92
5.1	Introduction.....	92
5.2	Structural Analysis.....	95
5.2.1	Samples Preparation.....	96
5.2.2	Pressure Experiments.....	99
5.3	FEA Simulation	103
5.3.1	Defining Model and Boundary Conditions.....	104
5.3.2	Static Stress Analysis.....	106
5.3.3	Results Summary for Static Stress Analysis.....	110
5.3.4	Creep Analysis:.....	111
5.3.5	Results Summary for Creep Analysis.....	116
5.4	Conclusion	117
Chapter 6 Moisture Diffusion in Electronic Packaging Materials.....		119
6.1	Introduction.....	119
6.2	Mathematics of diffusion	121
6.3	Moisture Ingress Rate Calculations	128

6.4	Finite Element Simulation	132
6.4.1	Boundary Conditions	133
6.4.2	Moisture Ingress Simulation	134
6.4.3	Results.....	136
6.5	Conclusion	137
Chapter 7 Conclusions and Recommendations		141
7.1	Conclusion of Research	142
7.2	Recommendations and Future work	145
References.....		149
Appendix 1.....		159
Appendix 2.....		163

List of Tables

Table 2.1: Categories of current research on electronic devices	16
Table 3.1: Data-recorder tag specifications	37
Table 3.2: Failure rates of components.....	60
Table 3.3: Component importance for temperature circuit.....	63
Table 3.4: Component importance for pressure sensor circuit	65
Table 3.5: Component importance for communication circuit.....	67
Table 3.6: Component importance for power circuit.....	69
Table 3.7: Summary of Hazard plots	69
Table 4.1: Battery specifications.....	73
Table 4.2: Lifetime experiment results of virgin and tabbed cells under static load at 25°C	75
Table 4.3: Lifetime experiment results for tabbed cells under static load at -16°C.....	78
Table 4.4: Lifetime results for virgin and tabbed cells	79
Table 4.5: Table for boxplots.....	79
Table 4.6: Results of measurements taken through oscilloscope	87
Table 4.7: Life of data-recorder when used at 25°C and -16°C	88
Table 4.8: spreadsheet model of data-recorder life calculator	90
Table 4.9: Life of a data-recorder Vs number of data downloads	90
Table 5.1: Observation of pressure tests	100
Table 5.2: Material properties of the encapsulants	103
Table 5.3: FEA stress analysis results.....	110

Table 5.4: FEA creep analysis results.....	116
Table 5.5: Summary of static stress and creep analysis.....	117
Table 6.1: ASTM D570 Test methods.....	129
Table 6.2: Water absorption properties from polyurethane datasheet	130
Table 6.3: Diffusion coefficient for polyurethanes, soft and hard.....	131
Table 6.4: Variables map for FEA simulation.....	132
Table 6.5: Moisture ingress rate results	137

List of Figures

Figure 1.1: RF Tracking System, Courtesy of Lotek Wireless Inc.....	4
Figure 1.2: Acoustic Tracking System, Courtesy of Lotek Wireless Inc.	4
Figure 1.3: Data Recorders, Courtesy of Lotek Wireless Inc.	4
Figure 1.4: Components of Data Recorder Tracking Tag, Courtesy of Lotek Wireless Inc.	6
Figure 1.5: Data Recorder Tracking Tag, Courtesy of Lotek Wireless Inc.....	7
Figure 3.1: Data Storage Tag	36
Figure 3.2: Temperature Chart of Tag	38
Figure 3.3: Pressure Chart of Tag.....	39
Figure 3.4: Temperature Data of Tag from start till evening just before the tag was left outside for overnight recording.....	40
Figure 3.5: Temperature Chart of Tag recording overnight cold temperatures	40
Figure 3.6: Pressure Chart of Tag with scale change.....	41
Figure 3.7: Full data (regardless of failure mode)	48
Figure 3.8: Bathtub Curve.....	50
Figure 3.9: Failure modes Pareto chart	51
Figure 3.10: Hazard plot of power failure data.....	52
Figure 3.11: Hazard plot of packaging failure data	53
Figure 3.12: Hazard plot of communications failure data	54
Figure 3.13: Hazard plot of pressure sensor failure data	55
Figure 3.14: Hazard plot of temperature failure data.....	56

Figure 3.15: Block Diagram of Data Recorder Tag.....	59
Figure 3.16: FTA for Temperature Failure	61
Figure 3.17: FTA of Pressure sensing failure	64
Figure 3.18: FTA for communications failure.....	66
Figure 3.19: FTA for Battery failure.....	68
Figure 4.1 Dimensions of battery.....	72
Figure 4.2: Tabbed battery	74
Figure 4.3: Tabbed and Virgin Cells under static load test.....	75
Figure 4.4: Experimental setup of lifetime analysis for tabbed cells at -16°C	77
Figure 4.5: Tabbed cells under static load at -16°C	77
Figure 4.6: Box plot diagram for lifetime experiments	80
Figure 4.7: Comparison of lifetime of tabbed cells at +25°C and -16°C	81
Figure 4.8: Current draw at reset activity	84
Figure 4.9: Time measurement for reset activity	84
Figure 4.10: Current draw at sampling activity	85
Figure 4.11: Time measurement for sampling activity	85
Figure 4.12: Current draw at data download activity	86
Figure 4.13: Time measurement at data download activity	86
Figure 4.14: Relationship between data download activity and life of the data-recorder tag.....	89
Figure 5.1: Anatomy of the data-recorder tag showing polyurethane body	93
Figure 5.2: Sketch of data-recorder under study.....	93

Figure 5.3: Silicone moulds	97
Figure 5.4: Silicone moulds for soft polyurethane.....	97
Figure 5.5: Cobalt Chloride test strip.....	98
Figure 5.6: Fully moulded test samples in silicone mould	99
Figure 5.7: Hydraulic pressure vessel.....	100
Figure 5.8: Test samples after 2800psi pressure for 13 hours showing moisture on the test strip	101
Figure 5.9: Micro-cracks on soft polyurethane, sample 1	102
Figure 5.10: Micro-cracks on soft polyurethane, sample 2	102
Figure 5.11: Sketch of data-recorder tag showing only two polyurethane moulding compounds	104
Figure 5.12: Dimensions of data-recorder tag and soft polyurethane compound.....	105
Figure 5.13: Soft polyurethane compound model showing restraints and pressure	105
Figure 5.14: Von Mises stresses when 1420psi pressure is applied	107
Figure 5.15: Displacement when 1420psi pressure is applied.....	108
Figure 5.16: Von mises stresses when 2800psi pressure is applied.....	109
Figure 5.17: Displacement when 2800psi pressure is applied.....	110
Figure 5.18: Von mises stresses when 1420 psi pressure is applied for 5 hours	114
Figure 5.19: Displacement when 1420psi pressure is applied for 5 hours	114
Figure 5.20: Von mises stresses when 2800 psi pressure is applied for 5 hours	115
Figure 5.21: Displacement when 2800 psi pressure is applied for 5 hours	116
Figure 6.1: Sketch of data-recorder tag showing bi-material interface	120

Figure 6.2: Sketch showing diffusion paths for water through hard and soft polyurethane materials.....	121
Figure 6.3: Example of Fickian curve.....	127
Figure 6.4: Boundary conditions for moisture diffusion FEA model.....	133
Figure 6.5: Moisture diffusion after 1.8 days	134
Figure 6.6: Moisture diffusion after 10 days	135
Figure 6.7: Moisture diffusion after 35 days	135
Figure 6.8: Moisture diffusion after 185 days	136
Figure 6.9: Moisture diffusion time through two polyurethane materials.....	137
Figure 6.10: Sketch of tag showing interfaces of polyurethane materials.....	140

List of Symbols and Abbreviations

β	Scale Parameter
θ	Shape Parameter
e	exponent function
ln	natural logarithm
m	meter
y	intercept
V	volts
F(t)	cumulative density function
f(t)	probability density function
$\lambda(t)$	hazard rate function
min	minute
sec	seconds
RH	relative humidity
C	Celsius
deg	degree
wt	weight
MTTF	mean time to failure
PoF	physics of failure
CFD	computational fluid dynamics
Wcf	warranty correction factor

FEA	finite element analysis
LED	light emitting diode
GPS	global positioning system
RF	radio frequency
amp	ampere
msec	milli second
mm	millimeter
psi	pounds per square inch

Chapter 1

Introduction

1.1 Introduction to Microelectronics

Electronics is the study of the flow of charge through various materials and devices such as semiconductors, resistors, inductors, capacitors and microprocessors.

Electronic devices or systems are used in many fields, such as;

1. Communication
2. Computing
3. Entertainment
4. Measuring or scientific equipment
5. Biomedical
6. Other

Among such fields of application is, Biomedical, in which physiological data is monitored or maintained by small electronic devices, hence known as “Biomedical devices”. When such data is remotely obtained or transferred to data storage or

monitoring station through RF, Acoustic or GPS (global positioning system) signal, it is known as “Biotelemetry”.

Biotelemetry (or Medical Telemetry) involves the application of telemetry in the medical field to remotely monitor various vital signs of ambulatory patients. Telemetry is a technology that allows the remote measurement and reporting of information of interest to the system designer or operator, typically refers to wireless communication. These devices can be mounted externally to the body of the subject or implanted.

This thesis is only going to address the system Reliability of biotelemetry devices designed to study wildlife, mainly marine animals.

1.2 Biotelemetry Devices and Components

Biotelemetry devices designed for marine life study varies in size and technology based upon environment and size of the animal, for example;

1. **RF Transmitter Tags:** for shallow or fresh water application and capable of transmitting data to the on-shore data receiving stations through radio frequency.
2. **Acoustic Transmitter Tags:** mainly for shallow or fresh water application and capable of transmitting physiological data to either on-shore receiving stations directly or indirectly through floating data recording devices in water.

3. **GPS Transmitter Tags:** For terrestrial animals and capable of transmitting data through satellite to remotely located receiving station.
4. **Data Recorder Tags:** these tags are for deep water application, and usually deployed for long time study (2-5 years). These tags record all the information to an on-board memory and the recorded data can only be recovered when the tags are physically retrieved from the animal.

These tags can be equipped with multiple sensors like;

- Temperature sensors (environment and body temperature measurements)
- Pressure sensors (elevation for in-land and depth sensing for water animals)
- Motion sensors (mobility)
- ECG sensors (to measure heart rate)
- Compass (to determine heading or positioning)
- Light Sensors (to determine day and night)

Some types of biotelemetry systems are shown below;

1. Radio Transmitters and Receivers:



Figure 1.1 RF Tracking System, *Courtesy of Lotek Wireless Inc.*

2. Acoustic Transmitters and Receivers:



Figure 1.2 Acoustic Tracking System, *Courtesy of Lotek Wireless Inc.*

3. Data Recorders:



Figure 1.3 Data Recorders, *Courtesy of Lotek Wireless Inc.*

1.3 Data Recorders – System Description

The electronics of biotelemetry devices (tags) consist of the following essential components;

1. Integrated circuit with Microprocessor
2. Sensor(s)
3. Data download or upload circuit
4. Battery
5. Wireless communication mode, like antennas or circuits.

Data recorder tags do not include any antenna as they are not designed to transmit data periodically like other tags. However, these tags do contain memory chips to record data on-board, till it needs to be recovered. Data from recovered tag is downloaded through optical mechanism (LED) to a computer by using a reading device.

Biotelemetry devices, especially data recorder tags, for wildlife research are designed to study animal behaviors by tagging animals either externally on the body or internally (implanted) that monitors and records data over the mission of the study. This important data is usually recovered after a long wait by scientists and single tag can carry up to 32,000 data points which depict the behavior of the animal over a period of 3-4 years. The recovery rate of these tags is very low, in the range of 3.9-10%, (Walker and Urawa, 2007), which makes it very important for these devices to have high system Reliability so that during mission, tags record data reliably and after mission data can be obtained

reliably from the recovered tags. Therefore, due to risks involve, these data recording tags needs to have high reliability.

Figure 1.4 shows some main components of data recorder tag.

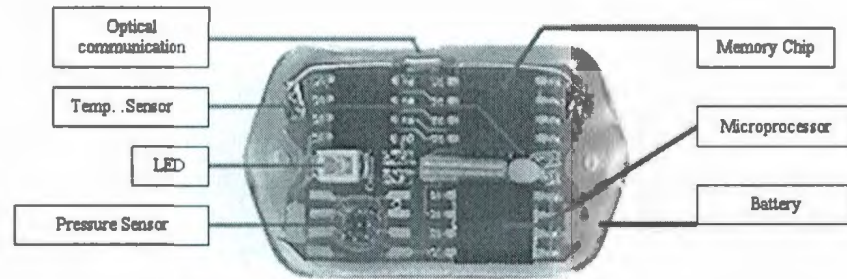


Figure 1.4 Components of Data Recorder Tracking Tag, *Courtesy of Lotek Wireless Inc.*

This thesis is based on the study of data-recorder device as shown in figure 1.4 and figure 1.5.

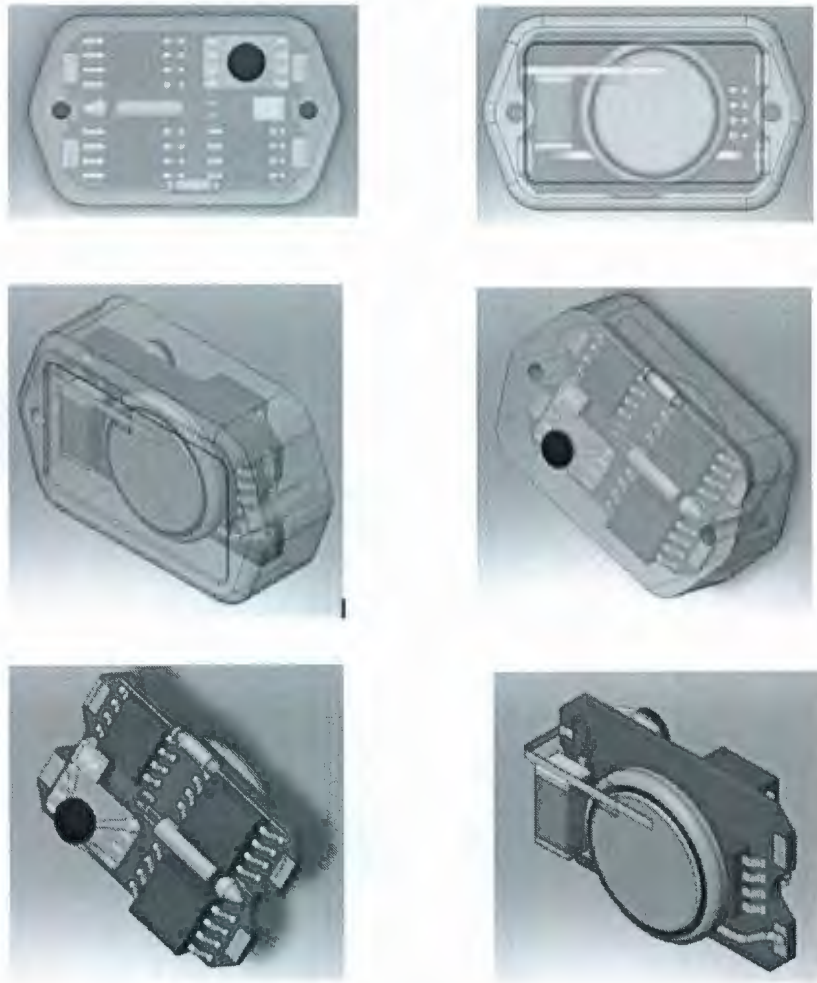


Figure 1.5 Data Recorder Tracking Tag, *Courtesy of Lotek Wireless Inc.*

1.4 Scope and Purpose of Research

The ultimate goal of this work is to determine ways for improving the reliability of the data recording tags. To achieve this goal it is important that failure modes of the system are identified and studied. This is done by studying the failure data that is gathered from

field performance record. Also critical components of the system are identified and studied. These studies were done analytically and experimentally.

The first component of this research is to perform a detailed analytical analysis on historical field failure data of the data recorder tag, which will lead into Reliability Analysis of the whole system. Failure data of these data-recorder tags, which is available from the last six years, was studied. Failures were defined and grouped under these categories and Pareto chart was created. Then each failure mode was analytically studied using Weibull analysis to understand the mechanisms of failure rate. Shape parameter, β , is used to determine the failure mode.

Using failure rates obtained from MIL-STD-217F and MIL-STD-338B, failure rates and probability of failure data of each component is calculated depending upon working conditions and environmental loads. Fault Tree analysis is performed for each failure modes to understand the failure mechanics. The analysis also helped in understanding the overall reliability of the system. As a result of this analysis of the most sensitive components came into light.

The second component of this research utilizes the information from the first part of the research in which the failure modes were identified and takes into deeper understanding of the root cause of these failures. Experiments at component level are conducted to find the root cause of all failure modes, which are due to power, packaging and component

failures. These experiments include testing of battery at continuous and intermittent load conditions to determine the discharge life of the battery. The experiment was conducted at two different temperatures to understand the life of battery at extreme temperature conditions.

Similarly, packaging failure which is defined as water penetration to electrical circuit related to structural strength and moisture diffusion was also studied, both analytically and experimentally by conducting pressure experiments and FEA simulation. These experiments gave insight to the design limitations of data-recorder tags and moisture problem which is related to most of the failures in these data-recorder tags.

1.5 Outline of Thesis

Chapter 1 gives a general introduction to the biomedical equipment and biotelemetry devices. The chapter also includes a statement of the objectives and an outline of the thesis. The next chapter, chapter 2, is review of the literature. Literature on the moisture diffusion problem in electronic packaging materials which leads to failures of circuits is also reviewed. This part of the research is necessary to understand the theory behind moisture diffusion and conduct experiments to determine the moisture ingress rate through packaging materials.

Detailed field data analysis is presented in chapter 3. Hazard rate plots are created for the whole dataset and then also for separate failure modes. The data was fitted to Weibull distribution so that we can determine the failure mode of the tags. It was found that the prominent failure mode is infant mortality. Therefore, in later chapters more extensive study and experiments are conducted to determine the root cause of these failures.

Battery failure is studied extensively in chapter 4. Experiments were conducted to determine the preferred characteristics of batteries to be used for powering the tags at different temperatures. Conclusions and experiments details are presented in chapter 4.

Packaging failures, which means mostly structural failures, resulting in water penetration from outer environment and damaging electrical circuit, are discussed in chapter 5. This chapter also includes experiments and simulations using FEA to determine the design limitations of the data-recorder tag and qualify the design specifications and modifications necessary to the design to meet improved specifications.

Another significant problem that is a subset of packaging failures is the moisture diffusion problem. Water diffuses through the packaging material and through the soft and hard polyurethane interface causes potential for excess current draw, thus, resulting in failure of battery and components. Chapter 6 discusses this problem in detail along with analytical calculations and FEA simulations to determine the impact of moisture diffusion on the suitability of the current design.

The conclusions, recommendations and future work are presented in chapter 7.

Chapter 2

Literature Review

2.1 Introduction

Reliability engineering is an engineering field that deals with the study of reliability, defined as, “the ability of a system or component to perform its required functions under stated conditions for a specified period of time”. It is often reported in terms of a probability.

Even though a product has a reliable design, when the product is manufactured and used in the field, its reliability may be unsatisfactory. The reason for this low reliability may be that the product was poorly manufactured. So, even though the product has a reliable design, it is effectively unreliable when fielded which is actually the result of a substandard manufacturing process. As an example, cold solder joints could pass initial testing at the manufacturer, but fail in the field as the result of thermal cycling or vibration. This type of failure did not occur because of an improper design, but rather it is the result of an inferior manufacturing process. So while this product may have a reliable design, its quality is unacceptable because of the manufacturing process.

Microelectronics integration density is limited by the reliability of the manufactured product at a desired circuit density. Design rules, operating voltage and maximum switching speeds are chosen to insure functional operation over the intended lifetime of the product. Thus, in order to determine the ultimate performance for a given set of design constraints, the reliability must be modeled for its specific operating condition.

According to Denson (Denson et. al., 1998), over the last several decades, our knowledge about the root cause and physical behavior of the critical failure mechanisms in microelectronic devices has grown significantly. Confidence in the reliability models have led to more aggressive design rules that have been successfully applied to the latest VLSI technology. One result of improved reliability modeling has been accelerated performance, beyond the expectation of Moore's Law. A consequence of more aggressive design rules has been a reduction in the weight of a single failure mechanism. Hence in modern devices, there is no single failure mode that is more likely to occur than any other as guaranteed by the integration of modern failure physics modeling and advanced simulation tools in the design process.

In order to understand the current trends in reliability modeling and prediction, we have to look at it from historical point of view. Reliability modeling and prediction is a relatively new discipline. Only since World War II has reliability become a subject of study. This came about because of the relatively complex electronic equipment used during the war and the rather high failure rates observed.

Since then, we can indicate two different approaches for reliability modeling corresponding to different time periods. Until the 1980s, the exponential, or the constant failure rate (CFR) model had been the only model used for describing the useful life of electronic components. It was common to six reliability prediction procedures, which were reviewed by Bowles (1956) and was the foundation of the military handbook for reliability prediction of electronic equipments, known as MIL-HDBK-217. Although the CFR model was used without physical justification, it is not difficult to reconstruct the rationale for the use of the CFR model which mathematically describes the failure distribution of systems in which the failures are due to completely random or chance events. Indeed, throughout that period, electronic equipment complexity has begun to increase significantly. Similarly, the earlier devices were fragile and had several intrinsic failure mechanisms, which combined together to result in a constant failure rate.

During the 1980s and early 1990s, with the introduction of integrated circuits (ICs), more and more evidence was gathered suggesting that the CFR model was no longer applicable. Phenomena, such as infant mortality and device wear out dominated the field failures and they could not be described using the CFR model. In 1991, two research groups, IIT Research Institute/Honeywell SSED and the Westinghouse/University of Maryland teams both suggested that the CFR model should not be used, Nash et al. (1994), based on their research to provide guidelines to update the MIL-HDBK-217. They suggested that the exponential distribution was unacceptable and should not be blindly applied to every type of component and system.

Since then, the Physics-of-Failure approach has dominated reliability modeling. In this approach, the root cause of individual failure mechanism is studied and corrected to achieve some determined lifetime. Since wear out mechanisms became better understood, the goal of reliability engineers has been to design dominant mechanisms for the useful life of the components by applying strict rules for every design feature. The theoretical result of this approach, of course, is that the expected wear out failures has become unlikely to occur during the normal service life of microelectronic devices. Nonetheless, failures do occur in the field and reliability prediction had to accommodate this new theoretical approach to the virtual elimination of any one failure mechanisms limiting the useful life of an electronic device.

2.2 Current Research

Since all biomedical/biotelemetry devices are microelectronics in nature so all the challenges currently being faced by electronic industry is truly applicable to such devices. Research can be seen on finding better materials, assembly methods, high performing components or hardware design, etc.

The technology or limitations to technology are constantly being challenged by industry engineers; the reliability of such components or systems made out of such components is also a challenge to calculate. Previously available reliability models need to be updated as the technology changes to keep them validated. Same is the case with MIL-HDBK-

217 standard which is used by industry as a standard but usually modified so that predicted values are not very off from the tested values.

Current research can be divided into three categories as shown in table 2.1;

Table 2.1 Categories of current research on electronic devices

Electronics Packaging	Electronics Hardware Design	Reliability Analysis of Electronic Devices
Materials	Power Supply (life)	Prediction Models
Mechanical Packaging	Mechanical Packaging, including size and weight reduction (Limited)	Failure Rates Accuracy
Algorithms	Algorithms and System Architecture	Accelerated Life Testing
Data Transfer	Data Transfer (RF/ACS/GPS) Uplink/downlink	Algorithms

2.3 Hardware Design of Biotelemetry Electronic Devices

Addressing the need for more power efficient microprocessors to prolong the life of battery, Cook and Fernald (1990), designed a custom microprocessor for implantable telemetry devices making them more power efficient and be able to package smaller in size. To further reduce the size of the microprocessor, DeMichele and Troyk (2003), designed an ASIC (assigned specific integrated circuit) which reduced the electronics physical size significantly by adding circuitry into a very small die. Tanase and Marinca (2005), proposed a concept of frequency exchanger as a part of telemetry devices to help capture the true movements of subject at low speeds. Whereas, Hsu and Luo (2006)

created a biotelemetry chip using analog modulation technique, which greatly enhance the wireless monitoring of ECG data. On the other hand, Betancourt-Zamora and Lee (1998) proposed a new architecture based upon CMOS technology that saves power as significant portion of the power budget for any implantable telemetry system is allocated to the generation of the RF carrier.

Similarly, Valdastri and Menciassi (2004), derives a microcontroller based multi-channel telemetry system which can read different types of sensors simultaneously. This is widely used in industry as a common platform for most of the biotelemetry devices available today. Wang and Johannessen (2005) also designed a whole new biotelemetry device which is a system-on-chip and programmable.

2.4 Specific Reliability Models for Electronics

Since solder joints are the common part of any electronic devices, Jorez (1999) presented an optical method to study the thermo-mechanical behaviour of electronic power devices to understand the reliability of solder joints. Studies like these provide real data that can be used to calculate failure rates of devices.

Park and Osenback (2005) found that a 3-parameter exponential function is useful to predict the degradation of T_g (glass transition temperature) under the given aging condition.

2.5 Prediction Modeling and Assessment

Reliability prediction is one of the most common forms of reliability analysis, usually employed at the earlier design stages, in order to evaluate inherent reliability of product design as well as to identify potential reliability problems. The most common reliability prediction techniques of the past were based on empirically driven MIL-HDBK-217; the military standard widely used for three decades by many electronics companies. Reliability prediction models such as described by MIL-STD-217 are widely accepted in industry. However, they do not provide accurate values in a number of situations. Therefore, during the last years this method's popularity has been gradually declining mostly due to proliferation of new electronic packaging technologies, continuous improvement in quality and reliability, and thus subsequent inability of MIL-HDBK-217 to make accurate failure rate predictions.

However, most of the mathematical models in MIL-STD-217 along with the relevant principles of physics remain largely valid. In the past years there have been multiple efforts to improve the accuracy of MIL-STD-217 predictions. The examples include PRISM, developed by RAC, British Telecom HRD-5, European IEC 1709, Telcordia SR-332, French developed CNET 93, and others. Following is the list of standards available;

1. MIL-HDBK-217 (parts count and parts stress method)

2. Telcordia
3. Prism (RAC rate models)
4. RDF 2000 (previously CNET 93)
5. NSWC-98/LE1
6. HRD5
7. GJB/z299B

Out of all the above references, only MIL-HDBK-217 is widely available and most commonly used. Due to assumptions made in MIL-HDBK-217 and some deficiencies which are explained in detail by Pecht and Nash (1994), lot of work has been done in modifying these prediction models to obtain accurate results.

Kleyner and Bender (2003) presented a comparison of prediction methods by merging military standards and manufacturer's warranty data in an attempt to enhance the process of reliability prediction. This paper presents an attempt to further enhance the process of reliability prediction by linking the results to the product field data. This is done by introducing a warranty correction factor, W_{CF} into the equation.

Since each of the two reliability prediction methods have advantages and disadvantages, it is appropriate to combine both that helps to overcome their shortcomings and make the most of their benefits. The merging of the two methods can be accomplished by adjusting the appropriate empirical equations and coefficients from MIL-HDBK-217 by

multiplying them by W_{CF} . Where; W_{CF} is a “warranty correction factor”, derived from the analysis of manufacturer’s warranty return data.

Kleyner and Bender (2003) states that MIL-STD-217 advantages include useful empirical equations allowing the user to account for component type and specific operating conditions. The disadvantages include low accuracy of predicting absolute values of components failure rates, which are further weakened by the effect of lesser-defined parameters. Similarly, advantages of applying warranty or other field data to reliability prediction include relative accuracy of prediction and consistency of the results with product’s performance in the field. Moreover, reference to the field data provides more credibility with the customer examining the data. The disadvantages include inability to account for specific usage conditions and to distinguish between different parts within the same part family.

The limitations of MIL-HDBK-217 are limited by definition of dynamic states, most of these calculations were done assuming steady-state conditions where power is continuously supplied and the environment conditions remain constant. This is contradictory with real environment conditions that most of these devices are operated in. Considering this Rodgers and Evely (2000), demonstrated the use of CFD (computational fluid dynamics) as current feasible reliability predictive technologies in early design stages to evaluate thermal performance of the electronics.

Moisture induced failures is the number one cause of failures of most of the electronic equipments today and many efforts and studies has been done to understand this phenomenon. While Rodgers and Evely (2000) demonstrated use of CFD modeling for heat transfer studies, Zhao and Chaers (2003), developed a prediction model for the moisture induced failures in flip chip on flex interconnections. Zhao and Chaers (2003) used FEM simulations (finite element modeling) and experimental modeling for material characterization and model validation. Finite element simulation was used to calculate the contact pressure between the bumps and the copper contacts. Then a simulation methodology was established that models the stress relaxation from contact pressure and bonding process when exposed to steady-state temperature and humidity conditions. The mechanical contact pressure obtained in finite element modeling was translated to the electrical contact resistance for practical interpretation and validation with reliability ageing test, which was validated by damp heat tests were performed. The experimental setup and methodology provided important information to understand and to quantify the degradation mechanisms during aging.

Considering the deficiencies in the current prediction models and the inaccuracies caused by neglected factors, Wong (1995) developed a framework for prediction models by also incorporating environmental and internal stresses, parts and material selection, parts vendors and the exact usage profile.

He proved that even if just one factor, storage conditions at vendor, is considered in prediction model, one can see that it varies from vendor to vendor, which provides another factor that is missing from the classic methods. The inaccuracies of MIL-STD-217D were also discussed, for example; MIL-STD-217D cannot be used to predict MTBF to within 500% accuracy even for similar equipment use in the same environment.

The issues of uncertainties and inaccuracies in the MIL-STD-217 are further illustrated by Parry and Clemens (2002), by discussing the knowledge gap between temperature/stress analysis and system lifetime assessment. Parry and Clemens (2002) discussed that straight forward application of the Arrhenius model has led to widespread misconceptions that are then followed blindly. Parry and Clemens (2002) also mention the difficulty of using MIL-STD-217 type models for new emerging technologies. Since there is lack of wide, environmentally relevant database of test data and experience of field failures, the MTTF calculations would be based on many assumptions.

The PoF (physics of failure) approach is a good trustworthy method which takes user defined load and environmental conditions in combination with layout and other input data and physics of failure mechanisms to result in a ranking of most probable failures. The downside of PoF approach is the correct identification of failure mechanisms. For example; for package and interconnect failure mechanisms, wire bond fatigue might be due to delamination at the die surface, while misregistration of the part during placement or inadequate solder paste could reduce the life of the package interconnect. Parry and

Clemens (2002) described the deficiencies in the thermal analysis by pointing out the environmental and design uncertainties while also describing the gaps that need to be filled in order to conduct a reliable thermal model.

It is often and very commonly required to conduct accelerated life tests to predict reliability of the designed system in a short time. Zhao and Elsayed (2004) conducted such experiment by developing an IPL-Weibull Brownian model for analyzing competing risk data involving performance degradation and hard failures obtained at accelerated operating conditions. The models are also validated experimentally by conducting an accelerated testing on the LED's subject to high test driving current.

When there are multiple failure modes, commonly, it is important to use the relationship of these competing modes in order to predict the life. Huang and Askin (2003) described how the reliability analysis are conducted considering competing failure modes involving performance aging degradation. An experimental dataset was used as an example where two kinds of failures were kept under discussion, solder/Cu pad interface failure (catastrophic) and light intensity degradation (degradation failure).

First the MTTF of system is calculated by using each individual failure modes and the combined effect. The results shows that catastrophic failures has more impact on degradation of life then any other failure modes, $F_h \gg F_s$. It can also be seen that after certain time the catastrophic failure mode is not dominant.

Pfau and Ferrari (2007) went in completely different direction and proposed a hidden markov model based segmentation technique that can be applied to large data set with various degrees of freedom. Stochastic pattern recognition based on hidden markov model can be successfully applied to the task of automated segmentation and classification of inertial sensor data.

Although there is not much research that can be found on the Reliability analysis of biomedical or biotelemetry devices, but lot can be found considering general electronics. As discussed and presented in previous chapter that biotelemetry or biomedical devices are basically microelectronics the research on reliability of electronic devices is applicable. Bernstein and Gurfinkel (2006) presented a comprehensive paper, in which, two state-of-the-art degradation-based reliability simulation methodologies are reviewed and a new failure rate-based SPICE reliability simulation methodology is proposed to address some limitations inherent in the former methods. The simplicity and power of this reliability simulation method make it an additional tool for designers and users to estimate product reliability and allow system designers to de-rate products for longer life applications.

Similarly, Cushings and Mortin (1993) presented very interesting approach and study by comparing MIL-STD-217 with PoF (physics of failure) approach. Cushings and Mortin (1993) presented data showing the difference in failure rates of components using the two

methods. In conclusion, emphasizes was made on understanding the actual failure mechanism rather than generalizing all types of failures into single type.

Nash and Pecht (1994) also presented a very comprehensive overview of reliability prediction and assessment methods and also provided deficiencies in currently available methods which lead to future work. For example; development of PoF model to better represent the effects of material, stress and structure towards failure of components or systems.

Guo and Zhao (2006) reviewed two popular used models for repairable systems. In order to overcome the drawbacks of these models, a new model which considers both time trend and repair effects was proposed. Comparison results show that the proposed model is very useful in practice.

Jones and Hayes (2001) also presented a new approach to calculate non-constant failure rate model for reliability estimation of a system which does not depend upon constant failure rates. Lall (1996) compared the two approaches in calculation of the temperature acceleration of microelectronics device failure. The comparison showed different results obtained from using MIL-HDBK-217 model and PoF approach.

2.6 Moisture Diffusion Problem

Since many contemporary electronic packages utilize epoxy based materials such as underfill and molding compounds, they are highly susceptible to moisture absorption, which can lead to undesirable changes in mechanical performance and interfacial adhesion. Consequently, moisture can be attributed as being one of the principal causes for many premature package failures. Central to understanding the effect of moisture to interfacial adhesion in microelectronic assemblies is to first identify the rate as which moisture is delivered to the interface, followed by understanding the response of the interfacial adhesion to increasing levels of moisture concentration. Moisture can affect the interfacial adhesion both directly by being physically present at the interface itself and indirectly by changing the mechanical properties of the adhesive and substrate due to moisture uptake. Moisture can also cause both reversible and irreversible damage to interfacial adhesion. Therefore a comprehensive study on the effect of moisture on interfacial adhesion in microelectronic assemblies will need to consider moisture transport to the interface, moisture effects on epoxy adhesives, moisture effects at the interface, and recovery of adhesion and bulk properties from moisture uptake.

The deleterious effect of moisture not only damages interfacial adhesion by being physically present at the interface, but also through the degradation of the elastic modulus of the adhesive and substrate due to moisture uptake. The change in the elastic modulus after moisture uptake can be substantial, which can significantly affect material performance and interfacial fracture toughness results. Consequently, the variation in the

elastic modulus of the adhesive and substrate as a function of moisture concentration should be determined to completely characterize the loss in interfacial adhesion due to moisture absorption. Since the substrates in this study are metallic and impermeable to moisture, it is only necessary to characterize the change in the elastic modulus as a function of moisture concentration for the underfill adhesive, which is epoxy based and highly susceptible to moisture uptake.

Epoxy adhesives are found in many microelectronic packaging applications and widely used throughout the industry. One of the more substantial developments within the last ten years is underfill, which is an epoxy based encapsulant that mechanically couples the chip to the board. Underfill drastically enhances the fatigue life of microelectronic assemblies when compared to unencapsulated devices, Tencer (1994). However, since underfills are epoxy based, they are also particularly vulnerable to moisture ingress, as discussed and explained by Uschitsky and Suhir (2001), Wong and Lim (1998), Ferguson and Qu (2003). Although the absorbed moisture can significantly alter its mechanical performance and the overall microelectronic assembly reliability, very few studies in the electronic packaging literature have addressed the issue of moisture on the mechanical properties of epoxies, and no known papers found to address the effect of moisture on the elastic modulus. Consequently, it is a necessary requirement to step outside of the electronic packaging community in order to gain a better understanding of the state of the art of the effect of moisture on the mechanical properties of bulk epoxies.

Throughout the literature, the availability of information regarding the effect of moisture on the mechanical properties of epoxy adhesives is in general limited and more work is needed to adequately characterize this response, Crocombe (1997), and Harper and Kenner (1997). From the work that has been published, it has been found that water absorption can severely modify the mechanical properties of epoxy adhesives by decreasing the elastic modulus, Zanni-Deffarges and Shanahan (1995), shear modulus, Jurf and Vinson (1985), and Zanni-Deffarges and Shanahan (1994), yield and ultimate stress, Wahab (2002) while increasing the failure strain, Crocombe (1997), and Wahab (2002) as water concentration increases.

Moisture primarily affects the mechanical properties of adhesives through three mechanisms: plasticization, crazing, and hydrolysis. The first is considered reversible upon drying, while the latter two are irreversible. Several studies attribute the decrease in modulus due to the plasticizing action of the water on the adhesive, Jurf and Vinson (1985), Brewis and Neval (1990), DeNeve and Shanahan (1992), Zanni-Deffarges and Shanahan (1995), Crocombe (1997), and Wahab (2002). By acting as an external plasticizer to the polymer adhesive, the water spreads the polymer molecules apart and reduces the polymer-polymer chain secondary bonding. This provides more room for the polymer molecules to untangle and move, which results in a softer, more easily deformable mass, Rosen (1993). Other studies show the decrease in epoxy modulus after moisture absorption resulting from crazing, Morgan and Lu (1979), where the absorbed water can act as a crazing agent continuously decreasing the mechanical strength of

epoxies with exposure time in water. This is supported by scanning electron micrographs of epoxies, which show cavities and fractured fibrils that could only be explained by moisture induced crazing mechanism, Fremont, Pintus, Deletage and Danto (2001). Consequently, the moisture induced swelling creates dimensional changes and internal stresses that can ultimately craze and/or crack the material. As a result, lightly cross-linked networks will be more susceptible to crazing than highly cross-linked networks, Ma, Jansen and Ernst (2006). Last, moisture can also affect the mechanical properties of adhesives by causing hydrolysis leading to chain scission. Short term exposure to moisture results in chain scission with a chemical addition of water that remains permanently in the epoxy system even after subsequent drying, while long term exposure to moisture can result in an increased probability of chain scission detaching segments from the polymer network, yielding a permanent loss in weight after subsequent drying, Xiao and Shanahan (1997).

Studies by Zanni-Deffarges and Shanahan (1994 and 1995) and DeNeve and Shanahan (1992) depict the decrease in elastic and shear modulus of an epoxy as a function of time exposure to moisture. Although this information is useful in evaluating the effect of exposure time to moisture on the modulus, it does not depict how the inherent wet modulus values change as a function of concentration since a gradient of mechanical properties will exist in the adhesive until saturation is reached and water concentrations become steady and uniform. Other studies have evaluated the effect of moisture on epoxy adhesives after saturation is established for a given level of moisture preconditioning.

These studies have shown a decrease in the elastic modulus of epoxy adhesives of 24%, Zanni-Deffarges and Shanahan (1994), 29%, Su and Yang (1992), and 86%, Su and Yang (1992) for saturation concentrations of 4 wt%, 0.9 wt%, and 3.1 wt% respectively. However, they only tested one level of moisture preconditioning to compare to fully dried test results. Consequently, information regarding the mechanical response of epoxy adhesives to different levels of moisture concentrations is incomplete and fundamental insight into the intrinsic response of the adhesives to increasing saturation concentrations of moisture cannot be ascertained.

There are several factors to be considered in interfacial adhesion. Such factors include the material and physical properties of the adhesives, the bulk and surface characteristics of adherends, and the nature of the forces involved in the bonding, Lee (1979). Loss of adhesion resulting in delamination intensifies singular stress behavior, inducing higher stress concentrations between the adherend and adherate. This will result in more rapid crack growth than in comparison with undamaged devices, Vroonhoven (1993).

Last, environmental factors such as temperature and moisture can also have an adverse effect on adhesion. Ferguson and Qu (2002) showed that interfacial fracture toughness is significantly affected by the presence of moisture, with the interfacial adhesion of two different underfill/solder mask interfaces decreasing by approximately one half after 725 hours of exposure at 85°C/85%RH. Gledhill and Kinloch (1974) tested joints consisting of a mild steel substrate and an epoxy adhesive at 20°C/56%RH and submersion in water

at 40°C, 60°C, and 90°C for up to 2500 hours. They found that the 20°C/56%RH specimens suffered no significant change in joint strength; however, all specimens submerged in water resulted in a significant loss in joint strength. They also noted that joints exposed to 20°C, 40°C, 60°C, and 90°C and 0%RH had no significant loss in joint strength even after prolonged exposure. Consequently, the testing temperatures themselves did not contribute to the loss of joint strength, and all the observed losses in joint strength were attributed to moisture. Similarly, Cotter (1977) showed that after 4 years of exposure of epoxy-polyamide/aluminium-alloy joints to a hot-wet tropical environment resulted in a significant loss in die shear strength, whereas the same amount of exposure to a hot-dry climate had little effect in die shear strength.

As a result, the deleterious effect of moisture was much more damaging to the bond strength of the joints than temperature when comparing the two environments. Although the temperature had no effect in the two aforementioned studies, Kinloch (1979) warns that in general temperature will affect the durability of adhesive joints, with an increase in temperature generally yielding an increase in the rate of strength loss. However, a study by Rogers and Evely (2000) found that lap shear joints consisting of a low-modulus thermoset adhesive bonded to fiber-reinforced plastics (FRP) and galvanized steel had higher lap shear strength for joints exposed to 60°C for 6 weeks when compared to controls kept at laboratory conditions (23°C). Consequently, temperature actually increased the lap shear strength of the joints. Based on the results of the above studies, it is clear that both temperature and moisture can play a critical role in interfacial adhesion.

Works from other authors were also considered in regards to modeling of moisture diffusion using finite element analysis method. Wong and Rajoo (2003) presented the wetness fraction approach for concentration discontinuity in the application of Fick's law to multi-material system such as in the plastic packages. Due to this approach commercial thermal diffusion analysis software packages can be used to model the transient moisture diffusion phenomenon. Galloway and Miles (1996) presented a partial pressure approach to understand moisture diffusion problem. Wong and Lim (1998) challenges the approach presented by Galloway and Miles (1996) as it is limited for gas if it retains its state in solid but this is not the case with moisture which condenses into water. To further add to his approach, Wong, Koh, Lee and Rajoo (2002) presented a 99% sorption approach which helped in defining the limit of Fickian diffusion, hence eliminating error caused by non-fickian sorption. Adding further, Wong and Rajoo (2003) experimented and presented a comprehensive relationship between the aspect ratio of the test specimen and errors in moisture diffusion models.

Wang, Koh, Lee and Rajoo (2003) presented a normalized analogy for FEA replacing concentration with solubility which assumes that solubility remains constant regardless of the level of concentration. Others like Fremont, Horaud and Weide-Zaage (2006), Ma, Jansen, Ernst, Van Driel, Sluis and Zhang (2007) added more research work by conducting various experiments using the methods describe by Wong, Teo and Lim (1998).

2.7 Significance of Current Research

The previously mentioned work does cover many aspects of reliability modeling and assessment related issues in electronics reliability, but all the research is either at component level, assembly level or focusing on general technology and technology issues. One can learn a lot from these research and available information in books but application of such knowledge to a complete system comprising of customized packaging methods requires experience to modify methods and equations for best fit.

Biotelemetry product manufacturers and designers can benefit a lot from the understanding of numerical and experimental analysis and methodology prescribed in reliability engineering at earlier design stage. As explained in previous chapter that due to risks involve in these costly studies of animals using biotelemetry devices, it is desirable to understand the true system Reliability of data-recorder tags so that probability of having a successful mission is well understood.

This thesis focuses on presenting methodology of assessing system reliability by analyzing the field failure data of data recorder tag. The analyses of failure data is used to find out different failure modes and the root cause of those failure and their current reliability in given design.

To further, design analysis and qualification of micro-electronics is evaluated by using analytical and experimental approach for determining structural and materials specifications.

Chapter 3

Failure Data Analysis

3.1 Introduction

In this chapter field data of recovered tags will be analyzed to determine the failure modes for the tags. Field data for a number of Data Recording Tags was collected through the warranty claims database, shown in appendix 1 and 2.

Before the failure data analysis, description, functionality and recorded data is described in next topic to better understand the product and type of data under study.

3.2 Data Recorder Tag

Biotelemetry instruments and systems are used around the world by biologists to study wildlife behaviour. The complete system comprises of hardware and software. Hardware includes implantable data recording tags and data download/upload device, whereas, software is provided for post processing of recorded data for easy viewing in graphical format.

A data storage tag (DST) is used to study marine life, especially in deep oceans where acoustic and radio telemetry is not possible. These devices are designed to collect data at specific intervals and store the data into onboard memory till it is retrieved back which could be after years.

The data recorder tags, product under study, records a time series of temperature and depth (absolute pressure) measurements to provide insight into detailed animal behavior. Standard depth measurement ranges include 50m, 500m and 1000m, where “m” means meters depth of water. Figure 3.1 shows a picture of this product.

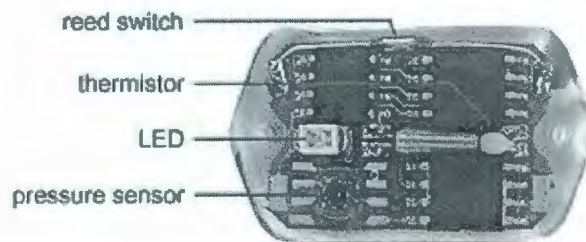


Figure 3.1 Data Storage Tag

Table 3.1 shows the product specifications, in general;

Table 3.1 Data-recorder tag specifications

Dimensions	8mm X 16mm X 27mm
Weight in air	5 grams
Weight in Fresh Water	~ 2 grams
Max Operation Temperature	35° C
Min Operation Temperature	-5° C
Data Points (Temp and Pressure)	16K, 32K
Standard Depth Range	50, 500, 1000 m
Sensors	Temperature and Pressure
Pressure Accuracy	+/-1% of Current Scale
Pressure Resolution	Scale / 256
Temperature Measurement	-5° to 35° C
Temperature Accuracy	better than 0.3° C
Temperature Resolution	0.20° C (avg.)
Typical Life	>3 years
Number of Records	32K, 64K

Since the recorded data from the data-recorder tags provides life pattern of in study living species by capturing temperature of the body and depths in ocean where the animal lives, it also contains failure time and failure mode history. A test is conducted to show the functions of the data-recorder tag and understand the interpretations of the recorded data.

To do this, tag, as mentioned in figure 1 was used to record data for approximately 1 day. The tag was reset and left on desk in a room environment from afternoon till evening, then after 5:30 pm tag was left on outside in an open environment to collect data overnight in cold temperature. Retrieved back and brought back inside for download.

Start: November 20, 2007, 11:23.02 am

Finish: November 21, 2007, 08:44:08 am

Total Data Points Recorded: 5467 (1 every 14 seconds)

Below are the graphs from Figures 3.2 to 3.6 shows the recorded data;

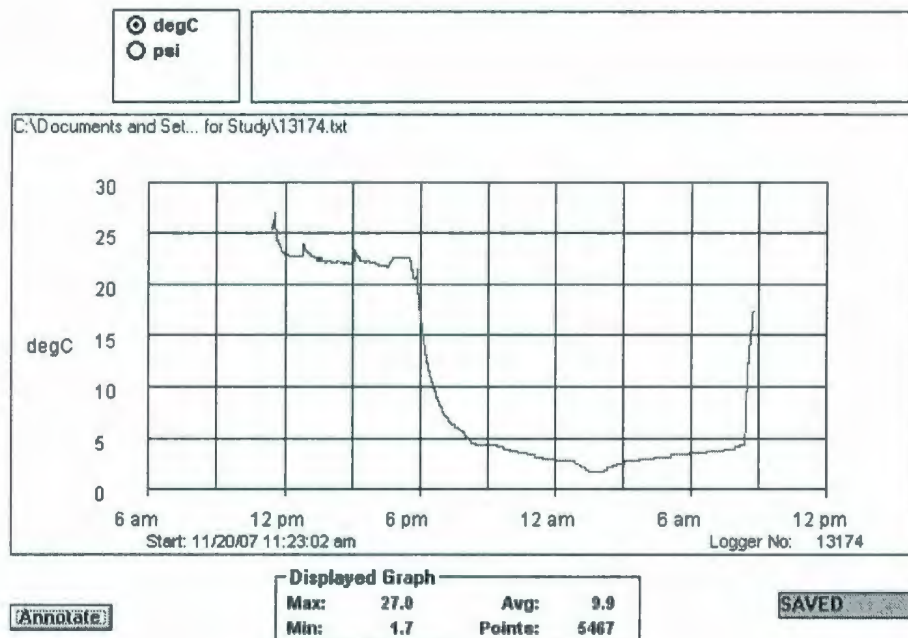


Figure 3.2 Temperature Chart of Tag

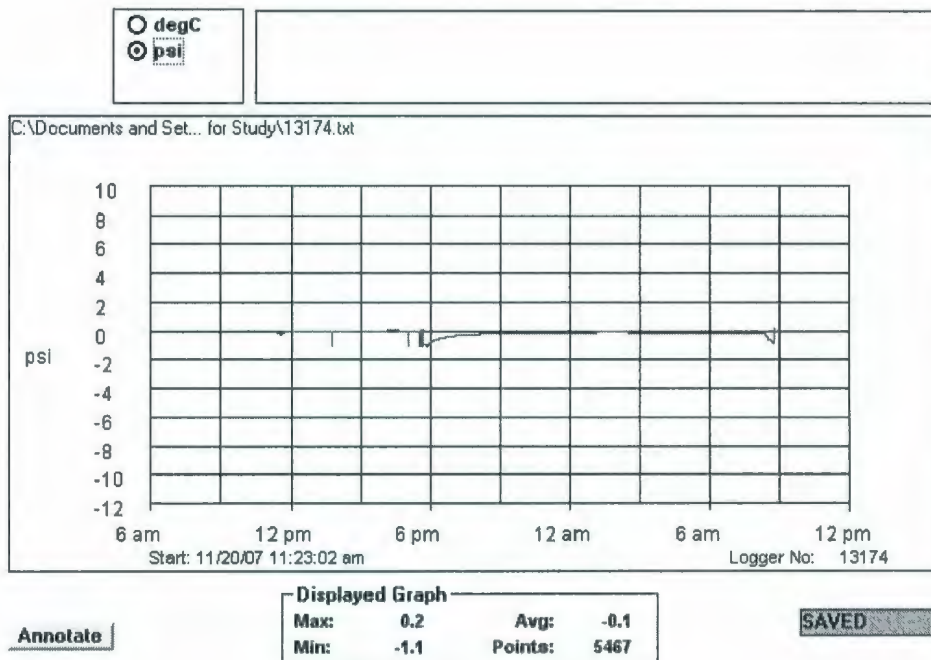


Figure 3.3 Pressure Chart of Tag

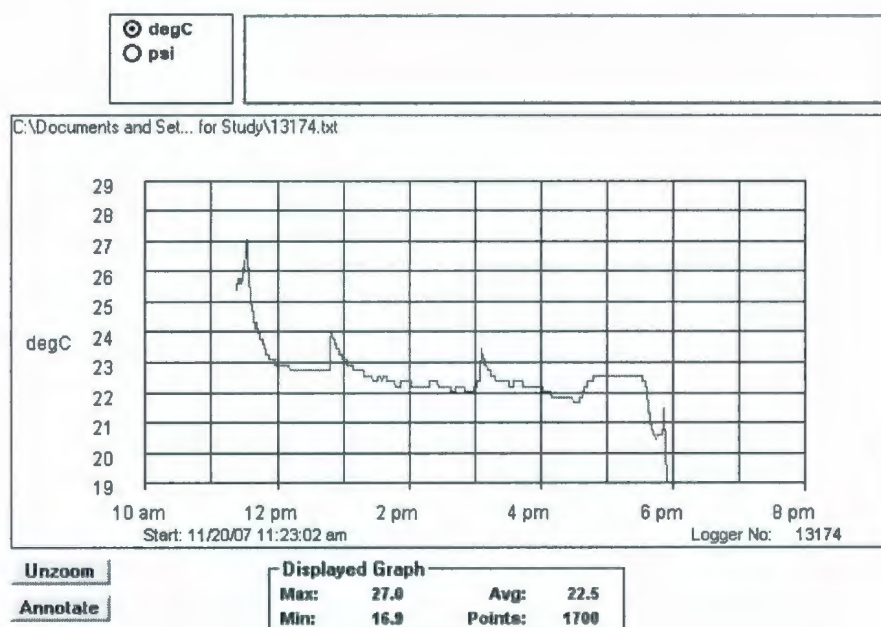


Figure 3.4 Temperature Data of Tag from start till evening just before the tag was left outside for overnight recording

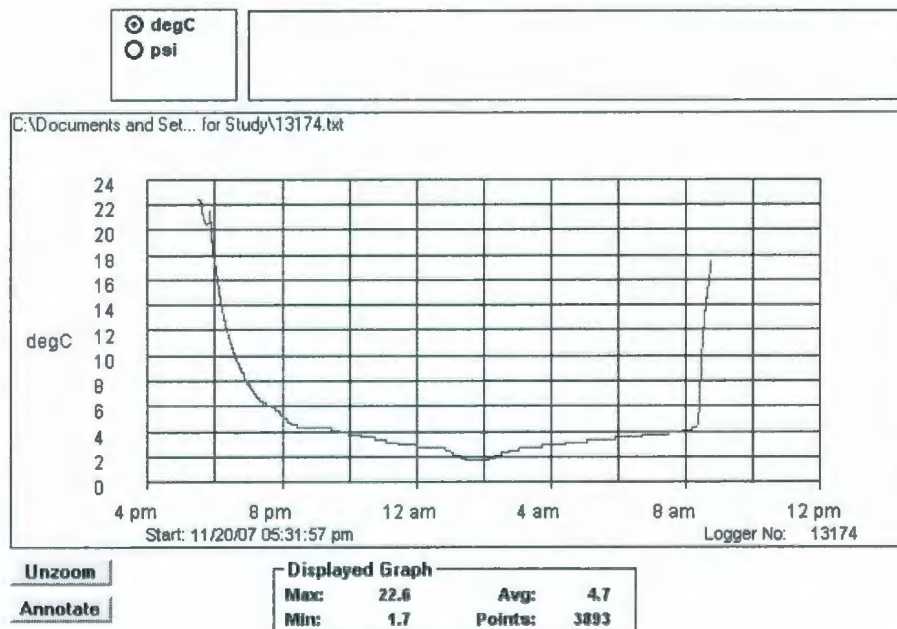


Figure 3.5 Temperature Chart of Tag recording overnight cold temperatures

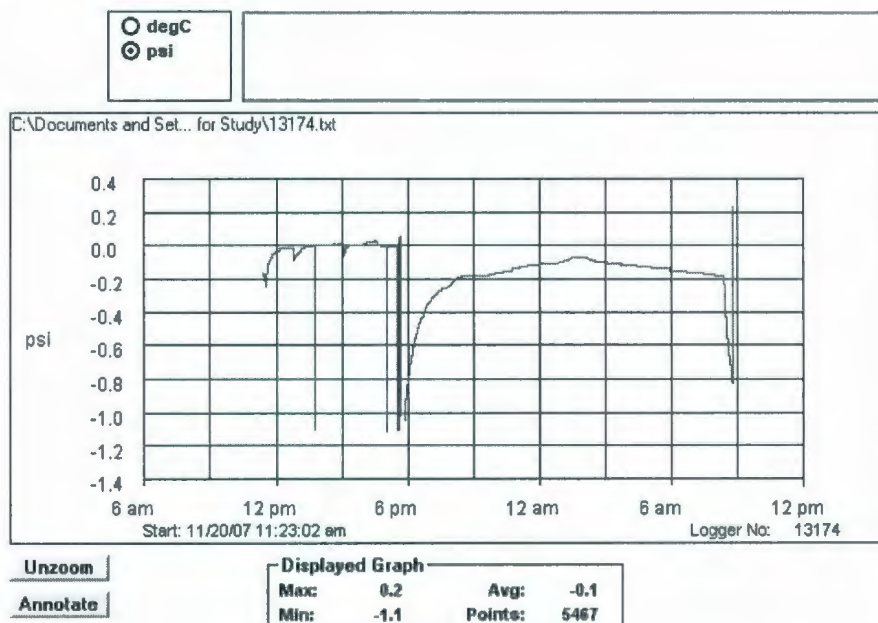


Figure 3.6 Pressure Chart of Tag with scale change

One can see that the temperature reached a maximum of 27°C during day and a minimum of 1.7°C at night, whereas the pressure stayed around zero (absolute pressure) all the time.

This test shows the significance of recorded data in terms of;

- Mission life
- Performance and accuracy of pressure and temperature sensors
- Failure of each sensor. This is not evident from this test as tag did not fail during the test. If any of the sensors had failed during the mission life it could be seen here recorded as flat line.

After understanding about the operation of product and data presentation, failure data was analyzed to establish different failure modes.

3.3 Failure Data Analysis

Hazard rate plotting method is used to determine the probability distribution that best describes the failure process. This is a powerful graphical approach to perform failure data analysis. The method is popular because of its advantages such as;

- Fits the data to a straight line
- Results obtained through plotting are convincing
- Easy to understand
- Straight forward to visualize the theoretical distribution that fits the field data

The complete observations may be described as data in which the times to failure of all units of a sample are known. On the other hand, when the running times of unfailed units and the failure times of failed units are given, the data are called incomplete or “Censored data”. In turn, the running times of unfailed units are called the “Censoring times”.

In the event of having different censoring times of the unfailed units, the data is known as “Multi-censored data”. In contrast, when the censoring times of all the unfailed units are

the same and greater than the failed units failure times, the data are said to be “Singly censored”. Nonetheless, the multi-censored data occur due to factors such as follows;

- Removing items/units or terminating their use prior to their failure
- Some extraneous causes were responsible for the units/items failure
- Collecting data from active units/items

Censoring was used to filter out the tags that did not fail and can be seen in Appendix 2.

3.4 Hazard Rate Plotting

Hazard rate is defined by Equation 3-1 and 3-2;

$$\lambda(t) = \frac{f(t)}{R(t)} \quad (3-1)$$

$$\lambda(t) = \frac{f(t)}{1 - F(t)} \quad (3-2)$$

Where;

$\lambda(t)$ = hazard rate or instantaneous failure rate

$R(t)$ = reliability at time t

$f(t)$ = probability density function (PDF)

$F(t)$ = cumulative distribution function (CDF)

Weibull distribution consists of a family of distributions which can be used to describe a wide range of failure data. The Weibull density function is defined by Equation 3-3;

$$R(t) = e^{-\left(\frac{t}{\theta}\right)^\beta} \quad (3-3)$$

For $t \geq 0$

Where;

R = reliability of system at given time, t

t = time

β = shape parameter

θ = scale parameter (characteristic life)

The Exponential and the Raleigh distributions are two of the many special distributions that can be obtained from the Weibull distributions by changing the value of the shape parameter, β . An Exponential distribution is obtained by setting the shape parameter to 1, while a Raleigh distribution is obtained by setting the shape parameter to 2.

The failure and reliability functions are related by;

$$F(t) = 1 - R(t) \quad (3-4)$$

By substituting equation 3-3 into 3-4, we get;

$$F(t) = 1 - e^{-\left(\frac{t}{\theta}\right)^\beta} \quad (3-5)$$

Rearranging and applying natural log on both sides;

$$\ln\{1 - F(t)\} = -\left(\frac{t}{\theta}\right)^\beta \quad (3-6)$$

Taking natural log again,

$$\ln \ln \left\{ \frac{1}{1 - F(t)} \right\} = \beta \ln t - \beta \ln \theta \quad (3-7)$$

Comparing this with the general equation describing a straight line,

$$Y = mx + c \quad (3-8)$$

Where,

$$Y = \ln \ln \left\{ \frac{1}{1 - F(t)} \right\}$$

$$X = \ln t$$

One can also plot a graph between $\ln \ln[1/(1-F(t))]$ and $\ln(t)$.

To determine the statistical distribution fit to the given data and estimate the values for its parameters by using the hazard plotting steps is described below:

3.4.1 Plotting Steps

The following 8 steps are used to construct a hazard plot;

1. Ordering the data containing "t" times from smallest to largest without making any distinction whether these data are running (censoring) or failure times of units. A separate column adjacent to the times is showing the status of the tags for identification.
2. Labeling the ordered times with reverse ranks.

3. Computing hazard value for each failure using 1/reverse rank. The hazard value may be described as the conditional probability of failure time. In other words, it is the observed instantaneous failure rate at a certain failure time.
4. Obtaining the cumulative hazard value for each failure by adding its hazard value to the cumulative hazard value of the preceding failure.
5. Choosing a statistical distribution, in this case Weibull, and prepare times to failure and corresponding cumulative hazard data for use in the selected distribution to construct a hazard plot.
6. Excel is used to calculate values and plot charts. Even though the running times are not plotted, they do determine the plotting points of the times to failure through the reverse ranks.
7. Determining if the plotted data points roughly follow a straight line. If they do, it is reasonable to conclude that the selected distribution adequately fits the data and draw a best fit straight line.
8. Estimating the values of the distribution parameters using the hazard plot. For example; for Weibull distribution values of θ and β can be calculated.

Following the steps mentioned above, a graph is plotted for the complete failure data as shown below in Figure 3.7.

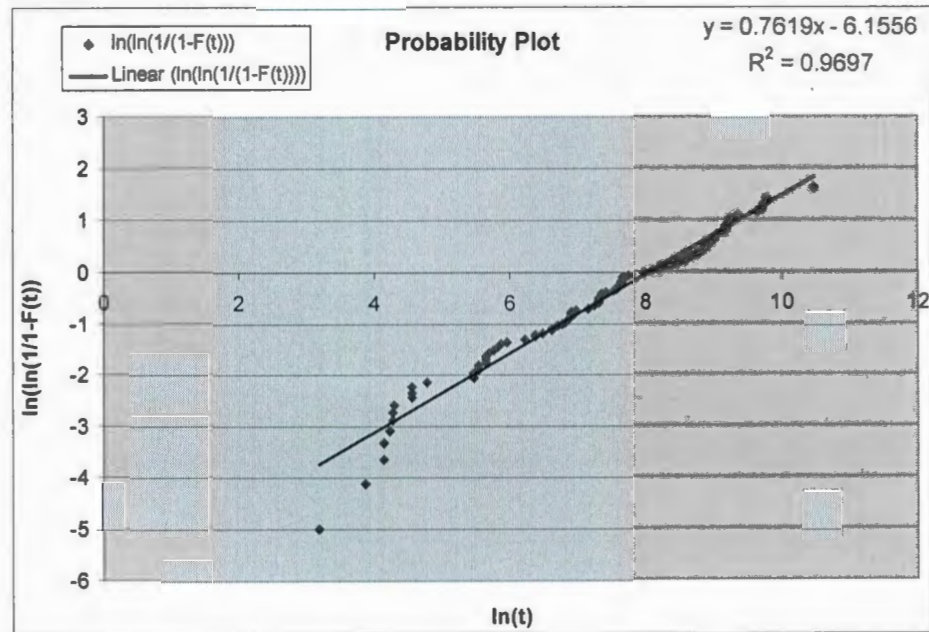


Figure 3.7 Full data (regardless of failure mode)

Considering equation 3-7 and comparing with the equation of the straight line, equation 3-8, from graph, we can see that;

$$\text{Slope} = m = \beta = 0.7619$$

$$\theta = e^{-\frac{y}{\beta}} = e^{-\left(\frac{-6.1556}{0.7619}\right)} = 3225.89 \text{ hours} \quad (3-9)$$

Where,

$$Y = y \text{ and intercept} = C$$

Similarly, MTTF for Weibull distribution can be calculated using Equation 3-10;

$$MTTF = \theta \cdot \Gamma \left(1 + \frac{1}{\beta} \right) \quad (3-10)$$

Inserting the values of θ and β from the graph and determining the value of Γ from the tables, we get;

$$MTTF = 3225.89 \cdot \Gamma \left(1 + \frac{1}{0.7619} \right)$$

$$MTTF = 6711.77 \cdot \Gamma(2.317)$$

$$MTTF = 3786.45 \text{ HOURS}$$

$$MTTF = 0.43 \text{ YEARS}$$

We can see that the distribution is showing decaying hazard rate, $\lambda(t)$, which is the infant mortality part of the bathtub curve as shown in Figure 3.8.

$0 < \beta < 1 = 0.76 =$ exponentially decreasing function, describes infant mortality

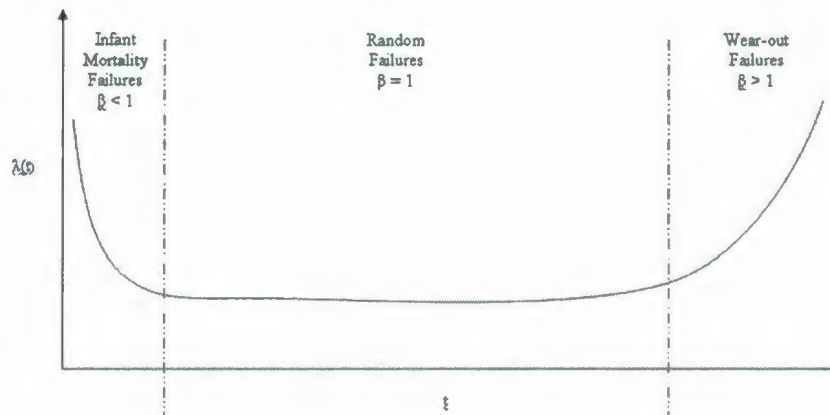


Figure 3.8 Bathtub Curve

After analyzing the complete failure data, it is broken down into different failure modes by first defining the failure criteria. Definitions of failures are as described below;

1. **Power failure:** when tag stops working < 2 years in mission life due to no power from battery.
2. **Packaging failure:** when single or multiple components on the circuit board stops working due to presence of water.
3. **Communications failure:** when photodiode stops working and data cannot be downloaded from the tag. Means, only component failure and all the other components are functioning normally.
4. **Pressure sensor failure:** when pressure sensor stops working and no data is recorded. Means, only component failure and all the other components are functioning normally.

5. **Temperature sensor failure:** when temperature sensor stops working and no data is recorded. Means, only component failure and all the other components are functioning normally.

Pareto chart, Figure 3.9, shows all failure modes and their contribution.

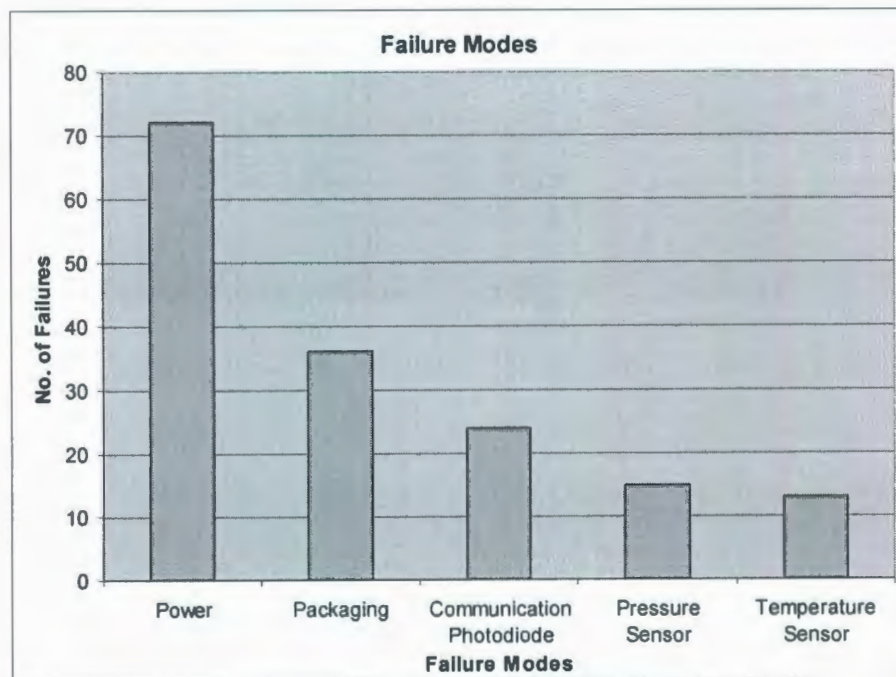


Figure 3.9 Failure modes Pareto chart

Weibull analysis of each failure mode is separately done in following sections.

3.5 Failure Mode 1: Power Failure

Figure 3.10 shows the data distribution for power failure.

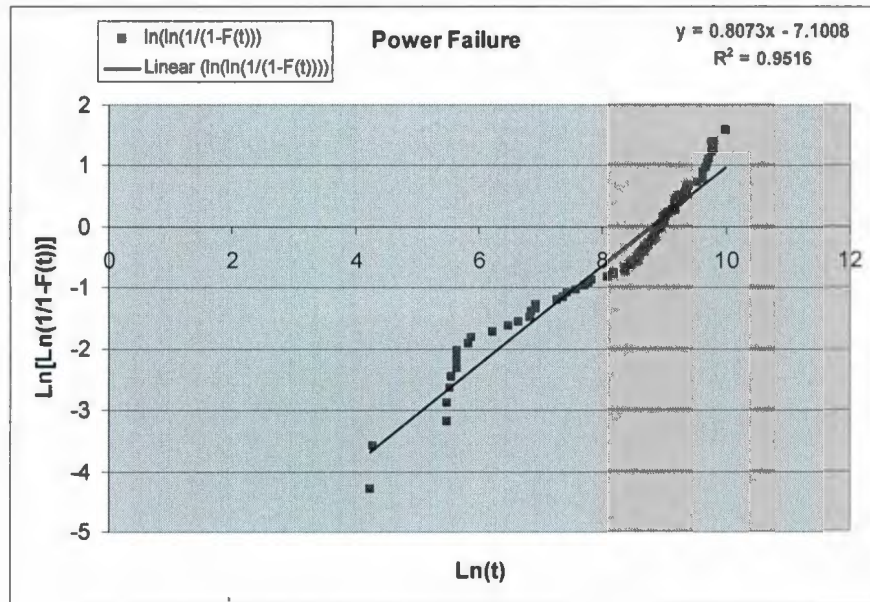


Figure 3.10 Hazard plot of power failure data

Similarly using Equations 3-9 and 3-10,

$$\text{slope}(m) = \beta = 0.8073$$

$$\theta = e^{-\frac{y}{\beta}} = e^{-\left(\frac{-7.1008}{0.8073}\right)} = 6606.03 \text{ hours}$$

$$\text{MTTF} = 0.8 \text{ years}$$

$0 < \beta < 1 = 0.80 =$ exponentially decreasing function, describes infant mortality

3.6 Failure Mode 2: Packaging Failure

Figure 3.11 shows the data distribution for packaging failure.

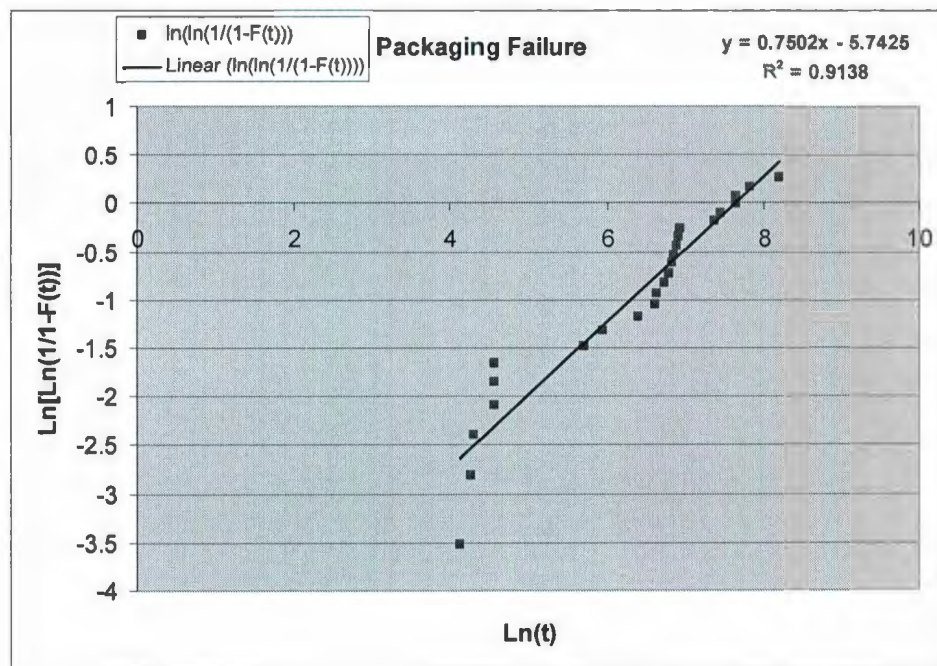


Figure 3.11 Hazard plot of packaging failure data

Applying equations 3-9 and 3-10, we get;

$$\text{slope}(m) = \beta = 0.7502$$

$$\theta = e^{-\frac{\gamma}{\beta}} = e^{-\left(\frac{-5.7425}{0.7502}\right)} = 2110.3 \text{ hours}$$

$$\text{MTTF} = 0.28 \text{ years}$$

$0 < \beta < 1 = 0.75$ = exponentially decreasing function, describes infant mortality

3.7 Failure Mode 3: Communications Failure

Figure 3.12 shows the data distribution for communications failure.

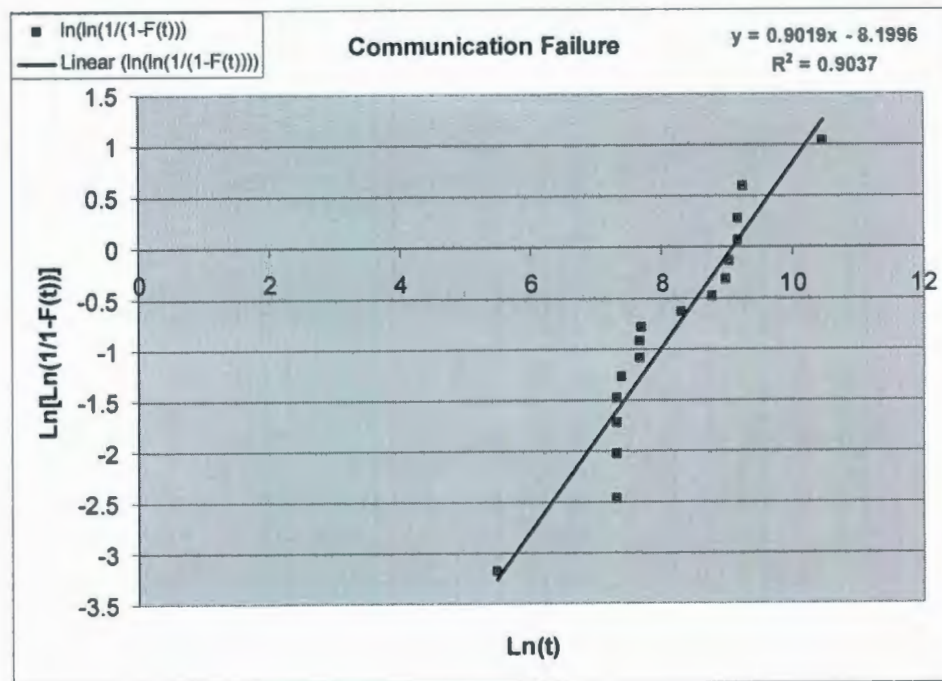


Figure 3.12 Hazard plot of communications failure data

Using Equations 3-9 and 3-10, we get;

$$\text{slope}(m) = \beta = 0.9019$$

$$\theta = e^{-\frac{y}{\beta}} = e^{-\left(\frac{-8.1996}{0.9019}\right)} = 8879.26 \text{ hours}$$

MTTF = 1 year

$0 < \beta < 1 = 0.90$ = exponentially decreasing function, describes infant mortality

3.8 Failure Mode 4: Pressure Sensor Failure

Figure 3.13 shows the data distribution for pressure sensor failure.

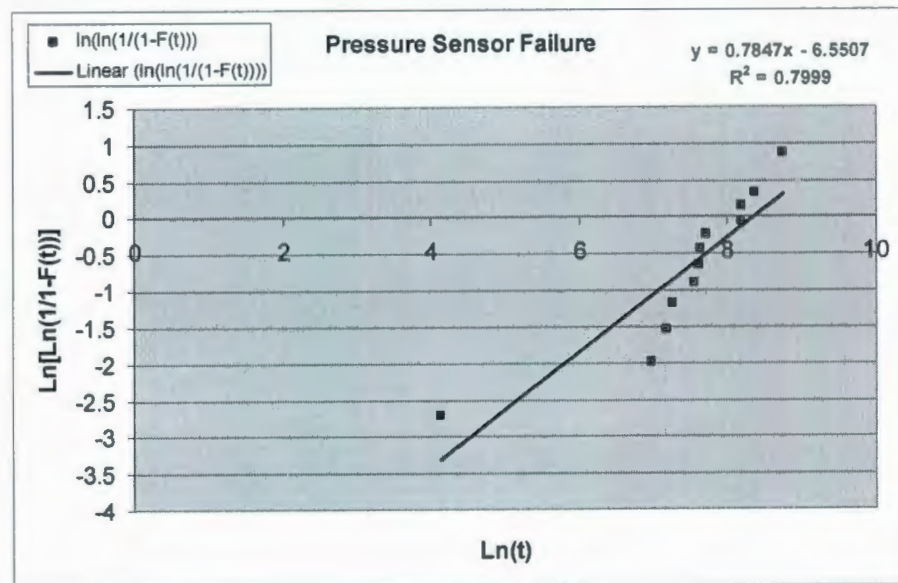


Figure 3.13 Hazard plot of pressure sensor failure data

Using equations 3-9 and 3-10;

$$\text{slope}(m) = \beta = 0.7847$$

$$\theta = e^{-\frac{y}{\beta}} = e^{-\left(\frac{-6.5507}{0.7847}\right)} = 4221.36 \text{ hours}$$

$$\text{MTTF} = 0.5 \text{ years}$$

$0 < \beta < 1 = 0.78 =$ exponentially decreasing function, describes infant mortality

3.9 Failure Mode 5: Temperature Sensor Failure

Figure 3.14 shows the data distribution for temperature sensor failure.

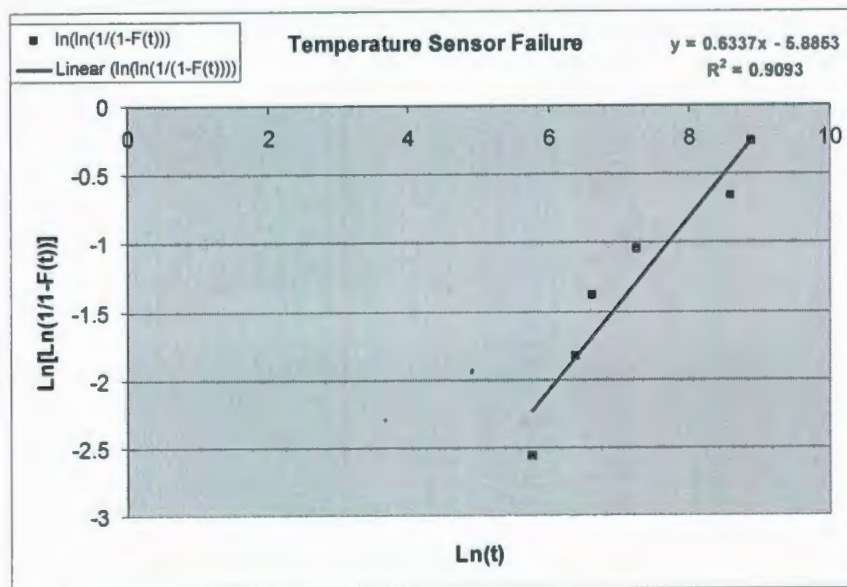


Figure 3.14 Hazard plot of temperature failure data

Again, applying Equations 3-9 and 3-10, we get;

$$\text{slope}(m) = \beta = 0.6337$$

$$\theta = e^{-\frac{1}{\beta}} = e^{-\left(\frac{-5.8853}{0.6337}\right)} = 10793.92 \text{ hours}$$

$$\text{MTTF} = 1.7 \text{ years}$$

$0 < \beta < 1 = 0.63 =$ exponentially decreasing function, describes infant mortality

3.10 Fault Tree Analysis

FTA can be simply described as an analytical technique, in which an undesired state of the system is specified, usually events that result in failure. The system is then analyzed to find all realistic ways in which the undesired event (top event) can occur. The fault tree itself is a graphic model of the various parallel and sequential combinations of faults that will result in the occurrence of the predefined undesired event. The faults can be events that are associated with component hardware failures, human errors, software errors, or any other pertinent events which can lead to the undesired event. A fault tree thus depicts the logical interrelationships of basic events that lead to the undesired event, the top event of the fault tree.

FTA is a deductive, failure-based approach. In determining the causes, a fault tree is constructed as a logical illustration of the events and their relationships that are necessary and sufficient to result in the undesired event, or top event.

In the previous section failure data obtained from field was analyzed and the following failure modes were noted;

1. Temperature sensor failure
2. Pressure sensor failure
3. Communications failure
4. Power failure

In this section a Fault Tree Analysis will be conducted to further investigate the root cause of these failures. Each mode of failure is plotted to show root cause of the failure and the probability of each component failure is looked upon to determine the root-cause of the failure.

Before fault tree analysis of the above mentioned failure modes are conducted it is important to understand the block diagram of the whole circuit so that relationship between components can be seen, which will help in creating and understanding the fault tree diagrams. Following Figure 3.15 shows the block diagram of the data recorder that is under study;

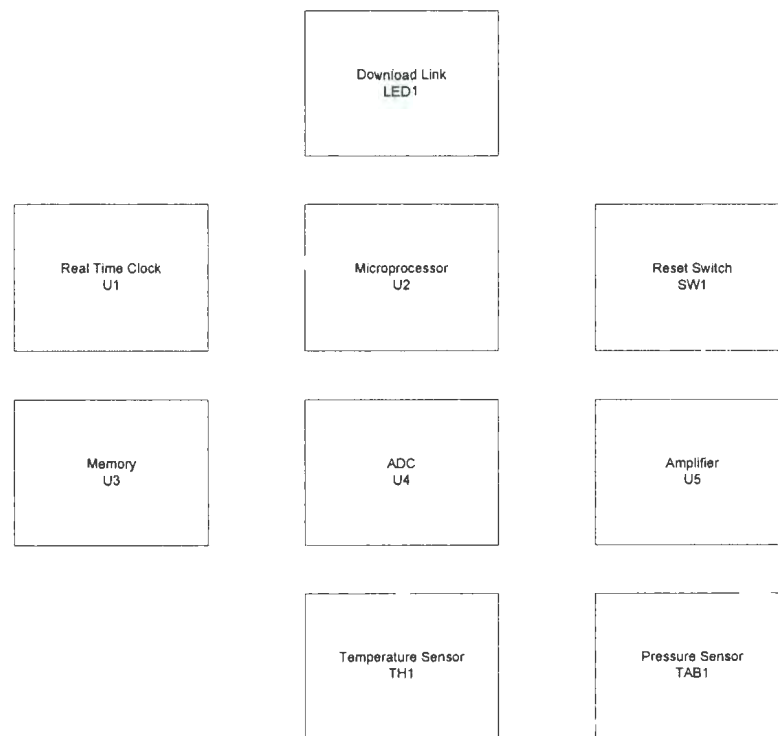


Figure 3.15 Block Diagram of Data Recorder Tag

The DC power is supplied to the microprocessor (U2) which runs the embedded firmware to control the rest of the circuitry.

Using MIL-HDBK-217F, failure rates of each component was calculated and corresponding failure probability values were determined for Fault Tree Analysis. The values are shown in the following Table 3.2;

Table 3.2 Failure rates of components

Description	Ref. Designator	Failure Rate/10 ⁶ Hrs	Quantity Used	Total Failure Rate/10 ⁶ Hrs	R(t) = exp(-λt)	F(t) = 1-R(t)
Diode KA3020SRC	LED1	0.011664	1	0.011664	0.999693517	0.000306483
Crystal Tuning Fork 32.768Hz	X1	0.12432	1	0.12432	0.996738202	0.003261798
RTC PCF8563TS	U1	0.0416	1	0.0416	0.998907349	0.001092651
MICRO PIC12LC509A-04I/SN	U2	0.208	1	0.208	0.994548673	0.005451327
EPROM 24LC515-I/SM	U3	2.02	1	2.02	0.948298835	0.051701165
CONV MCP3202-CI/ST	U4	0.0372	1	0.0372	0.999022862	0.000977138
AMP LMV358MM	U5	0.1256	1	0.1256	0.996704674	0.003295326
Trans UN9214	Q1	1.75E-03	1	0.00175	0.999954011	4.59889E-05
CAP CER 1.0uF 16V 0603	C1	2.31E-03	1	0.00231	0.999939295	6.0705E-05
CAP CER 22pF NPO 0603 5% 50V	C2	0.013	1	0.013	0.999658418	0.000341582
CAP CER 220pF NPO 0603 5% 50V	C3	0.024	1	0.024	0.999369479	0.000630521
CAP CER 1000pF X7R 0603 10% 50	C4	0.029	1	0.029	0.99923817	0.00076183
CAP CER 1.0uF 16V 0603	C5	2.98E-03	1	0.00298	0.999921689	7.83113E-05
CAP CER 0.01uF X7R 0603 10%50V	C6	1.79E-03	1	0.00179	0.99995296	4.70401E-05
CAP Tantalum 220uF 6V C-Case	C7	0.078	1	0.078	0.997952259	0.002047741
Resistor 100Kohm 1% 0603	R3,R9,R10,R11, R13	8.62E-03	5	0.0431	0.999773492	0.000226508
Resistor 10Kohm 1% 0603	R2,R8,R15	7.84E-03	3	0.02352	0.999793986	0.000206014
Resistor 15Kohm 1% 0603	R5	7.84E-03	1	0.00784	0.999793986	0.000206014
Resistor 43Kohm 5% 0603	R7	7.84E-03	1	0.00784	0.999793986	0.000206014
Resistor 18K2ohm 1% 0603	R14	7.84E-03	1	0.00784	0.999793986	0.000206014
Resistor 15Mohm 5% 0603	R6	0.0196	1	0.0196	0.999485045	0.000514955
Resistor 0ohm 5% 0603	R18	7.84E-03	1	0.00784	0.999793986	0.000206014
Sensor NTC Thermistor	TH1	0.441	1	0.441	0.988477419	0.011522581
PCB LTD1100 Version 2	PCB	0.0323	1	0.0323	0.999151516	0.000848484
SWITCH REED SPST 10-15AT	SW1	10.2	1	10.2	0.764864947	0.235135053
TAB1	TAB	0.038	1	0.038	0.999001858	0.000998142
Battery	BATT	0.003886	1	0.003886	0.999897881	0.000102119
Packaging	PK1	0.6	1	0.6	0.984355664	0.015644336
Soldering	Slid	0.0002	1	0.0002	0.999994744	5.25599E-06

Total Failure Rate of System (λ_{sys}) = 14.1 failures/10⁶ hours
MTTF ($1/\lambda_{sys}$) = 70651 hours (8 years)
System Reliability R(t) = exp(-λt) 68.9% for 3 years
78% for 2 years
88.3% for 1 year

Fault Tree Analysis of failure modes are as follows;

3.10.1 Temperature Sensor Failure

This is mode of failure where only temperature sensor is failed and other parts of the circuit are working normally. This behavior is noticed when recorded data is plotted in post-processing software. When temperature sensor or temperature sensing circuitry stopped responding, a flat line is observed throughout the recorded data which is an indication of failed sensor reading.

The fault Tree of such failure event is as follows in Figure 3.16;

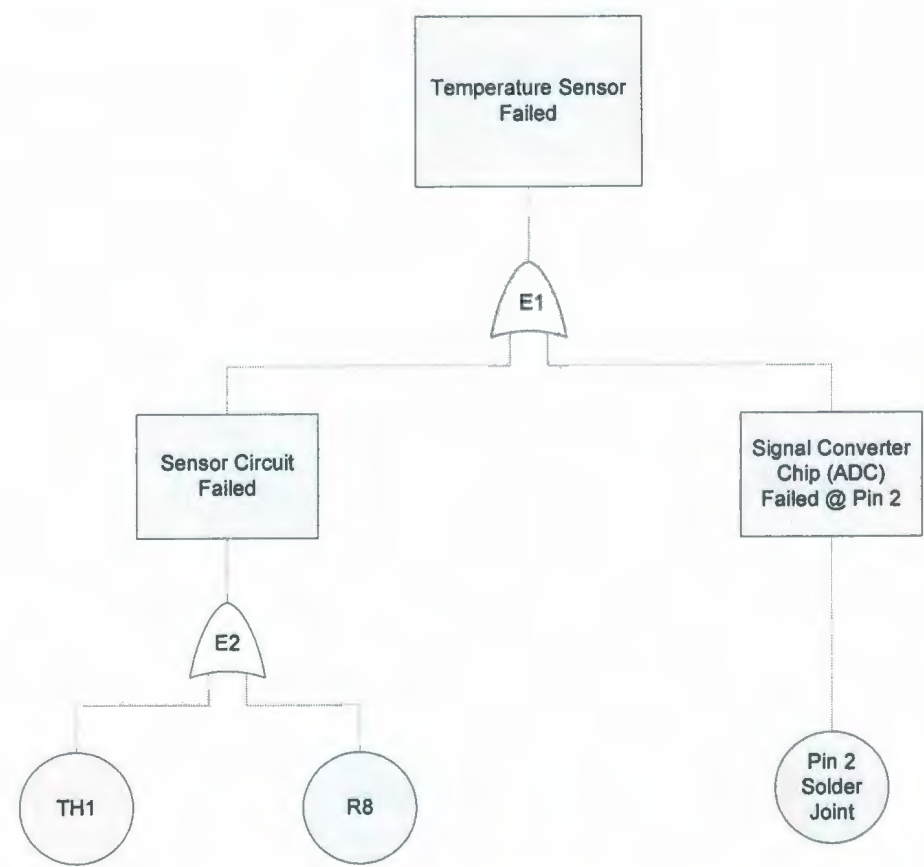


Figure 3.16 FTA for Temperature Failure

The analysis of the tree is conducted by expressing the top event as a Boolean algebraic equivalent of the tree itself. The top event “E1” is the union of 02 combinations, (intersections) of basic events, E2 and Pin 2.

$$E1 = E2 + \text{Pin 2}$$

$$E1 = \text{TH1} + \text{R8} + \text{Pin 2}$$

The failure rate (λ) of each component involved is used to calculate the Reliability (R) of each component, which is then subtracted from 1 to obtain the failure probability (P) of that particular component.

For above failure event,

$$\begin{aligned} P(\text{temperature sensor failing}) &= P(E2) + P(\text{Pin 2}) \\ &= P(\text{TH1}) + P(\text{R8}) + P(\text{Pin 2}) \end{aligned}$$

Inserting the values of from table 1, we get;

$$P(E1) = 0.011522581 + 0.000206014 + 5.25599\text{E-}06 = 0.01173385 = 1.1\%$$

The relative importance of each component can be obtained by taking the ratio of the individual value of failure of probability to the total system probability, P(E1).

Table 3.3 Component importance for temperature circuit

Component	Importance
TH1	98.24%
R8	1.75%
Pin 2	< 0.01 %

3.10.2 Pressure Sensor Failure

This mode of failure is described as when only pressure readings are not obtained due to pressure sensor circuitry failure, which also includes, amplifier and signal converter. This phenomenon is also observed, as temperature sensor failure, as flat line showing an infinite value of pressure in the data.

The fault tree of such failure event is shown in Figure 3.17;

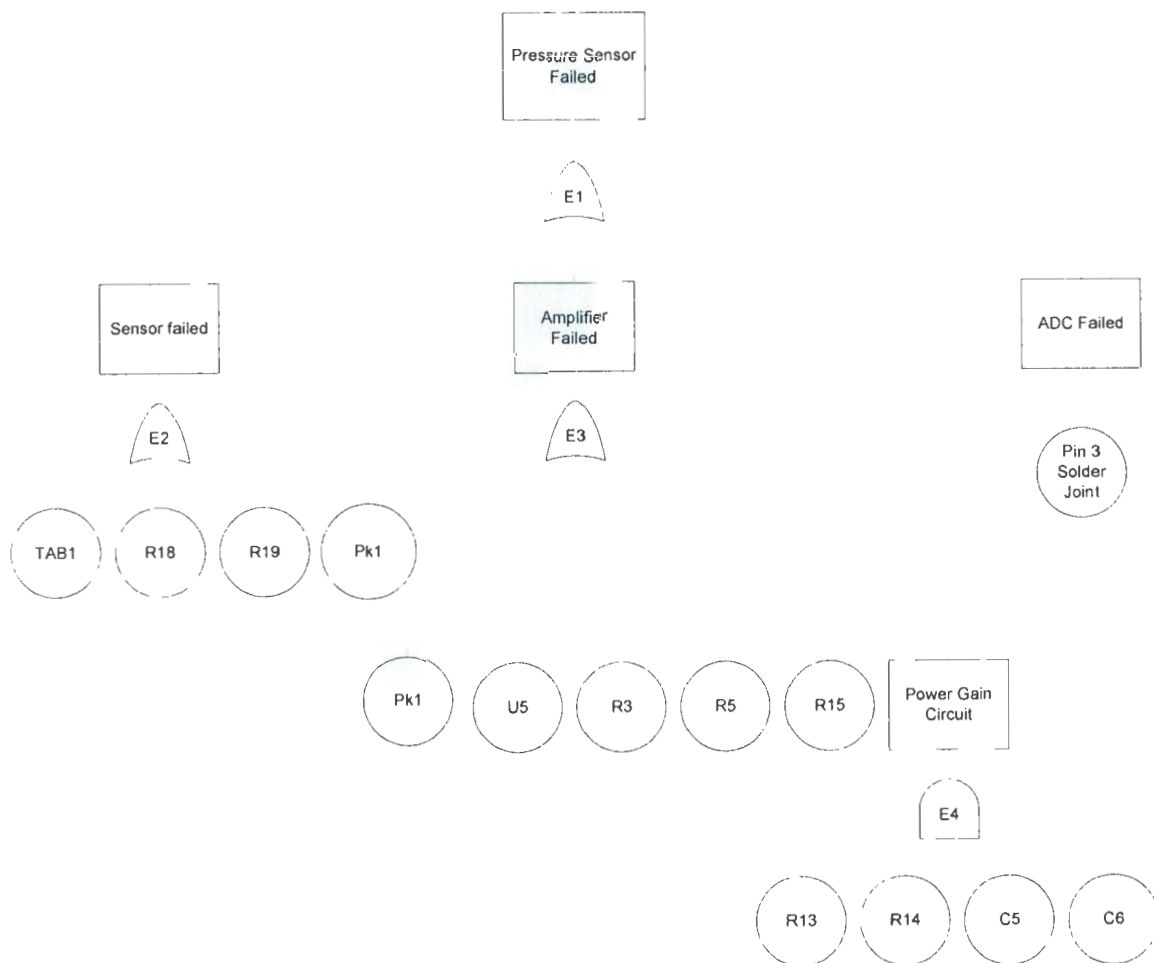


Figure 3.17 FTA of Pressure sensing failure

Again using same concepts as applied previously;

$$E1 = E2 + E3 + \text{Pin 3}$$

$$E1 = \text{TAB1} + \text{R18} + \text{R19} + \text{PK1} + \text{PK1} + \text{U5} + \text{R3} + \text{R5} + \text{R15} + \text{E4} + \text{Pin 3}$$

$$E1 = \text{TAB1} + \text{R18} + \text{R19} + \text{PK1} + \text{PK1} + \text{U5} + \text{R3} + \text{R5} + \text{R15} + (\text{R13} * \text{R14} * \text{C5} * \text{C6})$$

$$+ \text{Pin 3}$$

Or can be expressed in terms of probability of failures, as;

$$P(E1) = P(TAB1) + P(R18) + P(R19) + P(PK1) + P(PK1) + P(U5) + P(R3) + P(R5) + P(R15) + [P(R13)*P(R14)*P(C5)*P(C6)] + P(\text{Pin } 3)$$

Therefore,

$$P(E1) = 0.03643 = 3.64\%$$

The relative importance of each component can be obtained by taking the ratio of the individual value of failure of probability to the total system probability, P(E1).

Table 3.4 Component importance for pressure sensor circuit

Component	Importance
TAB1	19.42%
R18	0.4%
U5	34.13%
R3	0.4%
R5	0.4%
R15	0.4%
R13	0.4%
R14	0.4%
C5	0.2%
C6	0.91%
PK1	42.84%
Pin 3	< 0.01%

3.10.3 Communications Failure

This mode of failure results in no communication with the data recorder when an attempt is made to download recorded data. Fault tree for such a failure event is plotted and shown in Figure 3.18.

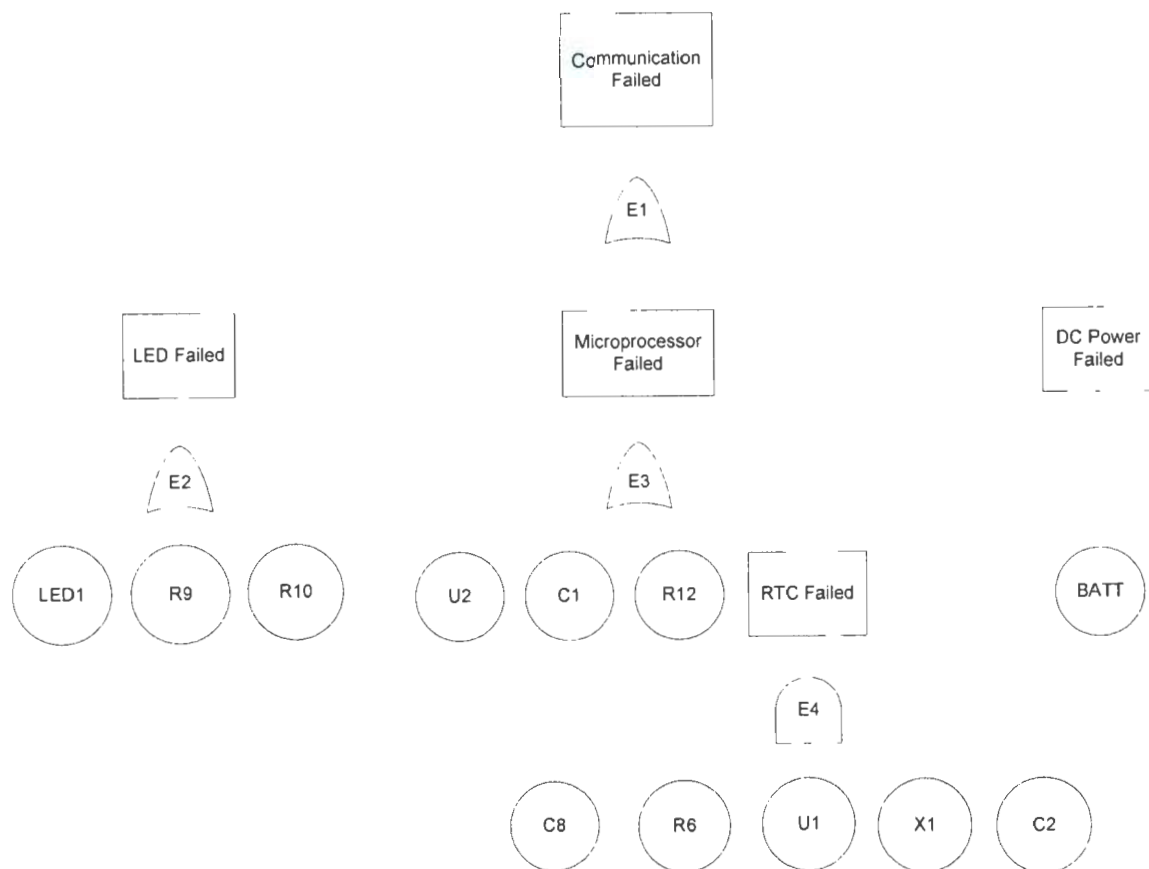


Figure 3.18 FTA for communications failure

$$E1 = E2 + E3 + BATT$$

$$E1 = LED1 + R9 + R10 + U2 + C1 + R12 + E4 + BATT$$

$$E1 = LED1 + R9 + R10 + U2 + C1 + R12 + (C8 * R6 * U1 * X1 * C2) + BATT$$

Hence,

Therefore,

$$P(E1) = 0.006579664 = 0.65\%$$

The significance of each component can be analyzed by considering the ratio of $P(E1)$ to individual failure probability, as shown below in Table 3.5;

Table 3.5 Component importance for communication circuit

Component	Significance
LED1	1.65%
R9	0.44%
R10	0.44%
U2	42.85%
C1	1.8%
R12	0.44%
BATT	1.55%
C8	0.71%
R6	7.82%
U1	10.60%
X1	29.57%
C2	2.13%

3.10.4 Power Failure

This mode of failure occurs when the total power of the system is failed. The fault tree for such failure event is described below in Figure 3.19;

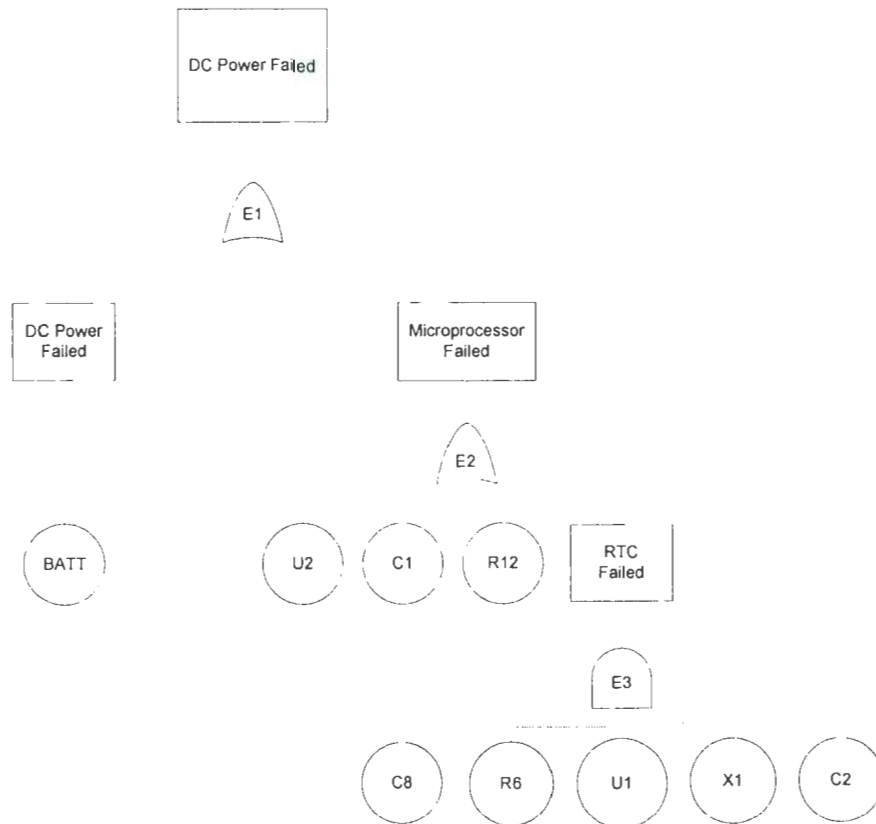


Figure 3.19 FTA for Battery failure

$$E1 = \text{BATT} + E2 = \text{BATT} + U2 + C1 + R12 + E3$$

$$E1 = \text{BATT} + U2 + C1 + R12 + (C8 * R6 * U1 * X1 * C2)$$

By inserting the values of probability of failure for each component, we get;

Hence,

$$P(E1) = 0.005320166 = 0.53\%$$

The significance of each component can be analyzed by considering the ratio of $P(E1)$ to individual failure probability, as shown below in Table 3.6;

Table 3.6 Component importance for power circuit

Component	Significance
BATT	1.91%
U2	55.27%
C1	1.14%
R12	3.87%
C8	0.88%
R6	9.67%
U1	10.53%
X1	10.31%
C2	6.42%

3.11 Conclusion

Summarizing the results from hazard plots in Table 3.7;

Table 3.7 Summary of Hazard plots

Data Set	Shape Parameter	Scale Parameter	Result
All failures combined	$\beta = 0.76$	$\theta = 3225$	Infant Mortality
Power failure	$\beta = 0.80$	$\theta = 6606$	Infant Mortality
Packaging failure	$\beta = 0.75$	$\theta = 2110$	Infant Mortality
Communication failure	$\beta = 0.90$	$\theta = 8879$	Infant Mortality
Pressure failure	$\beta = 0.78$	$\theta = 4221$	Infant Mortality
Temperature failure	$\beta = 0.63$	$\theta = 10793$	Infant Mortality

A summary of the results obtained for the analysis of failure data is given in Table 3.7.

These results show that the magnitude of the shape factor for the individual failure modes, as well as for the complete set of data is less than unity. This indicates that the tags failed in the “infant mortality” mode. This means that a better quality control system may actually reduce the failure rate of these tags and increase their service life. Reasons

for failure in the different modes need to be explored in detail and manufacturing and assembly defects need to be eliminated before the deployment of these tags.

In next chapter these failure modes will be looked upon in greater detail for determination of root cause of early life failures.

Chapter 4

Failure Mode Analysis: Power Failure

4.1 Introduction

The power failures are defined as system failure when tag stops working less than 2 years in its mission life due to no power from battery. This phenomenon is due to rapid discharge of battery. Rapid discharge of battery is due to excess current drawn from battery which can happen due to presence of additional unspecified resistance in parallel to the already present resistance resulting in lower resultant resistance causing battery to discharge rapidly. Probable causes of rapid discharge of battery are;

1. Excess current drawn by component(s) on circuit board
2. Operating or storing at extreme temperatures

A bottom-up approach is used to investigate the above probable failure causes. Starting with the battery, the battery type (chemistry), capacity and nominal life at different temperature conditions were experimentally investigated.

In next sections of this chapter all the experiments conducted on the battery and the methods of analysis applied to the experimental results are described. This leads to the conclusion that the battery type and capacity are well suited for the intended application.

4.2 Battery Type and Specification

The batteries under investigation are Lithium coin cells, in particular Lithium Manganese dioxide (LiMnO_2), as shown in Figure 4.1.

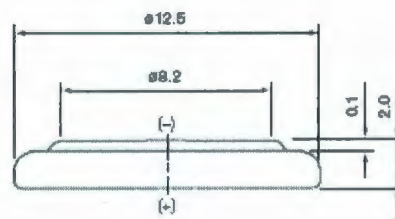


Figure 4.1 Dimensions of battery

Lithium batteries are primary batteries that have lithium metal or lithium compounds as an anode. Depending on the design and chemical compounds used, lithium cells can produce voltages from 1.5 V to about 3.0 V. Lithium batteries find application in many long-life critical devices such as artificial pacemakers and other implantable electronic medical devices. The specifications of the battery used in the data-recorder tags are shown in Table 4.2 below.

Table 4.1 Battery specifications

Nominal Voltage (V)	3.0
Nominal Capacity (mAh)	36
Nominal Discharge Current (mA)	0.1
Temperature Ranges (°C)	-20 to +85
Weight (grams)	0.8
Dimensions (mm)	Positive Cap Diameter: 12.5 Negative Cap Diameter: 8.2 Height: 2.0

4.3 Battery Lifetime Analysis

Two thin metal strips were welded to the positive and negative battery poles. This facilitated the attachment to the pads on the printed circuit board, known as “tabbed” cells, Figure 4.2. Heat generated during the welding process has a potential to burn some electrolyte in the cell and may consequently reduce the capacity of the cell.

An experiment was conducted to evaluate and compare the capacities of both virgin and tabbed cells at room temperature. Another experiment was conducted to compare tabbed cells at +25°C and at -16°C to determine the change in the capacity as a function of environmental temperatures.

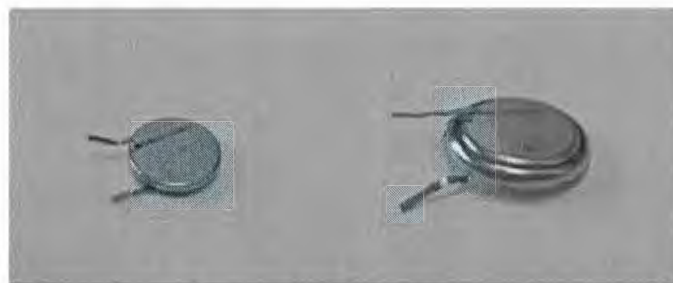


Figure 4.2 Tabbed battery

4.4 Experiment 1: Battery Lifetime in Continuous Drain Condition at +25°C

Cells were connected to an $18\text{k}\Omega$ resistor, as shown in Figure 4.3 and left at room temperature, $+25^\circ\text{C}$, to discharge. Periodic voltage readings were taken using digital multimeter till the battery voltage reached 1.99V which is the cutoff voltage for these batteries. The usable life of a battery is defined as the time it takes for its voltage to reach a level just under 2.00V .



Figure 4.3 Tabbed and virgin cells under continuous drain

Table 4.2 shows the results of continuous drain test at +25°C both for virgin and tabbed cells.

Table 4.2 Battery Lifetime experiment results of virgin and tabbed cells under continuous drain at +25°C

Component	Hours		Status
	Virgin	Tabbed	
Cell 1	263.5	259.0	Failed
Cell 2	254.5	254.0	Failed
Cell 3	252.5	251.5	Failed
Cell 4	264.0	262.5	Failed
Cell 5	261.5	261.0	Failed
Cell 6	261.0	258.0	Failed
Cell 7	257.0	247.5	Failed
Cell 8	260.0	261.0	Failed

Cell 9	278.5	262.5	Failed
Cell 10	250.0	254.0	Failed
Cell 11	256.5	250.5	Failed
Cell 12	254.0	251.0	Failed
Cell 13	253.5	261.5	Failed
Cell 14	261.0	253.5	Failed
Cell 15	260.5	272.5	Failed
Total =	3888.0	3860.0	15
Failure Rate (λ=Total cells/total hours) =	0.003858025	0.00389	
MTTF (hours) =	259.2	257.333	
Reliability =	0.99993241	0.99993	
Standard Deviation =	6.821185486	6.46603	
Coefficient of Variation =	2.62%	2.51%	
Standard Error =	3.101904762	2.7873	
Average Life (mAh) =	40.6	40.3	

4.5 Experiment 2: Battery Lifetime in Continuous Drain Condition at -16°C

The second experiment was conducted at -16°C by placing a number of tabbed cells in the freezer, under the same load of 18kΩ. A digital multi-meter was used to measure the voltage of the cells periodically. A voltage of magnitude 2.0V was used as a cutoff target. Figures 4.4 and 4.5 show the experimental setup.



Figure 4.4 Experimental setup of battery lifetime for tabbed cells at -16°C under continuous load of $18\text{k}\Omega$



Figure 4.5 Tabbed cells under continuous load at -16°C

Note that Figure 4.5 shows that although moisture appears to form on the cells but no rapid discharge was noticed on the recorded data.

Results of the continuous load test at -16°C are shown in Table 4.3

Table 4-3 Battery lifetime experiment results for tabbed cells under continuous load conditions at -16°C

Time	Cell 1	Cell 2	Cell 3	Cell 4	Cell 5
0	3.21	3.24	3.23	3.27	3.23
0:43:00	2.76	2.75	2.78	2.77	2.69
2:00:00	2.59	2.54	2.67	2.71	2.67
2:47:00	2.55	2.57	2.63	2.67	2.64
3:47:00	2.68	2.7	2.74	2.76	2.74
4:47:00	2.6	2.59	2.65	2.67	2.66
5:47:00	2.57	2.58	2.64	2.65	2.64
21:39:00	2.5	2.51	2.57	2.58	2.57
22:54:00	2.5	2.53	2.59	2.6	2.58
24:24:00	2.54	2.59	2.63	2.63	2.61
29:54:00	2.45	2.49	2.53	2.55	2.52
46:27:00	2.46	2.49	2.53	2.6	2.53
52:59:00	2.48	2.51	2.55	2.55	2.53
69:59:00	2.5	2.52	2.57	2.57	2.56
142:04:00	2.35	2.25	2.45	2.46	2.32
166:04:00	2.1	2.09	2.25	2.27	2.28
190:09:00	2.22	2.22	2.37	2.4	2.34
194:42:00	2.2	2.14	2.3	2.31	2.28
214:04:00	1.98	1.93	2.1	2.12	2.11
216:00:00	1.65	1.88	1.97	2.12	2.16
217:00:00	1.61	1.84	1.96	1.98	1.99

Total Discharge Hours =	1056
Failure Rate (λ) =	0.004734
MTTF (hours) =	211
Reliability =	0.9997
Standard Deviation =	7.3
Coefficient of Variation =	3.5%
Standard Error =	10.74

4.5.1 Results

Comparison between the battery life of the virgin and tabbed cells at +25°C and -16°C are shown in Table 4.4. It can be seen that tabbing reduces the MTTF by about 3.0 hours, while at a temperature of -16°C the reduction in MTTF reaches 48 hours.

Table 4.4 Battery lifetime results for virgin and tabbed cells

	Virgin +25°C (n=15)	Tabbed +25°C (n=15)	Tabbed -16°C (n=5)
Failure Rate (λ) =	0.003	0.003	0.004
MTTF (hours) =	259	257	211
Reliability =	0.999	0.999	0.999
Standard Deviation =	6.8	6.4	7.3
Coefficient of Variation =	2.6%	2.5%	3.5%
Standard Error =	3.10	2.79	10.74

The data obtained from both experiments can be compiled as shown in Table 4.5 so that box plots can be made for graphical representation, as shown in Figure 4.6.

Table 4.5 Table for box plots

		+25°C		-16°C
		Virgin	Tabbed	Tabbed
First Quartile	Q1	254.25	252.5	210
Smallest non-outlier value	MIN	250.0	247.5	199
Second Quartile	Median	260.0	258.0	214
Extreme Outlier	Max	278.5	272.5	217
Third Quartile	Q3	261.25	261.25	216
	Inter-quartile Range	7	8.75	6

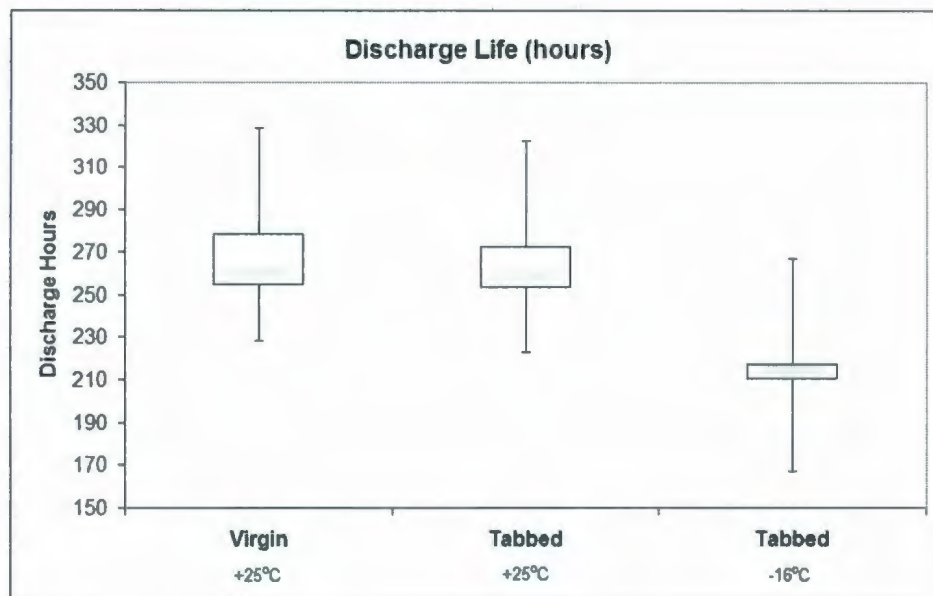


Figure 4.6 Box plot diagram for battery lifetime experiments

From the box plots shown in Figure 4.6, following comments can be made;

1. Total discharge life for both virgin and tabbed batteries tested at +25°C are close to each other with only 28 hours of difference
2. Standard deviation and coefficient of variation values for dataset belonging to virgin and tabbed batteries tested at +25°C indicates that the distribution of both the datasets is very similar to each other, meaning that there is approximately no difference between the test results of both virgin and tabbed batteries. This is also seen in resulting discharge life of only 28 hours of difference as indicated in item

3. Comparison of standard deviation and coefficient of variation values for datasets of tabbed batteries tested at $+25^{\circ}\text{C}$ and -16°C shows that a higher dispersion of data across the mean value for tabbed batteries tested at -16°C . This is mainly, due to the fact that total number of test samples were only 05 compared to 15 for tabbed batteries when tested at $+25^{\circ}\text{C}$
4. Life of battery reduces by 46 hours when operated at -16°C as compared to $+25^{\circ}\text{C}$

The difference in lifetime between tabbed cells at $+25^{\circ}\text{C}$ and -16°C can also be seen in Figure 4.7.

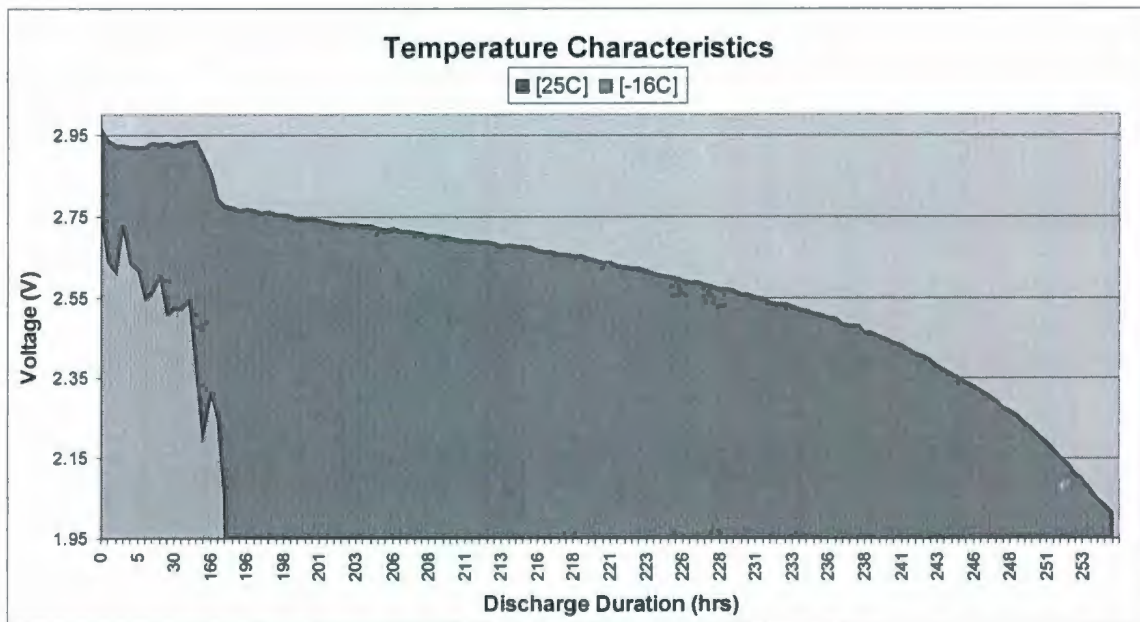


Figure 4.7 Comparison of lifetime of tabbed cells at $+25^{\circ}\text{C}$ and -16°C

The conclusion that can be made from experiments 1 and 2 is that there is a relationship between temperature and lifetime of battery. Lifetime of battery reduces as temperature is decreased. Similar experiments can be repeated at different temperatures and a curve can be plotted showing the relationship between temperature and life of battery.

To determine the true life of the battery when used in the data-recorder tag, battery needs to be tested at intermittent drain conditions also which mimic the real operation of the tag. The true battery life calculations requires knowledge of load at both continuous and intermittent drain conditions as the microprocessor intermittently runs the whole circuit when measurement is taken but rest of the time it stays in sleep mode which means low continuous drain from battery. Battery lifetime values at continuous drain conditions are completed in experiments 1 and 2. Experiment 3 is conducted to calculate battery lifetime at intermittent drain conditions as actually happens when data-recorder tag is operating normally.

The information gathered from experiments 1 and 2 will be used in experiment 3 and battery life will be calculated for temperatures, $+25^{\circ}\text{C}$ and -16°C .

4.6 Experiment 3: Battery Lifetime in Intermittent Drain Conditions

The cell provides power to the microcontroller chip which runs the circuit as needed. By using an oscilloscope, peak current values and pulse times are measured for each activity

of the tag to determine the rate of power usage at each stage and also to determine the depreciation in the cell's life when one activity is overused.

The tag once manufactured stays in running mode withdrawing a currents which depend on the type of activity. The activities are;

1. **Sleep:** it is amount of current needed by microprocessor to keep clock running. This is a continuous current draw condition which is fixed during mission life of the tag.
2. **Reset:** this is the amount of current microprocessor needs to reset the memory and start logging in readings from sensors from the beginning. This is an intermittent current draw condition that depends on user and not fixed.
3. **Sample:** it is the amount of current microprocessor needs when taking readings from pressure and temperature sensors. This is an intermittent current draw condition which is fixed during mission life of the tag.
4. **Download:** it is the amount of current microprocessor needs when recorded data is downloaded from tag's memory chip to computer. This is also an intermittent current draw condition that depends on user and not fixed.

Figures 4.8 to 4.13 show the measurements of time and currents used by the data-recorder tag. These measurements were taken using a highly accurate Oscilloscope.

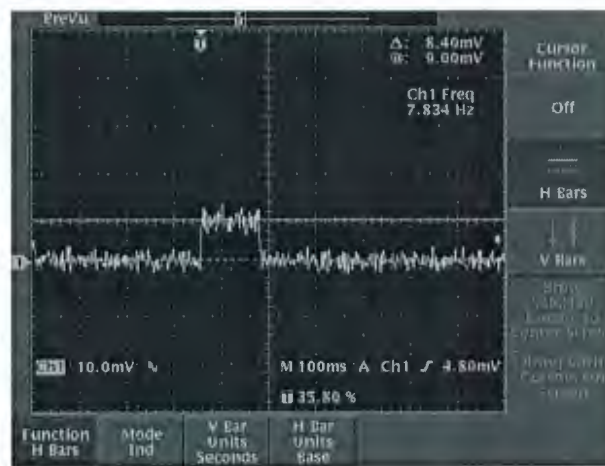


Figure 4.8 Peak current draw measurement at reset activity

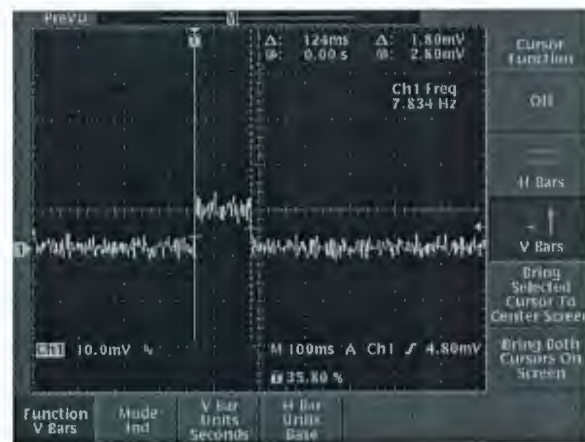


Figure 4.9 Pulse time measurement for reset activity

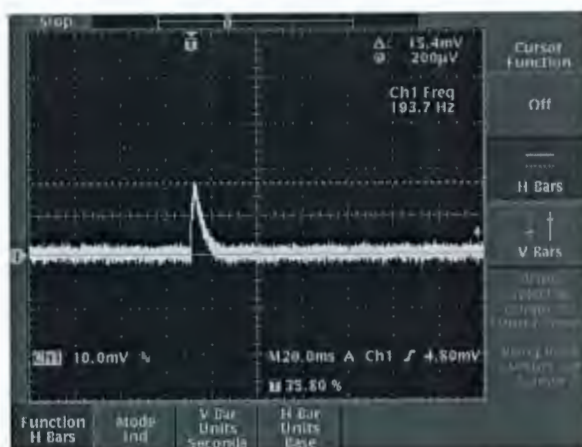


Figure 4.10 Peak current draw at sampling activity

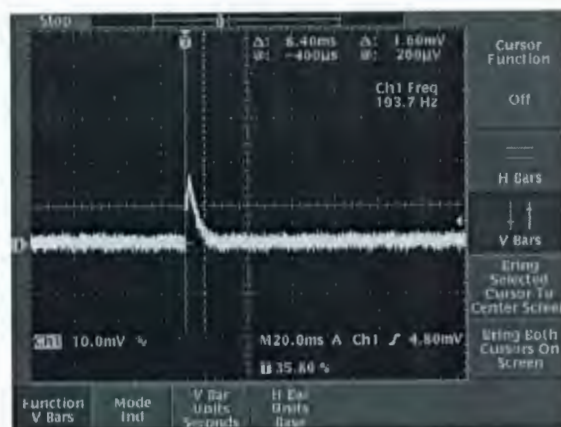


Figure 4.11 Pulse time measurement for sampling activity

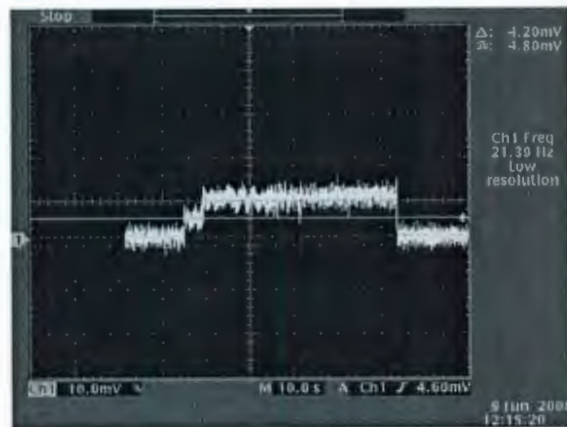


Figure 4.12 Peak current draw at data download activity

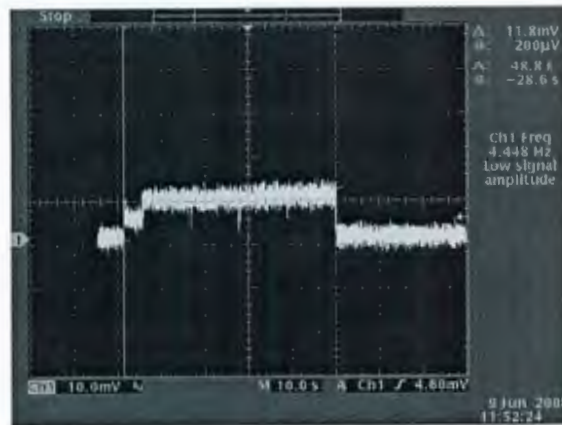


Figure 4.13 Pulse time measurement at data download activity

4.6.1 Calculations

Using the information of current and times measured through oscilloscope, summarized in Table 4.6, battery lifetime required by the data-recorder is calculated analytically.

Table 4.6 Results of measurements taken through oscilloscope

Activity	Current (uA)	Duration (seconds)
Reset	840	0.124
Sample	154	0.84
Download	880	44.2
Standby	1.19	continuous

Continuous Power Drain (standby mode or continuous drain):

$$1.19\text{E-}3 \text{ (mA)} \times 24 \text{ (hours)} \times 365 \text{ (days/year)} = 10.42 \text{ mAh/year}$$

Pulse power drain (sampling mode or intermittent drain):

For 32,000 samples

$$154\text{E-}6\text{A} \times 32000 = 0.00492 \text{ mA}$$

$$0.84 \times 32000 = 26.88 \text{ ms}$$

$$\text{As, } 60 \text{ (minutes)} \times 24 \text{ (hours)} \times 365 \text{ (days)} = 525,600 \text{ minutes/year}$$

$$525600 \times 26.88 = 14128128 \text{ seconds on load}$$

$$14128128/3600 = 3924.48 \text{ hours}$$

$$3924.48 \text{ (hours)} \times 0.00492 \text{ (mA)} = 19.30 \text{ mAh}$$

$$\text{Total power required to operate for 1 year} = 19.30 + 10.42 = 29.72 \text{ mAh}$$

$$\text{Average current drain} = 14.86 \text{ mAh} = 14.86/8760 = 1.69 \text{ uA}$$

$$0.036/1.69\text{E-}6 = 21301.775 \text{ hours} = 2.43 \text{ years}$$

So, at -16°C ,

$$= 21301.775 - 46.13 = 21255.64 \text{ hours}$$

In conclusion, life of data-recorder as calculated above is summarized in Table 4.7

Table 4.7 Life of data-recorder when used at +25°C and -16°C

Operating Temperature	+25°C	-16°C
Life of Data-Recorder	21301.77 hours 2.4 years	21255.64 hours 2.4 years

Since there was only 46 hours of difference in battery lifetime when tested at +25°C and -16°C, the life of the data-recorder tag, which includes continuous and intermittent drain conditions, is more than 2 years.

The data download and reset activities are user dependent and can be varied. Also, note from Table 4.6 that data download activity draws more current and for longer period. Addressing this relationship and its impact on tag life, a curve is plotted between the data download activity and tag life so that relationship can be understood, see Figure 4.14.

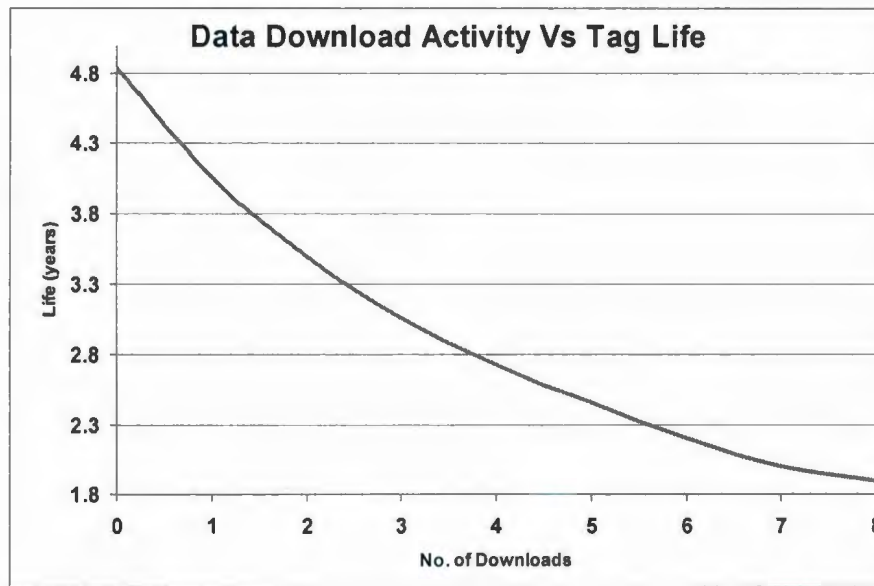


Figure 4.14 Relationship between data download activity and life of the data-recorder tag

Figure 4-14 shows that as the number of data download activity increases, life of the data-recorder tag decreases by a factor of 0.5 years for each additional activity. It also shows that maximum of 6 download activities is allowed in order to keep tag life above 2 years.

4.6.2 Results

It can be seen from the graph shown in Figure 4.14 that life of the data-recorder decreases linearly as the number of data downloads increases. Table 4.8 shows tag life as download activity increases.

Table 4.8 Life of a data-recorder Vs number of data downloads

No. of Downloads	Tag Life (years)
0	4.8
1	4
2	3.4
3	3
4	2.7
5	2.4
6	2.2
7	2
8	1.9

4.7 Conclusion

The following observations and results can be drawn from the experiments;

1. Loss of cell capacity between virgin and tabbed cells at +25°C is very low, which means welding process does not affect much on the life of the battery
2. Loss of cell capacity at different temperatures is not more than 46 hours of life
3. Cells are good for +2 years of life based on power requirement by microprocessor on circuit board
4. Power requirement by circuit that is using these cells still fits well within the design life of the product, > 2 years.
5. Data download activity which is user dependent needs to be controlled as it has significant affect on the life of the data-recorder tag.

In conclusion, premature battery failure which was observed in the analysis of failure data is most likely due to an excess current draw (short circuit) which drains battery

rapidly within few hours to few months depending on the type of the short circuit that occurred. It is assumed that the short circuit is due to moisture either already trapped inside the data-recorder at the time of moulding or diffused through the packaging material.

Since we have determined experimentally and analytically that rapid discharge of battery is the result of excess current drawn and not due to extreme operating temperatures, therefore power failures due to rapid discharge of cells is only a result of short circuiting of battery or any other component on-board the circuit. This will be discussed in-detail in Chapter 6

Chapter 5 and 6 investigates packaging failures which are related to penetration of water to the electrical circuit causing short circuit of component(s), thus resulting in either component failure only or rapid discharge of battery by drawing excess current.

Chapter 5

Failure Mode Analysis: Packaging Failure

5.1 Introduction

The biotelemetry data-recorder tag under study is designed for underwater applications where it remains immersed in water, attached to the animal, and collects pressure and temperature data periodically. Therefore, it is important that the electronic components should be completely insulated from water. The packaging should be designed to provide a water proof barrier that protects the electronic components from being subjected to moisture.

All electronic components along with the battery and sensors are moulded with polyurethane that provides such protection. Two kinds of polyurethanes are used to encapsulate the electronics, one is clear and hard with high tensile strength and the other is soft rubber like dark in colour with low yield strength. The later is used to cover the sensitive pressure sensor so that it remains protected from handling. The pressure sensor needs to be able to sense the compression of the soft polyurethane membrane as it deflects under the effect of pressure.

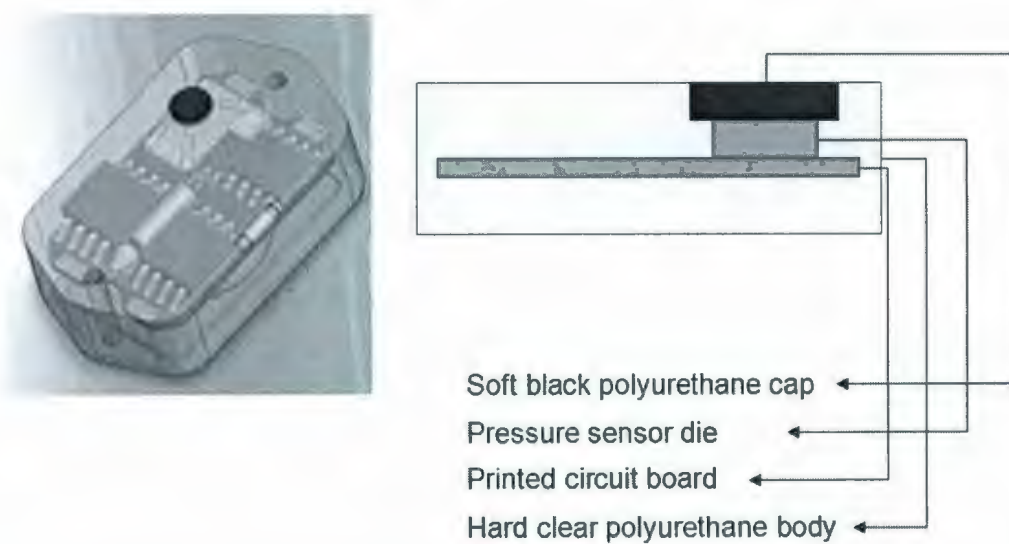


Figure 5.1 Anatomy of the data-recorder tag showing polyurethane body

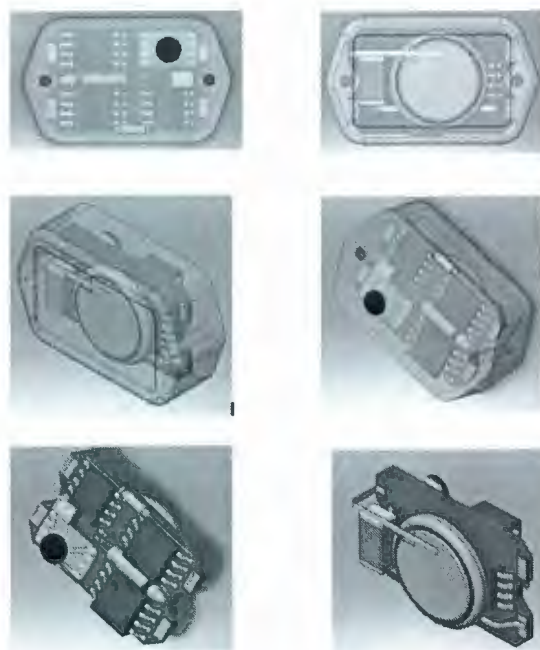


Figure 5.2 Sketch of data-recorder under study

Referring to Figures 5.1 and 5.2, it can be seen that there are only two ways water can penetrate to the electronic components and circuit;

1. Through cracks or openings in plastic encapsulation
2. Through polyurethane material by diffusion process

It is also suspected that water leaks through the interface between the black and the transparent urethane and causes damage to the pressure sensor and/or battery. Which results in either only pressure sensor failure or adds to rapid discharge of battery.

To investigate water penetration through the plastic body, structural analysis of the data-recorder is conducted both experimentally and numerically using finite element analysis. Chapter 6 describes more experiments and simulation modeling which were done to investigate moisture diffusion through the packaging materials. The focus of the structural analysis is on the stresses at the interface of the two types of polyurethanes used to package the tag. Since both types of the polyurethanes have different coefficients of thermal expansion, this may give rise to high residual stresses at the interface of the two materials and thus result in a lower tensile strength for the packaging.

In the next few sections of this chapter experiment details will be provided along with discussion on the results, and conclusions from the experiments and the simulation modeling.

As mentioned in Chapter 1, data-recorder tag is designed to have a design life of 2 years. The tag's function is to record temperature and pressure measurements in water of depths that may reach a depth of 1000 meters.

It is important to know if the materials used for encapsulation are strong enough to sustain such pressures. Any structural failure can cause water to ingress and cause damage to the electronics inside. Structural stress analysis is conducted using the finite element method at different pressures and results were compared with experimental analysis.

5.2 Structural Analysis

The tags were placed in a hydraulic pressure vessel capable of creating pressures up to 4500 psi. The first few data-recorder tags were subjected to pressures of 700, 1420 and 2800 psi for a period of 1 minute each. In another experiment, tags were subjected to the same pressures mentioned above for a period of 5 hours each to observe creep effect. The results obtained from this experiment are given in the following section.

Data-recorder tags are designed for marine animals study, which live in water and can reach depths of 1000 meters in cold oceans. Under such pressures, moulding compounds which encapsulates the electronics are subjected to pressures which create compressive

stresses on the surface of the data-recorder and has a potential to damage the soft and hard polyurethane body.

Pressure experiments are conducted to test these tags under such pressures and to determine the design limitations.

5.2.1 Samples Preparation

Few test specimens were made using the same manufacturing procedure used for the manufacture of the actual data-recorder tag. These test samples were moulded with moisture absorption test paper (Cobalt Chloride test strip), which turns white in colour when moisture is absorbed. Moisture tests strip replaces actual circuit board and electronic components to keep cost of test specimens low. Tag size and dimensions were exactly the same as the actual product.

5.2.1.1 Step 1

Preparation of moulds was done with moulding silicone. Once the silicone moulds were ready, after an overnight cure, it was filled to half its height with hard polyurethane and left for over night to cure at room temperature. Figure 5.3 shows the process.



Figure 5.3 Silicone moulds

5.2.1.2 Step 2

Another silicone mould was used for the soft polyurethane cap and after filling the moulds with the black soft polyurethane it was left overnight to cure fully. Figure 5.4 shows the moulds for the circular cap for pressure sensor.



Figure 5.4 Silicone moulds for soft polyurethane

5.2.1.3 Step 3

Once the overnight cure is complete, circular cap created from soft polyurethane was placed on the moisture test strip, as shown in Figure 5.5, and the assembly was laid in the mould which was half filled with hard polyurethane in step 1.

The mould is now filled to the top with the hard polyurethane, sandwiching the moisture test strip and circular cap, as shown in Figure 5.6. It is again left to cure for another 24 hours.



Figure 5.5 Cobalt Chloride test strip

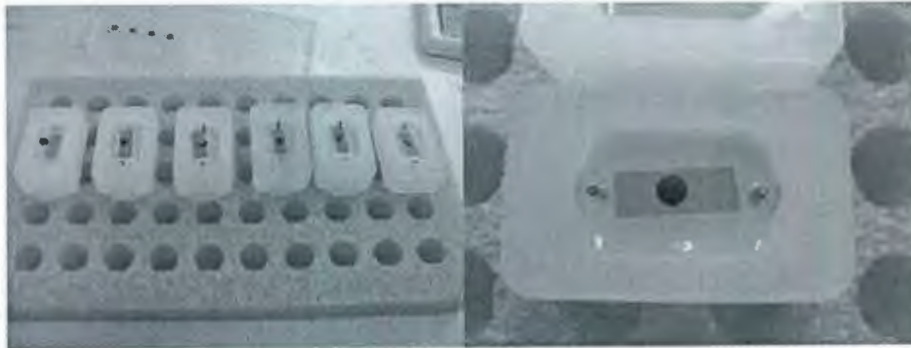


Figure 5.6 Fully moulded test samples in silicone mould

Test specimens are now ready for the pressure experiment.

5.2.2 Pressure Experiments

Test specimens were placed inside the hydraulic pressure vessel, as shown in Figure 5.7, and subjected to three pressures, 700, 1420 and 2800 psi for only 1 minute. In second stage of experiment same pressures were applied for 5 hours to create creep affect.



Figure 5.7 Hydraulic pressure vessel

After each applied pressure for specific time, samples of data-recorder tags were taken out of the vessel and inspected under the microscope for any cracks and visible damage. Table 5.1 shows the results at all applied pressure ranges.

Table 5.1 Observation of pressure tests

Applied Pressure	1 minute	5 hours
700psi	no damage noticed	not conducted
1420psi	no damage noticed	no damage noticed
2800psi	no damage noticed	damage noticed

Test samples subjected to 2800psi of pressure for 5 hours show signs of damage and presence of moisture on the test strip as shown in the Figures 5.8 to 5.10.



Figure 5.8 Test samples after 2800psi pressure for 5 hours showing moisture on the test strip

No damage was observed when samples were subjected to 700, 1420 and 2800 psi pressure for 1 minute. But when same pressures were applied continuously for 5 hours, micro-cracks were observed on the soft black polyurethane circular cap only. Figures 5.9 and 5.10 show cracks on the circular cap.

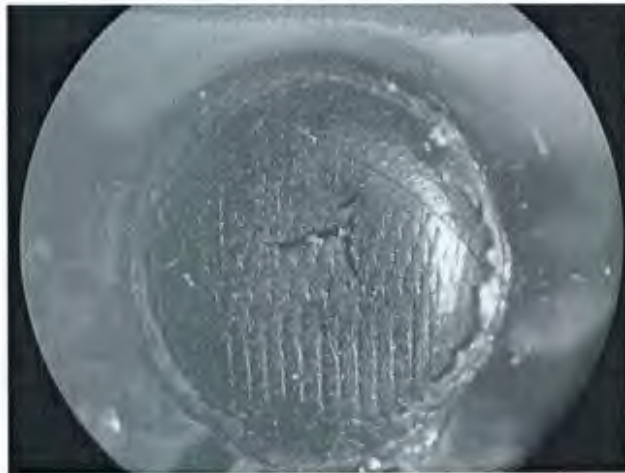


Figure 5.9 Micro-cracks on soft polyurethane, sample 1

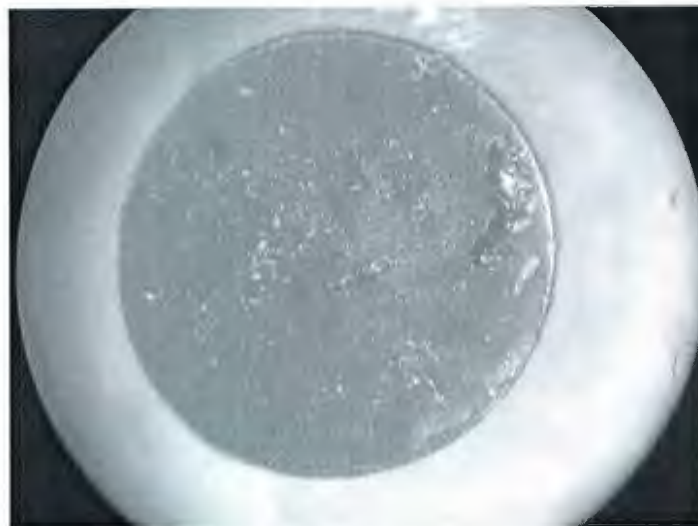


Figure 5.10 Micro-cracks on soft polyurethane, sample 2

Figures 5.9 and 5.10 show that cracks are not only in the middle of the soft polyurethane but also on the edges, which is the interface of soft and hard polyurethane. There was no damage observed on the hard clear polyurethane material.

5.3 FEA Simulation

Due to the cost of physical pressure experiment and specimens, FEA simulation is conducted using commercially available finite element package, CosmosWorks[®]. Same pressure values were used in FEA simulation as used in pressure experiments.

Material properties were obtained from the datasheets supplied by the manufacturer and presented in the Table 5.2.

Table 5.2 Material properties of the encapsulants

Material Properties	Soft Polyurethane (Black)	Hard Polyurethane (Clear)
Elastic Modulus (N/m ²)	9E06	300E07
Poisson's Ratio	0.49	0.39
Tensile Strength (N/m ²)	6.89E05	1.99E07
Yield Strength (N/m ²)	9E06	300E07
CTE (/K)	0.00067	0.00063
Thermal Conductivity (W/m.K)	0.14	0.189
Specific Heat (J/kg.K)	1	1

Since the soft polyurethane material, which is used to create the circular cap for the pressure sensor, resists flow in linear direction yet sustains large deformations, it is defined as non-linear visco-elastic material as the relation between stress and strain is non-linear. This is needed for creep analysis, which is the application of pressure for a long period of time. Therefore, the study is divided into two parts, one for static load analysis and the other for creep analysis.

5.3.1 Defining Model and Boundary Conditions

From our previous pressure experiments as described in the section 5.2.2, we learned that there is no damage on the hard polyurethane surface. It is mainly due to the fact that hard polyurethane has a very high tensile and yield strength compared to soft polyurethane, $1.99E07 \text{ N/m}^2$. Therefore, to reduce the simulation processing time, model size is reduced to only soft polyurethane, which means; only soft polyurethane is being modeled instead of modeling the whole structure. Figures 5.11 and 5.12 show the soft polyurethane circular cap as modeled in FEA.

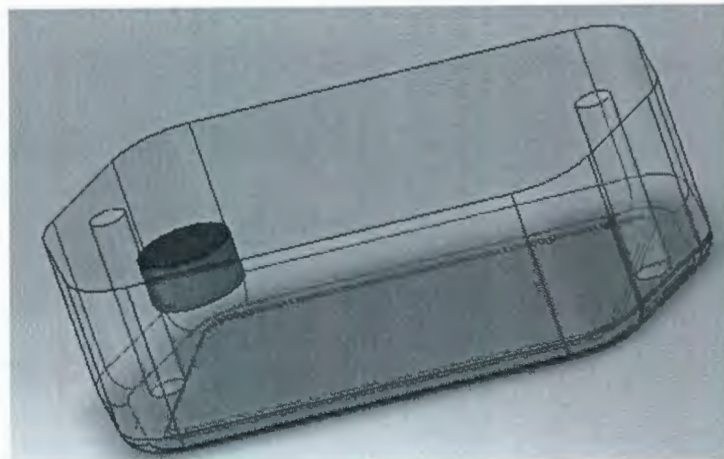


Figure 5.11 Sketch of data-recorder tag showing only two polyurethane moulding compounds

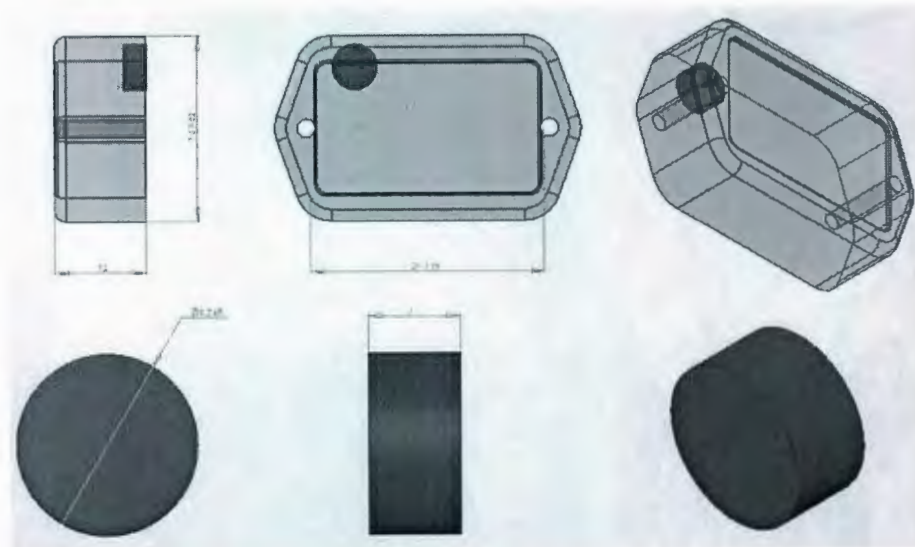


Figure 5.12 Dimensions of data-recorder tag and soft polyurethane compound

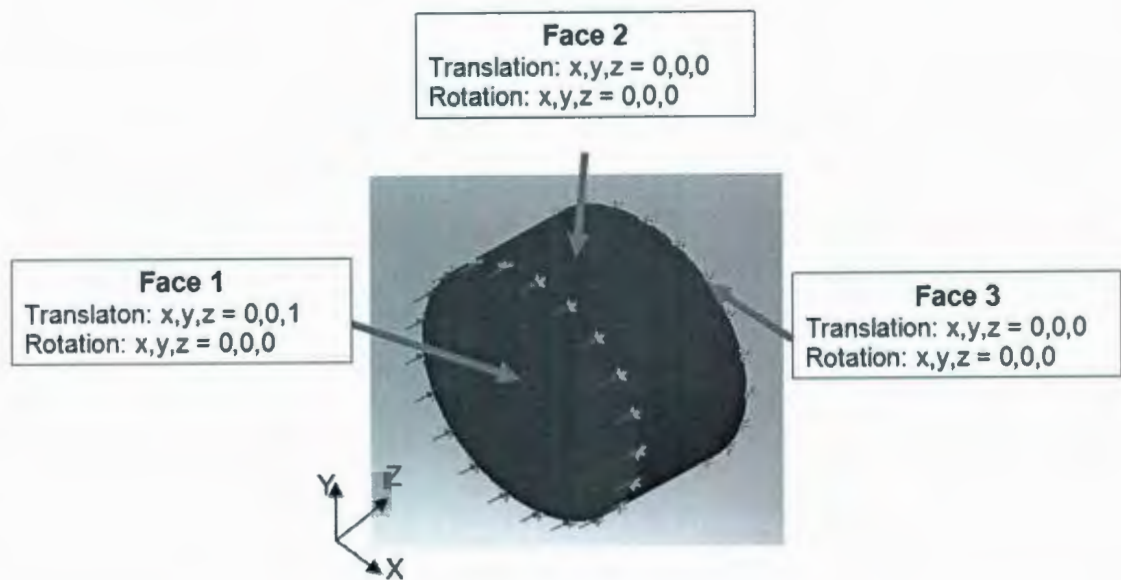


Figure 5.13 Soft polyurethane compound model showing restraints and pressure

Figure 5.13 shows the boundary conditions for the model. Face 1, which is considered as the top face of the component, is subjected to pressures, whereas, Face 3, is the bottom face of the component sitting on top of the pressure sensor. Face 1 is allowed to have translation in z-direction but translation in x and y direction is restricted. Rotation is also restricted in all directions for Face 1. However, Face 2 and 3 are restricted for translation and rotation in all directions.

5.3.2 Static Stress Analysis

Using the model as shown in Figure 5.13 and material properties as described in Table 5.2, pressure simulation study was conducted by applying 1420 psi and 2800 psi pressures to Face 1. Results were obtained for von-mises stresses, displacements and strains and shown in sections below.

5.3.2.1 Stresses and Displacement at 1420 psi

Results of FEA simulation for 1420 psi pressure are shown in Figures 5.14 and 5.15. It can be noted from Figure 5.14 that maximum stress value, $2.8E06 \text{ N/m}^2$, at 1420 psi is under the yield strength of the material which is $9E06 \text{ N/m}^2$.

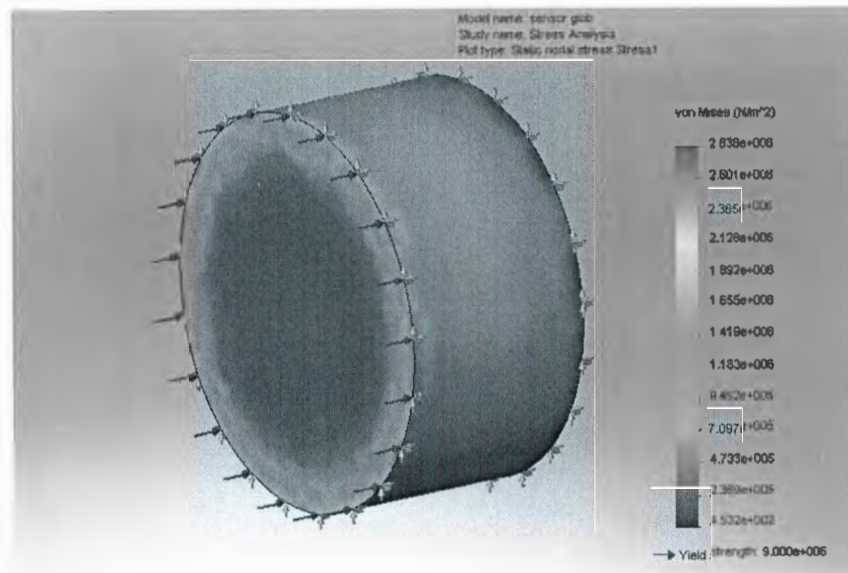


Figure 5.14 Von Mises stresses when 1420 psi pressure is applied

The maximum displacement is observed in the center of the circular cap, Figure 5.15. This behaviour is expected as the cap is constraint to deflect from sides, Face 2, so the maximum deflection from center is in z-direction and of magnitude of 0.19 mm.

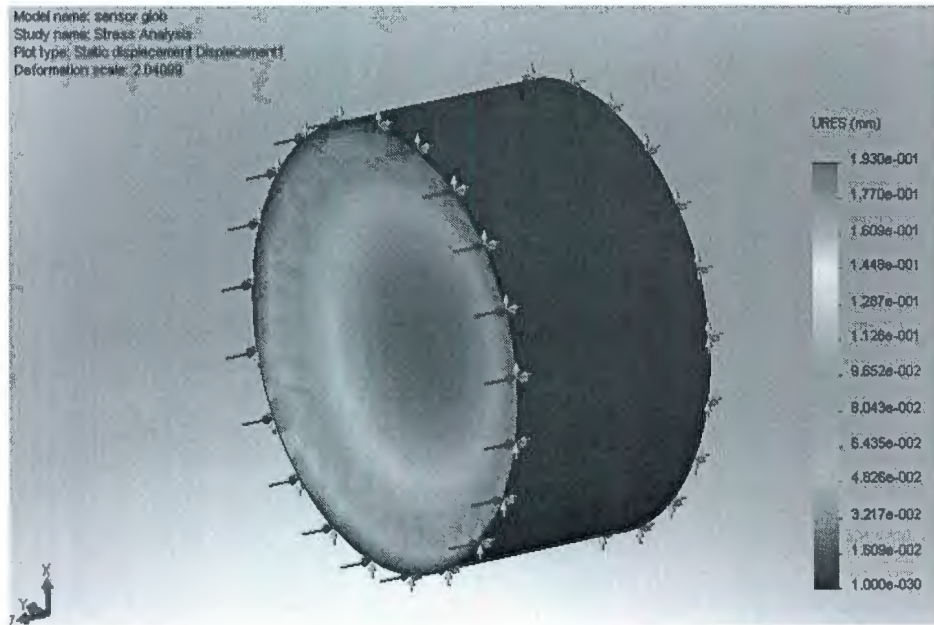


Figure 5.15 Displacement when 1420psi pressure is applied

5.3.2.2 Stresses and Displacement at 2800 psi

Results of FEA simulation for 2800 psi pressure are shown in Figures 5.16 and 5.17. It can be noted from Figure 5.16 that maximum stress value, $5.5E06 \text{ N/m}^2$, at 1420 psi is under the yield strength of the material which is $9E06 \text{ N/m}^2$.

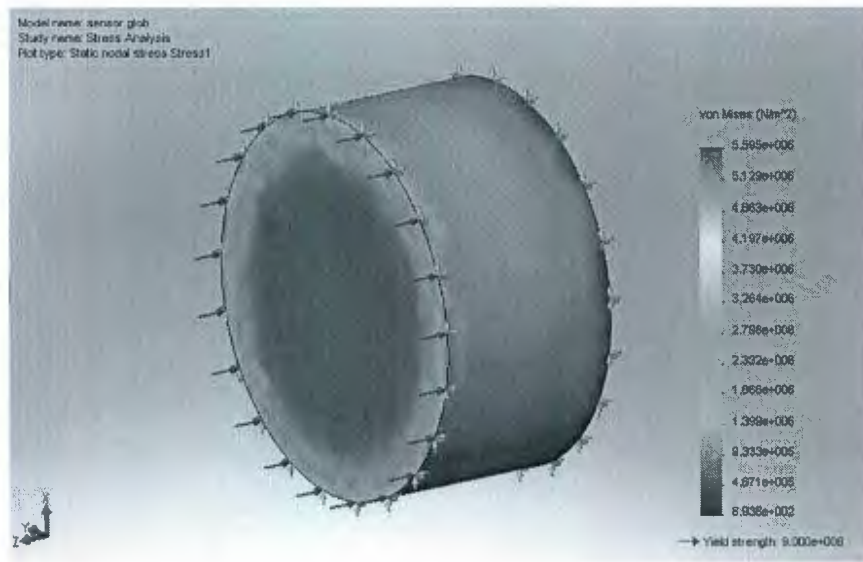


Figure 5.16 Von mises stresses when 2800psi pressure is applied

The maximum displacement is observed in the center of the circular cap, Figure 5.17. This behaviour is expected as the cap is constraint to deflect from sides, Face 2, so the maximum deflection from center is in z-direction and of magnitude of 0.38 mm.

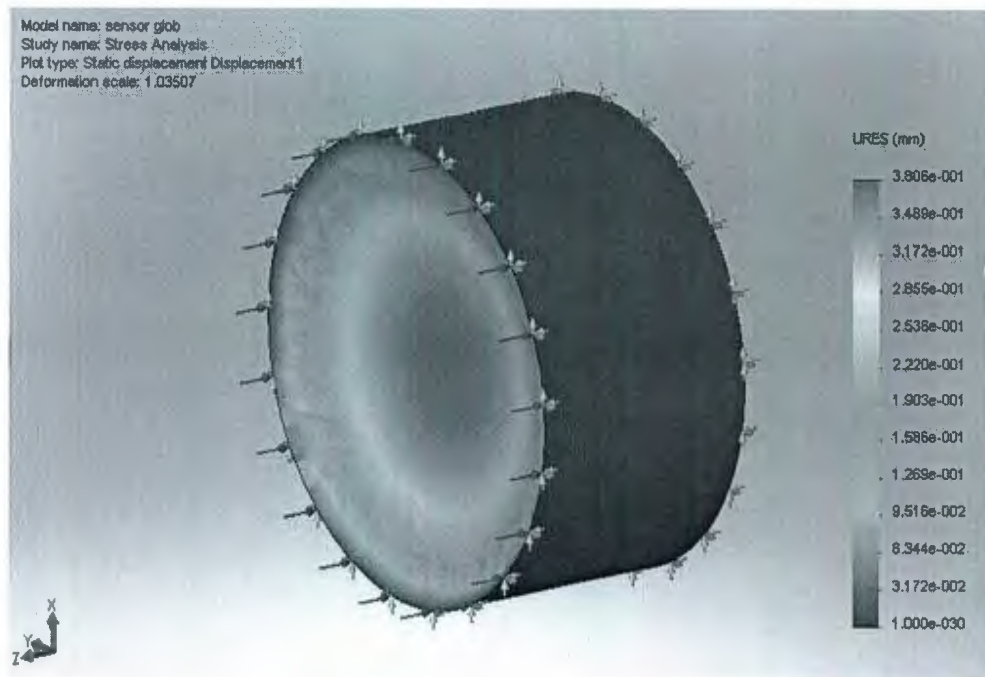


Figure 5.17 Displacement when 2800 psi pressure is applied

5.3.3 Results Summary for Static Stress Analysis

Results of static stress analysis are shown in Table 5.3.

Table 5.3 FEA stress analysis results

		1420 psi	2800 psi
Von Mises Maximum Stress	(N/m ²)	2.8E06	5.12E06
Displacement along Z-Axis	(mm)	0.19	0.38

Compared to yield strength of the material, 9E06 N/m², maximum value of stress is below the yield strength of the soft polyurethane circular cap at both applied pressures. The direction of deflection matches to the observations made in previous study of pressure experiments.

Since the maximum stress value is under the yield strength of the material, conclusion can be drawn that the material did not fail under applied pressure values.

In section 5.2.2, pressure experiments showed cracks on the soft polyurethane circular cap when pressure of value 2800 psi was applied for a longer period of time. This is due to creep affect and mainly due to the visco-elastic nature of the material. To study creep affects through FEA and also to determine the time it takes the material achieve stress greater than its yield strength, another FEA study was designed and conducted as described in section 5.3.4.

5.3.4 Creep Analysis

Tendency of a solid material to slowly move or deform permanently under the influence of stresses is known as “Creep”. It occurs as a result of long term exposure to levels of stress that are below the yield strength of the material. Creep is more severe in materials that are subjected to heat for long periods, and near the melting point. Creep always increases with temperature. Creep can occur in polymers and metals which are considered visco-elastic materials.

The rate of this deformation is a function of the material properties, exposure time, exposure temperature and the applied structural load. Depending on the magnitude of the applied stress and its duration, the deformation may become so large that a component

can no longer perform its function. Unlike brittle fracture, creep deformation does not occur suddenly upon the application of stress. Instead, strain accumulates as a result of long-term stress. Creep deformation is "time-dependent" deformation.

In the initial stage, or primary creep, the strain rate is relatively high, but slows with increasing strain. The strain rate eventually reaches a minimum and becomes near constant. This is known as secondary or steady-state creep. This stage is the most understood. The characterized "creep strain rate" typically refers to the rate in this secondary stage. Stress dependence of this rate depends on the creep mechanism. In tertiary creep, the strain rate exponentially increases with strain. The accumulation of large in-elastic strains may lead to failure.

When subjected to a step constant stress, visco-elastic materials experience a time-dependent increase in strain. This phenomenon is known as visco-elastic creep.

Polymers, like polyurethane, experience significant creep at all temperatures especially above 200°C. Polymeric creep is;

- Non-linear visco-elastic
- Irrecoverable
- Significant at high temperatures

Due to visco-elastic nature of soft polyurethane material, creep analysis were conducted using FEA simulation by applying pressures for long time keeping same boundary conditions as applied to the model in static stress analysis study. Several simulations were conducted by using time as variable. Time of each applied pressure was increased in each simulation starting from 1 hour to 5 hours. A same time increment was repeated for pressure values, 1420 psi and 2800 psi, thus 5 simulations at each pressure value.

5.3.4.1 Creep Analysis at 1420psi

Keeping pressure at constant value of 1420 psi, 5 simulations were run by changing time from 1 hour to 5 hours. Figure 5:18 shows the von-mises stress distribution when pressure of 1420 psi is applied for 5 hours. The value of maximum stress, $5.1E06 \text{ N/m}^2$, is under the yield strength of the material, which is $9E06 \text{ N/m}^2$. Stress values have changed significantly compared to static stress analysis study done in previous section.

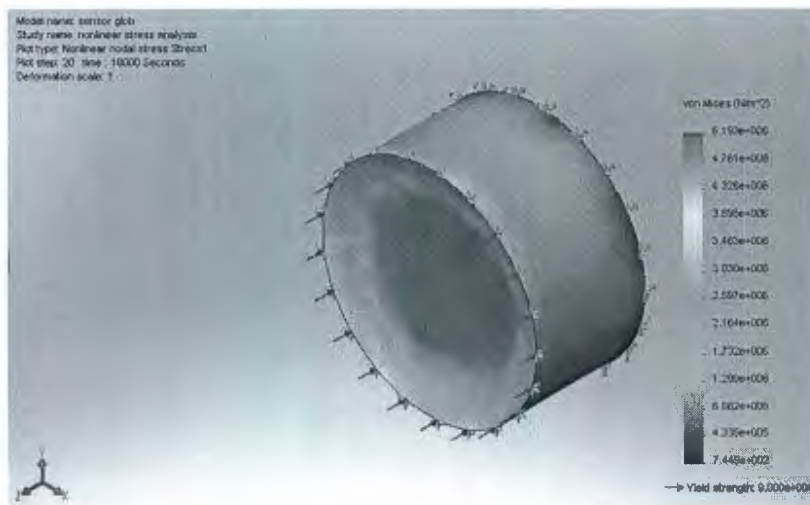


Figure 5.18 Von mises stresses when 1420 psi pressure is applied for 5 hours

The maximum displacement after 5 hours at 1420 psi is 0.4 mm. Maximum deflection is at the center of the circular cap as shown in Figure 5.19.



Figure 5.19 Displacement when 1420psi pressure is applied for 5 hours

5.3.4.2 Creep Analysis at 2800psi

Keeping pressure at constant value of 2800 psi, 5 simulations were run by changing time from 1 hour to 5 hours. Figure 5.20 shows the von-mises stress distribution when pressure of 2800 psi is applied for 5 hours. The value of maximum stress, $1E07 \text{ N/m}^2$, is greater than yield strength of the material, which is $9E06 \text{ N/m}^2$. High stress value will yield in deforming circular cap permanently and failure can be seen in the form of cracks.

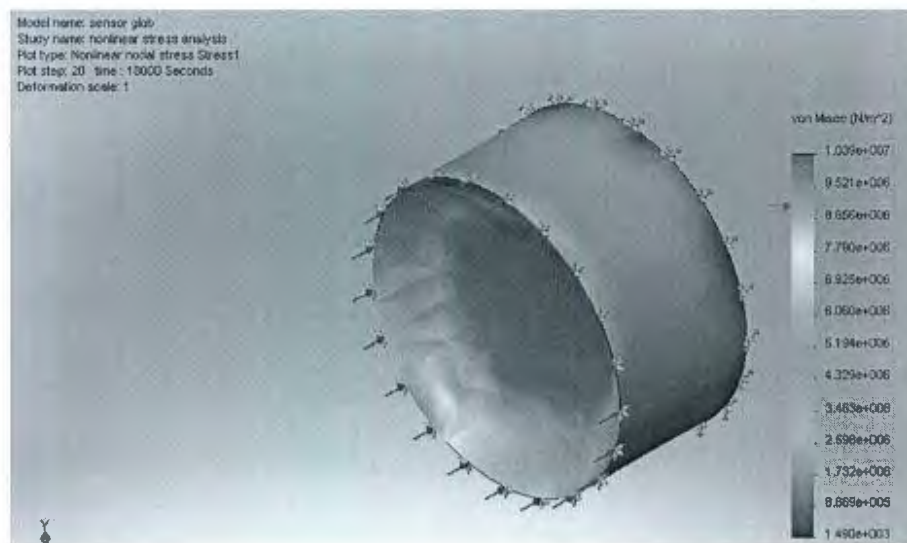


Figure 5.20 Von mises stresses when 2800 psi pressure is applied for 5 hours

The maximum displacement after 5 hours at 2800 psi is 0.81 mm. Maximum deflection is at the center of the circular cap as shown in Figure 5.21.

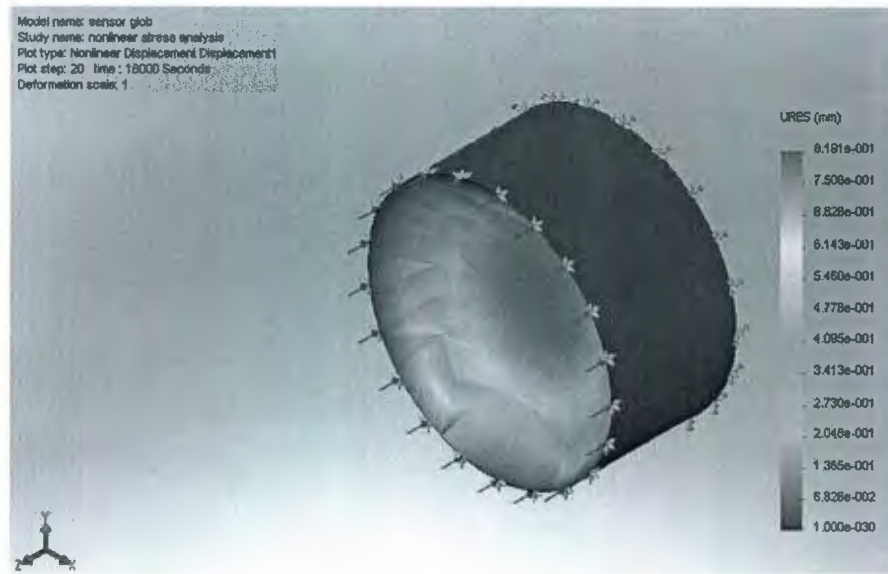


Figure 5.21 Displacement when 2800 psi pressure is applied for 5 hours

5.3.5 Results Summary for Creep Analysis

Results of creep analysis are shown in Table 5.4.

Table 5.4 FEA creep analysis results

		1420 psi	2800 psi
Von Mises Maximum Stress	(N/m ²)	5.19E06	1.039E07
Displacement along Z-Axis	(mm)	0.409	0.819

Compared to yield strength of the material, 9E06 N/m², maximum value of stress exceeds the yield strength of the soft polyurethane circular cap when pressure value of 2800 psi is applied for 5 hours. Deflections along the z-direction increase as the applied pressure and time increases. Large strain combined with the high stress value after 5 hours of 2800 psi pressure can cause this material to deform permanently and the reason for

cracks, which open path for water to enter the plastic polyurethane body and reach electrical circuit.

5.4 Conclusion

Summarizing the results from static stress and creep analysis, as shown in Table 5.5, it is clear that when 2800 psi pressure is applied for 5 hours, stresses exceed yield strength of the material and thus resulting in cracks which matches to results obtained from physical pressure experiments and shown in Figures 5.9 and 5.10.

Table 5.5 Summary of static stress and creep analysis

	Static Stress Analysis		Creep Analysis (5 hours)	
	1420psi	2800psi	1420psi	2800psi
Von Mises Maximum Stress (N/m ²)	2.8E06	5.12E06	5.19E06	1.039E07
Displacement (mm)	0.19	0.38	0.409	0.819

From the animal behaviour as observed through recorded data and published studies, it is not normal for any animal to dive to depths of 2800psi (1970 meters) and stay there for such a long time, 5 hours. The normal dive pattern of most the deep diving animals is between 3 to 9 minutes. Therefore, it can be concluded that the design of the data-recorder tag is good for the applications where the pressure, even as high as 2800 psi, is applied for a short period of time.

Recorded data from the tags that failed under packaging failure mode show that animals diving pattern was closer to 1500 psi (1000 meters) and also no physical damage was noticed on the casing of the failed tags, means no cracks. This means that the water penetration which is the effect of packaging failure was not caused by high stresses or openings through the plastic polyurethane body but could be due moisture diffusing through the polyurethane material.

Chapter 6 further investigates packaging failure from moisture diffusion perspective since it has been established that polyurethane packaging is strong enough to sustain high pressure, 2800 psi, when applied for few minutes, which is the normal behaviour of the marine animals. Root cause of other failure modes, power, temperature sensor, pressure sensor and communication diode failures will also become clear in Chapter 6.

Chapter 6

Moisture Diffusion in Electronic Packaging Materials

6.1 Introduction

Moisture poses a significant threat to the reliability of microelectronic assemblies and can be attributed as being one of the principal causes of many early-life failures. Since the vast majority of packaging materials are epoxy or polyurethane based, they have the tendency to absorb moisture, which can lead to undesirable changes in material properties. To ensure the reliability and durability of the electronic packages, the effect of moisture is discussed and researched by several researchers as discussed in chapter 2. In addition to being a moisture sensitive property, the interfacial adhesion is also affected by the elastic mismatch, relative mode mixity, temperature, and the corresponding surface chemistry and topology of the adherends. Therefore, the study of the moisture effect on interfacial adhesion is inevitably a multidisciplinary effort.

The presence of moisture in plastic packaging alters thermal stress through alteration of thermo-mechanical properties. For example; change of elastic modulus, shear strength and glass transition temperatures. Moisture also;

- Induces hygroscopic stress through differential swelling
- Reduces interfacial adhesion strength
- Induces corrosion
- Acts as an unwanted resistance when present between the two nodes of component and result in lowering the resistance

Despite the pivotal role of moisture, research activities in moisture induced failure remain relatively low, compared to thermal induced failure. This is partly due to the lack of material data and aggravated by the lack of material characterization techniques and procedures and the near absence of such properties from material vendors.

Chapter 6 presents a systematic knowledge and methodology to understand moisture diffusion through electronic packaging materials. Sketches presented in Figures 6.1 and 6.2 show the bi-material interface and the path for moisture to ingress to the printed circuit board through diffusion.

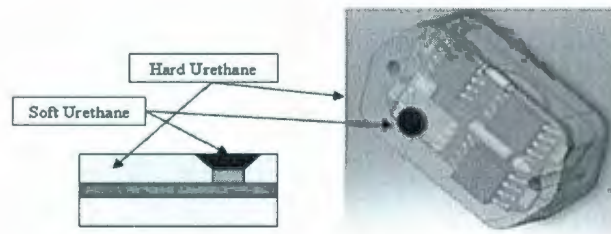


Figure 6.1 Sketch of the data-recorder tag showing bi-material interface

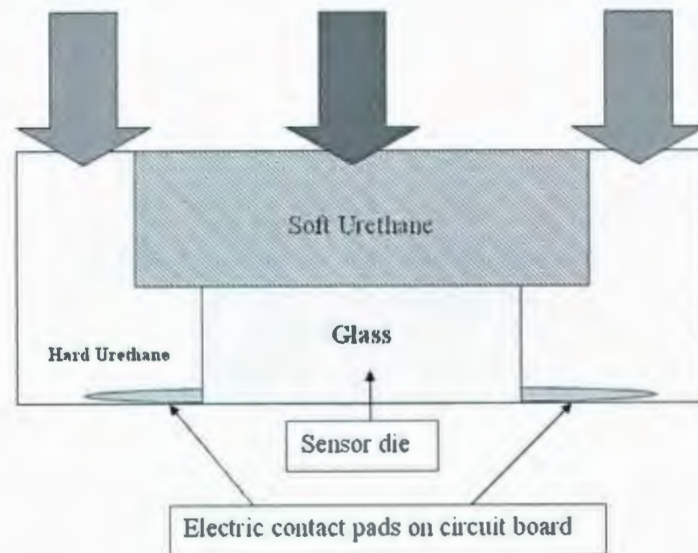


Figure 6.2 Sketch showing diffusion paths for water through hard and soft polyurethane materials

6.2 Mathematics of diffusion

Adolf Fick derived laws of diffusion in 1855 which are similar to heat diffusion equations by Fourier (Fourier, 1822). Fick's first law of diffusion, Equation 6-1, is used in steady-state diffusion which is when the concentration within the diffusion volume does not change with respect to time.

$$F = -D \frac{\partial C}{\partial x} \quad (6-1)$$

Where;

F = rate of transfer per unit area of section (cm^2/sec)

C = concentration of diffusing substance (g/cm^3)

x = space coordinate measured normal to the section

D = diffusion coefficient (cm^2/sec)

Fick's second law, Equation 6-2, is used in non-steady or continually changing state diffusion which is when the concentration within the diffusion volume changes with respect to time.

$$\frac{1}{D} \frac{\partial C}{\partial t} = \frac{\partial^2 C}{\partial x^2} + \frac{\partial^2 C}{\partial y^2} + \frac{\partial^2 C}{\partial z^2} \quad (6-2)$$

Where;

C = concentration of diffusing substance (g/cm^3)

D = diffusion coefficient (cm^2/sec)

x, y, z = dimensions in x, y and z direction (cm)

Polymeric packaging materials transport moisture primarily by diffusion, although secondary effects such as surface tension and pressure driven flows may also contribute. Moisture transport strictly by diffusion is modeled using the standard transient diffusion as per Fick's second law.

Wong, Koh, Lee and Rajoo (2002) showed that the crank's equation (mathematics of diffusion, 1956), can be modified into Equation 6-3 to calculate the diffusion coefficient for isotropic materials.

$$\frac{M_t}{M_\infty} = 1 - \frac{8}{\pi^2} \sum_{m=0}^{\infty} \frac{1}{(2m+1)^2} \exp\left[\frac{-D(2m+1)^2 \pi^2 t}{h^2}\right] \quad (6-3)$$

Where;

h = total sheet thickness (mm)

M_t = total mass of the diffusing substance absorbed at time t

M_∞ = Equilibrium mass of the absorbed substance

D = diffusion coefficient (mm^2/hour)

Since the Equation 6-3 assumes that there is no diffusion from the edges of the specimen or it is only true for large aspect ratio, Equation 6-4 is the correction factor needed to compensate diffusion in z -direction, as prescribed by Wong, Koh, Lee and Rajoo (2002)

$$D_z = C_f \times D_{1-D} \quad (6-4)$$

For square specimen,

$$C_f = \frac{1}{1 + \left(\frac{2z}{x}\right)^2} \quad (6-5)$$

Where;

C_f = correction factor

Z = thickness of specimen (mm)

X = length/width of the specimen

Zhou, Coffin and Arvelo (2006) suggested another correction factor, as shown in equation 6-6.

$$D_c = D \left(1 + \frac{h}{l} + \frac{h}{w}\right) \quad (6-6)$$

Where;

D = diffusion coefficient neglecting edge effect (mm²/hour)

D_c = diffusion coefficient including edge effect (mm²/hour)

h = height or thickness of the specimen (mm)

l = length of the specimen (mm)

w = width of the specimen (mm)

Using Crank's equation (Mathematics of Diffusion, 1956), shown in Equation 6-7;

$$\frac{C(x,t)}{C_\infty} = 1 - \frac{4}{\pi} \sum_{n=0}^{\infty} \frac{(-1)^n}{2n+1} \exp\left[\frac{-D(2n+1)^2 n^2 t}{4l^2}\right] \frac{\cos(2n+1)\pi x}{2l} \quad (6-7)$$

Where;

l = half thickness of sheet (mm)

D = Diffusion coefficient (mm²/hour)

t = time (hour)

C = concentration of diffusing substance in time t (g/mm³)

C_∞ = Saturated concentration of the absorbed substance (g/mm³)

In the initial stages of absorption where $M_t/M_\infty < 0.5$ and assuming a constant diffusion coefficient, D , above equation can be approximated to Equation 6-8 as shown by Wong, Koh, Lee and Rajoo (2002).

$$\frac{M_t}{M_\infty} = \frac{4}{h} \sqrt{\frac{Dt}{\pi}} \quad (6-8)$$

If absorption data is plotted with M_t/M_∞ as a function of $(t/h^2)^{1/2}$ and exhibits linear behaviour for $M_t/M_\infty < 0.5$, the diffusion coefficient can be determined by rearranging Equation 6-8 to Equation 6-9;

$$D = \frac{\pi}{16} \left[\frac{M_t / M_\infty}{\sqrt{t} / h} \right]^2 \quad (6-9)$$

The diffusivity, D , can now be experimentally determined using absorption data (M_t/M_∞) by weight gain experiment as prescribe in ASTM D570 method.

Once the diffusivity coefficient is known, theoretical Fickian curve can be plotted with the experimental data to see if the absorption is Fickian or not. This can be done by using the value of “ D ” calculated from weight gain experiment and plotting the graph with different time values. Equation 6-10 can be used;

$$\frac{M_t}{M_\infty} = 1 - \exp \left[-7.3 \left(\frac{Dt}{h^2} \right)^{0.75} \right] \quad (6-10)$$

Figure 6.3 represents an example of graph plotted between M_t/M_∞ and $t^{1/2}$, dotted marks are the data from experiment and the continuous line is a Fickian curve.

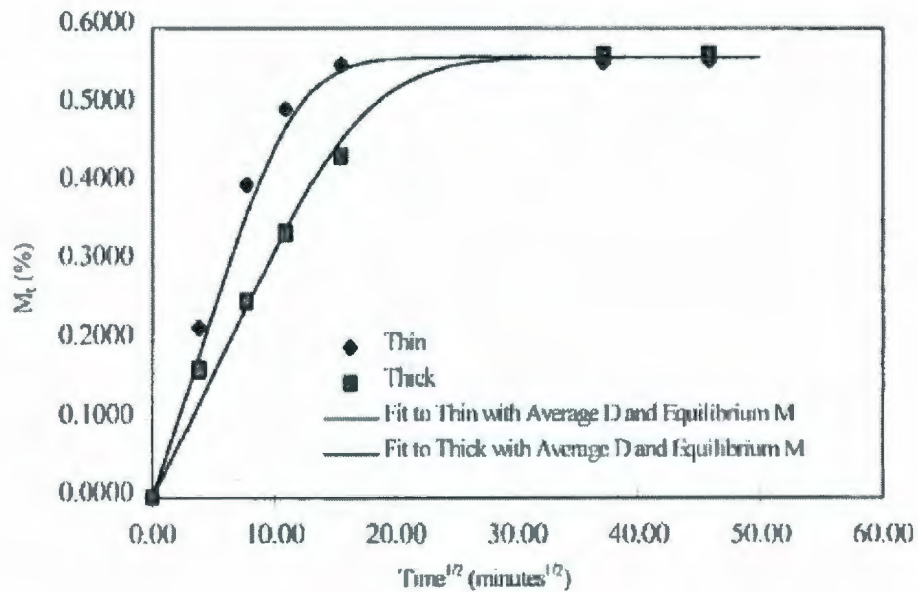


Figure 6.3 Example of Fickian curve

For very prolonged times curve becomes non-fickian, therefore, diffusion coefficient is calculated by considering only the linear part of the curve. For materials showing non-fickian behaviour, Wong, Koh, Lee and Rajoo (2002) suggested to use the following Equation 6-11;

$$t_{99\%} = \frac{0.45 h^2}{D} \quad (6-11)$$

Where;

$t_{99\%}$ = time to approach 99% saturation (hours)

h = height or the thickness of the specimen (mm)

D = diffusion coefficient (mm²/hour)

The 99% saturation approach helps to define the limit of Fickian diffusion hence eliminate error caused by non-fickian sorption.

6.3 Moisture Ingress Rate Calculations

Moisture diffusivity and solubility data can be gathered by periodically weighing samples soaked in a humidity chamber controlled to an accuracy of $\pm 1^{\circ}\text{C}$ and $\pm 1\% \text{RH}$ as prescribed by ASTM D570 standard. An analytical balance having an accuracy of $\pm 0.01 \text{mg}$ can be used to weigh samples. The samples are first dried in a convection oven above 100°C for at least 24 hours and weighed to determine the dry weight. It is considered complete dryness when two consecutive measurements are same. The samples are then placed in humidity chamber. Samples are periodically removed from the chamber and weighed. First few readings can be taken with a frequency of 10-15 minutes as sorption is higher in first few hours but can be relaxed later to 3-4 readings in a day. Samples are considered saturated when two consecutive readings are same.

The percent increase in weight of a material after exposure to water under specified conditions is calculated using Equation 6-12. Water absorption can influence mechanical and electrical properties. Factors such as the type of material, additives, temperature, and length of exposure can affect the amount of water absorbed.

$$M_t(\text{wt}\%) = \frac{M_t - M_o}{M_o} \times 100 \quad (6-12)$$

Where;

M_t = weight of wet specimen at time t (gms)

M_o = weight of dry specimen (gms)

For testing, the specimens are dried and cooled. Three testing procedures are commonly employed. Only data from the same testing procedures are readily comparable. The three tests prescribed in ASTM D570 method are described in Table 6.1.

Table 6.1 ASTM D570 Test methods

Procedure	Test Description
Water Absorption @ 24 hrs	Test specimens are immersed in distilled water at a specified temperature for 24 hours. Testing is most commonly done at 23°C
Water Absorption @ Saturation	Test specimens are immersed in distilled water at a specified temperature until the water absorption essentially ceases.
Water Absorption @ Equilibrium.	Test specimens are exposed to a humid environment at a specified temperature for 24 hours. Testing is most commonly performed at 50% relative humidity (RH) and 23°C

Datasheet obtained from materials manufacturer provided the information regarding water absorption (M_t/M_o) using ASTM D570 test method as shown in Table 6.2. Therefore, humidity chamber test was not conducted to calculate diffusion coefficient. Instead the values provided were used to calculate diffusion coefficient using Equation 6-9.

Table 6.2 Water absorption properties from polyurethane datasheet

	Soft Polyurethane	Hard Polyurethane
Water Absorption, % (168 hours at 25°C) ASTM D 570	0.3	0.2

Inserting the values of M_t/M_∞ in Equation 6.9 for soft polyurethane, we get;

$$D = \frac{\pi}{16} \left(\frac{0.3}{\sqrt{168}/2} \right)^2$$

$$D = 4.20 \times 10^{-4} \text{ mm}^2/\text{hr}$$

Using equation 6-11, moisture diffusion ingress rate can be calculated.

$$t_{99\%} = \frac{0.45(2)^2}{4.20 \times 10^{-4}}$$

$$t_{99\%} = 4285.71 \text{ hours} = 178.5 \text{ days}$$

Using equations 6-9 and 6-11 again for hard polyurethane, we get;

$$D = \frac{\pi}{16} \left(\frac{0.08}{\sqrt{168}/12} \right)^2$$

$$D = 1.07 \times 10^{-3} \text{ mm}^2/\text{hr}$$

$$t_{99\%} = 60560.74 \text{ hours} = 2523.36 \text{ days} = 6.913 \text{ years}$$

The results are summarized in Table 6.3 below;

Table 6.3 Diffusion coefficient for polyurethanes, soft and hard

	Soft Polyurethane	Hard Polyurethane
Diffusion Coefficient, D (mm ² /hr)	4.20 x 10 ⁻⁴	1.07 x 10 ⁻³
t _{99%} (days)	178.5	2523.36

Referring to Table 6.3, it takes approximately 6 months for the soft polyurethane circular cap to fully saturate with water whereas 7 years for hard polyurethane. Considering it takes 7 years to diffuse through the hard polyurethane, it is not considered for FEA simulation study. Only soft polyurethane circular cap was modeled in next section as it diffuses in 6 months which can be the cause of failures in the tag.

6.4 Finite Element Simulation

Since the Fick's moisture diffusion equation, Equation 6.2, follows the same governing differential equation as the diffusion of heat (Fourier,1822), with a change of the dependent variable, temperature, with moisture concentration and the thermal diffusivity with moisture diffusivity, commercially available heat transfer simulation software can be used to solve transient moisture diffusion problem. However, a unique problem arises in the diffusion of moisture. Since D is constant for particular material, for bi-material analysis, interfacial concentration discontinuity can not be analyzed. An interfacial discontinuity results where two materials having different saturated concentrations are joined.

To use heat transfer simulation software for moisture diffusion simulation, manipulation in defining material properties is required. This is done by replacing thermal conductivity of the material with moisture diffusion coefficient, which was calculated in previous section, and defining density and specific heat to unity. The method is prescribed by Yoon, Han and Wang (2007) and shown in Table 6.4.

Table 6.4 Variables map for FEA simulation

Heat Transfer (Temperature, T)	Moisture Diffusion (Moisture Concentration, C)
ρ , density (kg/m ³)	1
k , Conductivity (W/m.K)	D
c_p , Specific Heat (J/kg.K)	1

6.4.1 Boundary Conditions

As shown in Figure 6.4, Face 1 is exposing face of the circular cap where moisture is applied and therefore concentration on Face 1 is set to 1, meaning completely wet. Face 2 and 3 are defined as completely dry faces and concentration set to 0.

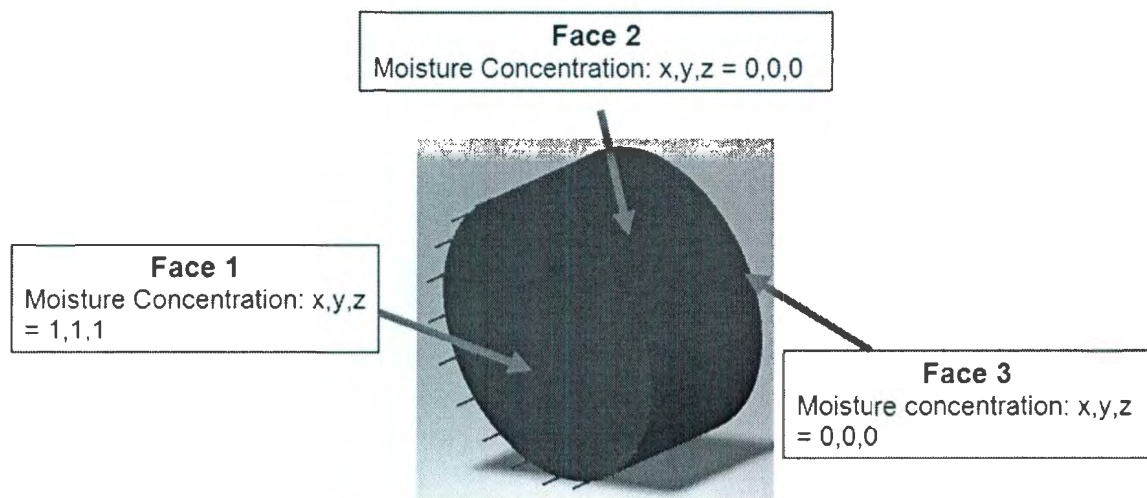


Figure 6.4 Boundary conditions for moisture diffusion FEA model

Where;

$C = 0$ for complete dryness

$C = 1$ for saturated wetness

6.4.2 Moisture Ingress Simulation

Following are the results of the moisture diffusion simulation as shown in Figures 6.5 to 6.8.

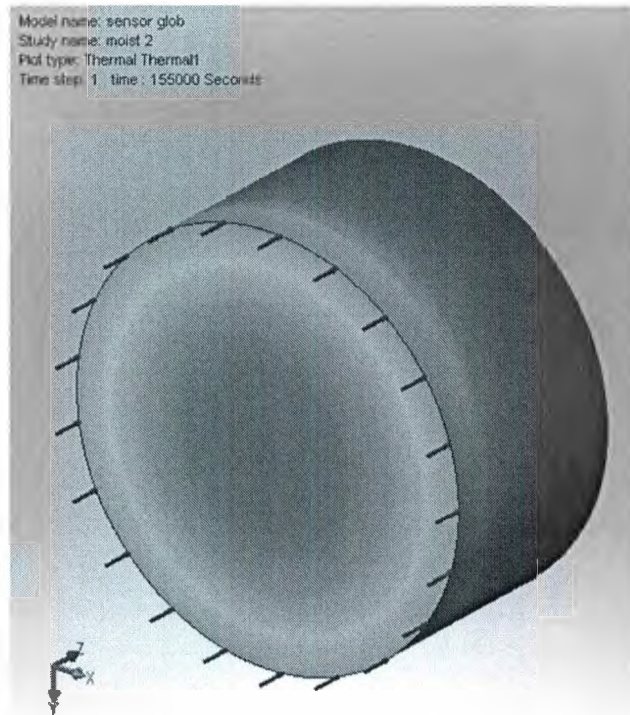


Figure 6.5 Moisture diffusion after 1.8 days

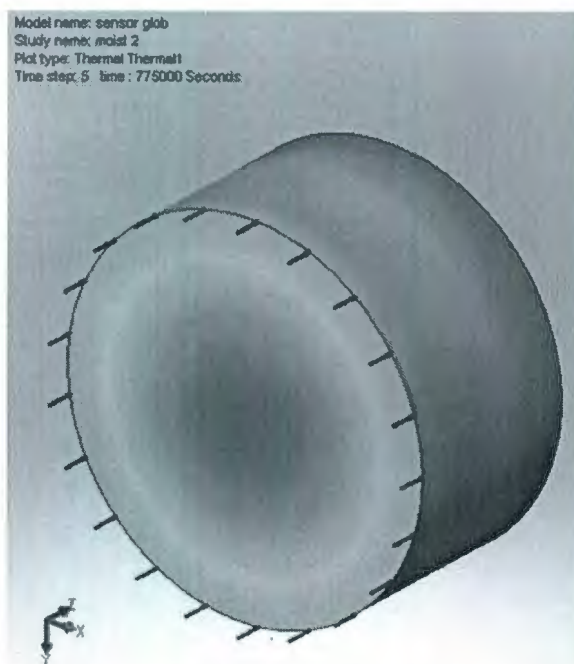


Figure 6.6 Moisture diffusion after 10 days

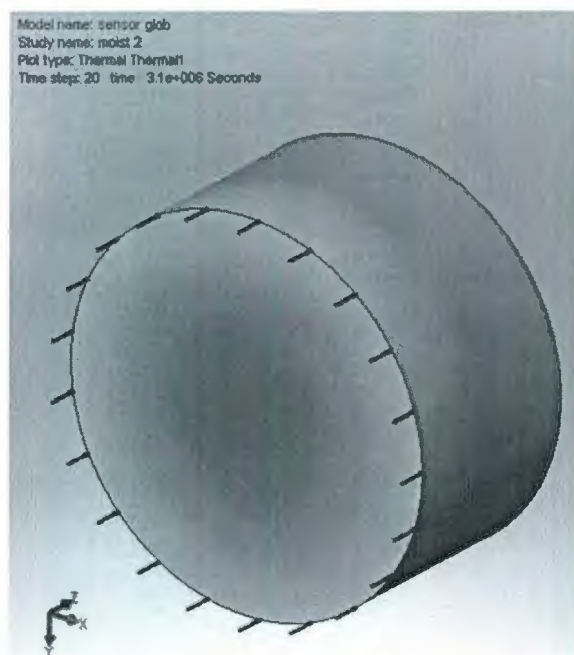


Figure 6.7 Moisture diffusion after 35 days

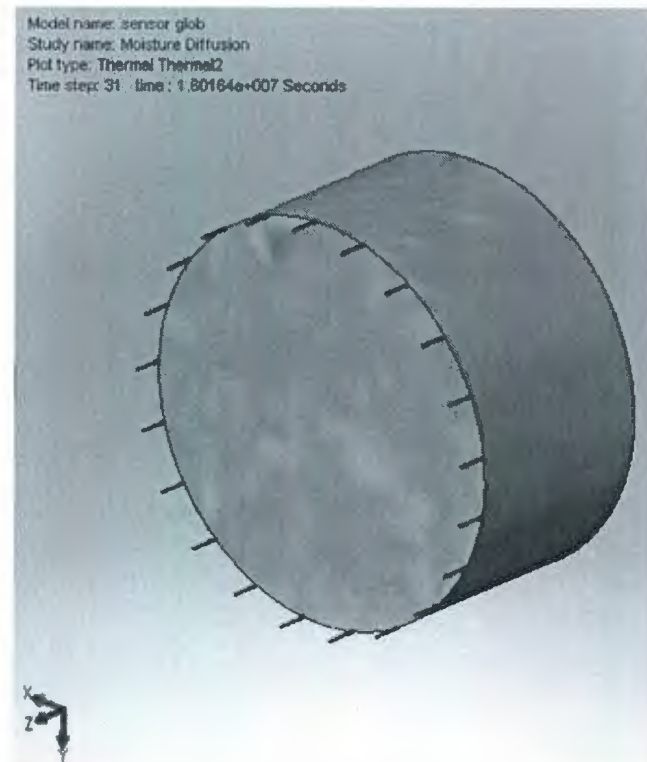


Figure 6.8 Moisture diffusion after 185 days

6.4.3 Results

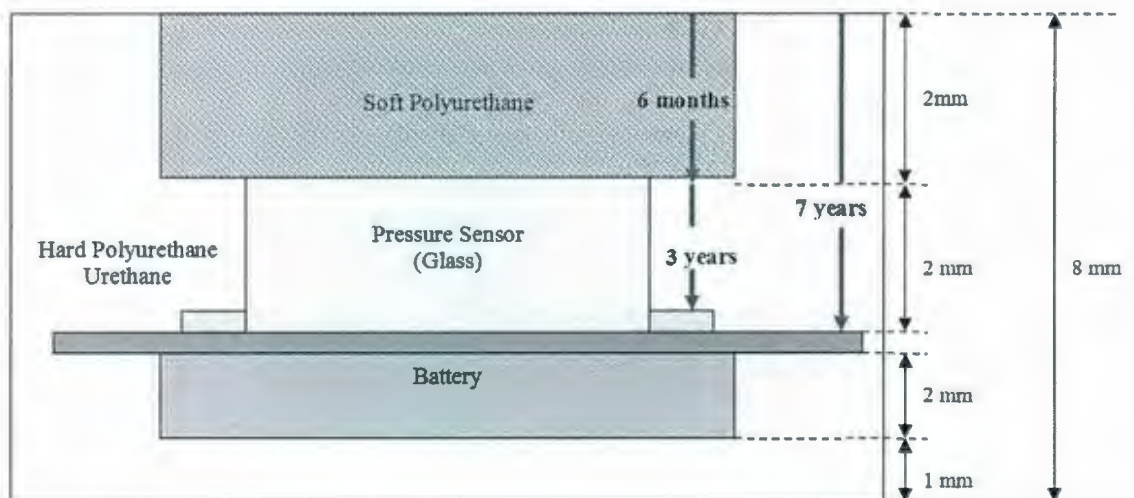
From the simulation results it is observed that it takes approximately 185 days for soft polyurethane to saturate 99%, which is close to the ingress rate result as calculated in previous section thus validating the FEA model. Table 6.5 shows the result from of moisture diffusion time obtained numerically and analytically.

Table 6.5 Moisture ingress rate results

Moisture Ingress Rate (Soft Black Polyurethane Circular Cap)	
Calculated	178 days
FEA	185 days

6.5 Conclusion

Moisture diffusion ingress rate is calculated and validated through finite element modeling. It takes approximately 6 months for soft polyurethane to saturate 99% with moisture, whereas approximately 7 years for hard polyurethane, as illustrated in Figure 6.9.

**Figure 6.9** Moisture diffusion time through two polyurethane materials

For moisture to reach interconnect pads of pressure sensor, when diffused through soft polyurethane material, which is at the bottom of the pressure sensor, it now needs to diffuse through hard polyurethane material of 2 mm in height as shown in Figure 6.9. Using Equation 6.11 to calculate the ingress rate for of moisture through 2 mm thick hard polyurethane material is almost 3 years. This means that all the electronic components in the tag, except pressure sensor which is encapsulated with soft polyurethane circular cap, can expect moisture to reach them through diffusion in 7 years. Whereas, sensing surface of pressure sensor can expect water, diffusing through soft polyurethane material, in 6 months.

Considering the design life of the data-recorder tag, which is from 2.5 years to 3 years, based on the maximum battery life, discussed in Chapter 4, time for moisture to reach to pressure sensor interconnect or the circuit board is 3.5 years, which is beyond tag's design life. Therefore, it can be concluded that packaging design is good to protect the electronic components and electrical circuit from moisture and does not allow moisture to penetrate polyurethane material during its life.

The failures observed from the failure data analysis, which are categorized as "packaging failures", are all well within 1 year of tag's mission life. This can happen if the manufacturing process of moulding the electronics in the two polyurethane materials is not in control.

Another important factor that is not considered in the study is the interface of two polyurethane materials, soft and hard, which is adhesively bonded to each other. If this bond is compromised, it will open up a path for water to travel faster to the components on the circuit board, Figure 6.10. One of the important factors for this bond to be reliable is the contact area, which is created during the moulding process when hard and soft polyurethane material in liquid form is poured by hand. If the process is not controlled it can result in achieving contact area which is beyond design specifications and cause bond to break during small pressure applications. Smaller contact area can also cause moisture to diffuse faster than calculated previously. Another important interface is the bond between hard polyurethane and pressure sensor components which is made of glass material. There is no data available on the bond strength of these two materials but if compromised, along with the bond of soft and hard polyurethane, will become an open channel for water to reach electrical circuit and result is either short circuiting one or more electronic components or creating an excess discharge phenomenon, which leads to rapid discharge of battery.

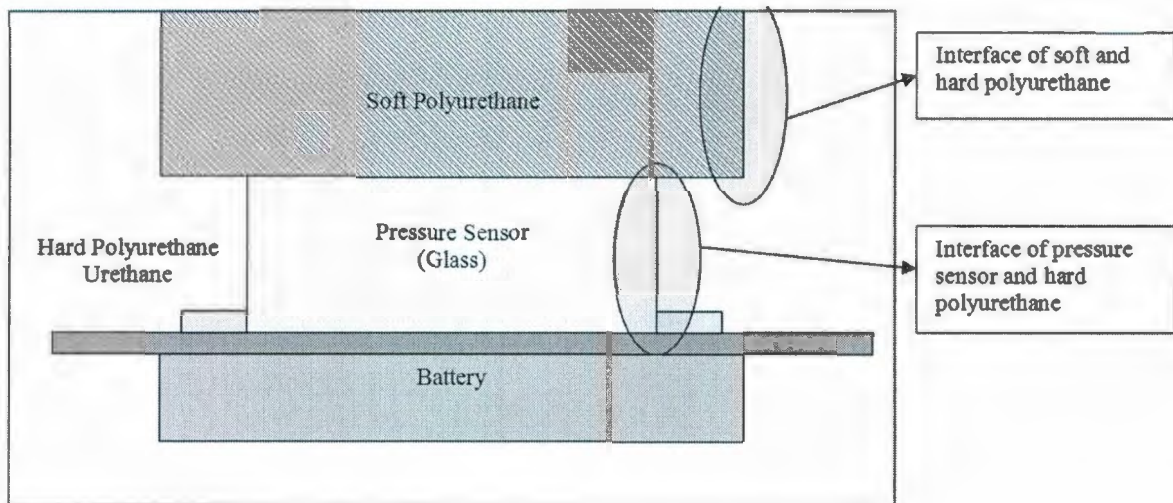


Figure 6.10 Sketch of tag showing interfaces of polyurethane materials

Chapter 7 presents the summary of the all the analysis and experiments done in previous chapter and lead to conclusions.

Chapter 7

Conclusions and Recommendations

Extensive experimental and analytical studies were performed to investigate the reliability of the biotelemetry data-recorder tag, to identify the critical factors and physical mechanisms that govern the early life failure of the tag during a mission. During this analysis it became apparent that moisture ingress stands out as the worst problem.

Before specifically researching moisture behaviour and its effects on microelectronic circuit, component reliability analysis was also considered and several experiments, calculations and models were created to understand the failure mechanisms which have an effect on life and reliability of these components. Among all, battery was studied with greater detail as most of the failures recorded were related to power failures.

Several fundamental conclusions can be made that will help advance current understanding of stress related and moisture induced failures. Future work can build upon this study to expand the knowledge of moisture degradation mechanisms to yield more

robust adhesive structures not only in microelectronic packaging applications, but also in aerospace and structural applications where high reliability is the key design element.

7.1 Conclusion of Research

Throughout the study both experiments and analytical models were developed to achieve greater understanding of the phenomenon. These conclusions can be divided into four primary sections.

Weibull analysis and hazard plots of failure obtained from field data show infant mortality. Fault tree analysis show that all electronic components on-board have high reliability as a system and even the critical component analysis for each sub-system surpasses design life of the tag. Battery is the only component that determines the ultimate life of the data-recorder tag and provides life to the electronics beyond 2 years, which is the design life of the tag. The result of infant mortality attributes to poor quality control in manufacturing process.

Second section of the thesis includes the experimental and analytical analysis of the tag to address each individual failure mode. Power failures which is related to rapid discharge of battery, is addressed by understanding the design limitations of the battery and calculating the true life of the battery. This is done by conducting experiments on the battery at room and sub-zero temperatures. This methodology helped in understanding

the life expectancy of battery and qualification at extreme operating conditions. An analytical model was also developed to calculate the real life of the battery when in-use with the data-recorder system. It is determined that choice of the battery is good at temperatures well below 0°C. The manufacturing process of welding tabs to the cells was also considered in the experiments which showed no significant impact on the life of the cell. After determining power failures are not due to poor performance of the battery, focus shifted towards external elements that can cause damage to electrical circuit or electronic components on the circuit.

Third section of the thesis is focused on the structural integrity and reliability at different pressures. This was done to address packaging failures which are related to presence of moisture inside the tag or on the electrical circuit short circuiting components to result in instant death of component or rapid discharge of battery. To investigate the process by which moisture can enter the plastic encapsulated body of the tag and reach electronics, pressure experiments were designed and conducted. Test specimen were subjected to different pressures to determine the ultimate strength of the encapsulating materials and bond strength of the bi-material interface as is the case in data-recorder tag under study. This was also repeated through FEA simulation and study was validated through comparison of results between the physical pressure experiments and FEA simulation. Conclusion was made that data-recorder tags qualify design pressure rating of 1500 psi when applied for short period of time. But creep affect was observed when 2800 psi was applied for 5 hours. Since the dive patterns of the marine animals is anywhere between 3

to 9 minutes reaching maximum depths of 2800 psi, the failure due to 5 hour creep affect is discarded and tag is considered qualified as per design specification. This also means that at normal operating conditions, temperature and pressure, polyurethane casing is strong enough to hold water penetrating to buried electronics. Therefore, the last hypothesis to investigate was moisture entering the tag through diffusion.

Last section of the thesis was specifically focused on providing a good understanding of the effect of moisture on the data-recorder tags. Moisture transport characteristics were studied by calculating the diffusion coefficient and using that information moisture ingress rate was calculated for both polyurethane materials, soft and hard.

It is determined that while it takes 6 months for moisture to diffuse through soft polyurethane circular cap, it takes 7 years through hard polyurethane material. Therefore, diffusion through soft polyurethane is faster and reaches the top sensing surface of the pressure sensor in 6 months. Water to reach electronics, after reaching the pressure sensor surface, need to first diffuse through 2 mm thick hard polyurethane layer, which slows down the diffusion process to another 3 years. The total time for moisture to reach electronics through soft polyurethane circular cap, takes approximately 3.5 years. It can be concluded here that there is no threat to electronics inside the moulded polyurethane materials during its design life, which is not more than 3 years.

After calculating diffusion coefficients of the two polyurethane materials, moisture ingress rate was also simulated through finite element analysis using heat transfer module. The results of ingress rate came close to the calculated values. Moisture absorption kinetics, elastic modulus variation due to moisture absorption, and the effect of moisture on interfacial fracture toughness were not studied in this thesis but can be analyzed in future work.

All the analytical calculations and finite element models developed in this thesis are verified by physical experiment results, except the moisture ingress finite element model, which provided same result as the calculations.

All reported and recorded failures in the data-recorder tag are in infant mortality stage. Moisture is the major role player for all the failures, whether it is a component failure as seen in temperature sensor, pressure sensor and communication diode failures or a system failure due to rapid discharge of battery which is due to presence of moisture between the two nodes of the component resulting in lower resistance which in-turn result in excess draw of current from battery, thus rapid discharge.

7.2 Recommendations and Future work

A multi-disciplinary study was conducted to advance the understanding of the microelectronics failures and use of reliability engineering theory. Several fundamental

mechanisms responsible for the change in adhesion from moisture uptake have been identified from this study; however, future contributions are needed to further advance the understanding of the role of moisture in the reliability moulded microelectronics and of adhesive joints in moulding materials.

Moisture can affect interfacial adhesion through two primary mechanisms. The first mechanism is the direct presence of moisture at the interface altering the interfacial integrity of the adhesive joint. The second mechanism is the absorbed moisture in either the adhesive and/or substrate altering the mechanical characteristics of those materials, which will indirectly affect the interfacial adhesion when an external load is applied to the structure.

Last, it should be noted that the basis of this work was founded on data-recorder tag test results. The results have provided groundwork for evaluating the effect of moisture; however, it would be interesting to conduct a study that focuses on the effect of moisture on the fatigue characteristics of adhesive joints. It is well known that fatigue loads much lower than static failure loads yield failures in adhesive joints, and future studies could build from the fundamental results of this study to identify the primary mechanisms responsible for the loss in fatigue life in the presence of moisture. Based on the data generated, a predictive model could be developed that characterizes the effect of moisture on joint reliability for fatigue environments. An additional consideration in addition to fatigue generated from externally applied loads is the issue of environmental fatigue.

Fatigue may occur due to repeated absorption and desorption of moisture in an adhesive joint. Recovery results in this study have shown a significant, permanent loss in interfacial fracture toughness upon fully drying after exposure to moisture. It would also be interesting to evaluate the effect of multiple cycles of environmental fatigue on interfacial fracture toughness, with one cycle consisting of saturated conditions followed by fully drying.

Further recommendations are as follows;

- Humidity controlled environment is needed at the manufacturing facility so that complete dry electronic assembly is moulded.
- Accelerated life testing models to be researched and developed for environmental stress testing
- Burn-in times and burn-in optimization should be calculated using reliability theory and practices before encapsulating the electronics
- Models for different types of stress tests to be developed for temperature, vibration, humidity and electrical stresses
- Further structural analysis using FEM to be conducted on the area of contact at the interface of the soft and hard polyurethane
- More mechanical tests to be conducted for bond strength of the two moulding materials
- More experiments and analytical analysis needed to understand characterization and modeling of moisture behaviour

- In-depth analysis of diffusion of moisture in multi-material system
- Using humidity chamber fickian curve for moisture behaviour to be developed for further clear understanding of moisture behaviour in moulding compounds
- Vapour pressure modeling for moisture diffusion to be conducted to understand the impact of moisture presence on the circuit board at different temperatures and pressures
- Further understanding of effect of moisture on loss of adhesion between moulding materials is needed for design qualification and evaluation

References

- Barlow, R.E., Proschan, F. (1975). *Statistical Theory of Reliability and Life Testing: Probability Models*. New York: Holt, Rinehart and Winston.
- Bernstein, J.B., & Gurfinkel, M. (2006). Electronics circuit reliability. *Microelectronics Reliability*, 46, 1957-1979.
- Crank, J. (1975). *The mathematics of diffusion*. Oxford: Clarendon Press.
- Conley, J.F., Jr. Lenahan, P.M., Wallace, B.D. (1996). Physically based predictive model of oxide charging [MOSFET gate oxides]. *IEEE Integrated Reliability Workshop*, 134-141.
- Coppola, A. (1984). Reliability engineering of electronic equipment: a historical perspective. *IEEE Transactions on Reliability*, 33, 29-35.
- Cushing, M.J., & Mortin, D.E. (1993). Comparison of electronics-reliability assessment approaches. *IEEE Transactions on Reliability*, 42-4, 542-546.
- Cook, T.A., & Fernald, K.W. (1990). A custom microprocessor for implantable telemetry systems. *IEEE Transactions on biomedical engineering*, 32, 708-713.
- Davis, D.J. (1952). An analysis of some failure data. *American Statistical Association*, 47, 113-150.
- DeMichele, G.A., & Troyk, P.R. (2003). Integrated multi-channel wireless biotelemetry system. *Proceedings of the 25th annual international conference of the IEEE members, Cancun, Mexico, September 17-21*, 3372-3375.
- Denson, W. (1998). The history of reliability prediction. *IEEE Transactions on Reliability*, 47, 321-328.

- Dhillon, B.S. (1983). Power System Reliability, Safety and Management. *Ann Arbor Science*, Ann Arbor, MI.
- Dhillon, B.S. (1991). *Robot Reliability and Safety*. New York: Springer-Verlag.
- Dhillon, B.S., Singh, C. (1981). Engineering Reliability: New Techniques and Applications. New York: John Wiley and Sons.
- Dhillon, B.S. (1983). *Reliability in systems design and operation*. New York: Van Nostrand Reinhold Company.
- Dhillon, B.S. (1979). A hazard rate model. *IEEE Transactions on Reliability*, 28, 150.
- Dhillon, B.S. (1992). *Reliability and Quality Control: Bibliography on general and specialized areas*. Gloucester, Ontario: Beta Publishers.
- Dhillon, B.S. (1988). *Mechanical Reliability: Theory, Models and Applications*. Washington, D.C.: American Institute of Aeronautics and Astronautics.
- Dhillon, B.S., Proctor C.L. (1976). Reliability analysis of multi-state device networks. *Proceedings of the annual IEEE reliability and maintainability symposium, Las Vegas*, 31-35.
- Dietrich, D.L. (2006). Reliability from design inception to product retirement. *Proceedings Annual Reliability and Maintainability Symposium. Newport Beach, California, USA, January 23-26*.
- Dilhaire, S., & Jorez, S. (1999). Optical method for the measurement of the thermomechanical behaviour of electronic devices. *Microelectronics Reliability*, 39, 981-985.
- Dodson, B., & Schwab, H. (2006). *Accelerated testing: A Practitioner's Guide To Accelerated And Reliability Testing*. Warrendale, Pennsylvania: SAE International.

- Fremont, H., Horaud, W., & Weide-Zaage, K. (2006). Measurements and FE-simulations of moisture distribution in FR4 based printed circuit boards. *7th International Conference on Thermal, Mechanical and Multiphysics Simulation and Experiments in Micro-Electronics and Micro-Systems, EuroSimE*, 781-883.
- Fremont, H., Deletage, J.Y., Pintus, A., Danto, Y. (2001). Evaluation of the moisture sensitivity of molding compounds of IC's packages. *ASME Transactions*, 123, 16-18.
- Galloway, J.E., & Miles, B.M. (1996). Moisture absorption and desorption predictions for plastic ball grid array packages. *IEEE Transactions, Intersociety Conference on Thermal Phenomena*, 180-186.
- Guo, H., & Zhao, W. (2006). Practical methods for modeling repairable systems with time trends and repair effects. *Proceedings Annual Reliability and Maintainability Symposium, California, January 23-26*.
- Haugen, E.B. (1980). *Probabilistic Mechanical Design*. New York: John Wiley & Sons.
- Henney, K. (1956). *Reliability Factors for Ground Electronic Equipment*. New York: McGraw-Hill.
- Hsu, C., & Lee, H. (2006). The implementation of biotelemetry chip by analog modulation technique. *IEEE Transactions on Circuits and Systems*, 48, 433-440.
- Huang, W., & Askin, R.G. (2003). Reliability analysis of electronic devices with multiple competing failure modes involving performance aging degradation. *Quality and Reliability Engineering International*, 19, 241-254.

- Jones, J. (2001). Estimation of system reliability using a "non-constant failure rate" model. *IEEE Transactions of Reliability*, 50, 286-288.
- Kang, J.M., & Yoo, T. (2006). A wrist worn integrated health monitoring instrument with a tele-reporting device for telemedicine and telecare. *IEEE Transactions on Instrumentation and Measurement*, 55, 1208-1215.
- Kleyner, A., & Bender, M. (2003). Enhanced reliability prediction methods based on merging military standards approach with manufacturer's warranty data. *IEEE Transactions, Proceedings Annual Reliability and Maintainability Symposium*, 202-206.
- Kleyner, A., & Boyle, J. (2003). Reliability predictions of substitute parts based on component temperature rating and limited accelerated test data. *IEEE Transactions, Proceedings Annual Reliability and Maintainability Symposium*, 518-522.
- Kocer, F., & Flynn, M.P. (2006). An RF-powered, wireless CMOS temperature sensor. *IEEE Sensors*, 6, 557-564.
- Kempe, M.D. (2005). Control of moisture ingress into photovoltaic modules. *31st IEEE Photovoltaics Specialists Conference and Exhibition, Florida*. January 3-7.
- Lall, P. (1996). Tutorial: temperature as an input to microelectronics reliability model. *IEEE Transactions on Reliability*, 45, 181-192.
- Lambert, H.E., Yadigaroglu, G. (1977). Fault tree for diagnosis of system fault conditions. *Nuclear Science Engineering*, 62, 20-34.
- Limaye, P., Vandavelde, B., Vries, H., Degryse, D., Slob, K., & Veen, C.V., et al. (2004). Finite element analysis of ultra thin BGA package: first and second level reliability. *IEEE*

Transactions, 5th International Conference on Thermal and Mechanical Simulation and Experiments in Micro-electronics and Micro-Systems, EuroSimE.

Ma, X., Jansen, K.M.B., Ernst, L.J., Van Driel, W.D., Sluis, O.V., Zhang, G.Q. (2007).

Characterization of moisture properties of polymers for IC packaging. *Microelectronics Reliability*, 47, 1685-1689.

Ma, X., Jansen, K.M.B., & Ernst, L.J. (2006). Moisture effects on the creep of thermosetting IC packaging polymers. *7th International Conference on Thermal, Mechanical and Multiphysics Simulation and Experiments in Micro-Electronics and Micro-Systems, EuroSimE.*

Department of Defense (1991). *Military Handbook MIL-HDBK-217: Reliability Prediction of Electronic Equipment*. Washington, D.C: DoD.

Department of Defense (1998). *Military Handbook MIL-HDBK-338B: Electronic Design Handbook*. Washington, D.C.: DoD.

Najmi, M., Kehoe, D.F. (2000). An integrated framework for post-ISO 9000 quality development. *Quality & Reliability Management*, 17-3, 226-258.

Park, J., & Osenback, J. (2005). Processability and reliability of epoxy adhesive used in microelectronic devices linked to effects of degree of cure and damp heat aging. *Microelectronics and Reliability*, 46, 503-511.

Parry, J.D., & Clemens, J.M. (2002). Enhanced electronic system reliability-challenges for temperature prediction. *IEEE Transactions on Components and Packaging Technologies*, 25, 533-538.

- Pecht, M.G., Ardebili, H., Shukla, A.A., Hagge, J.K., & Jennings, D. (1999). Moisture ingress into organic laminates. *IEEE Transactions on Components and Packaging Technology*, 22-1, 104-110.
- Pecht, M.G., & Nash, F.R. (1994). Predicting the reliability of electronic equipment. *IEEE Transactions*, 82, 992-1004.
- Pfau, T., & Ferrari, M. (2008). A hidden markov model based stride segmentation technique applied to equine inertial sensor trunk movement data. *Biomechanics*, 41, 216-220.
- Prendergast, J., Murphy, E., Stephenson, M. (1996). Predicting oxide reliability from in line process statistical reliability control. *IEEE Integrated Reliability Workshop*, 42-49.
- Rodgers, P. & Evely, V. (2000). Prediction of microelectronics thermal behaviour in electronic equipment: Status, challenges and future requirements, *IEEE Transactions*, 1-11.
- Sharma, R.K., Kumar, D., Kumar, P. (2005). Systematic failure mode effect analysis (FMEA) using fuzzy linguistic modeling. *Quality and Reliability Management*, 22, 986-1004.
- Shooman, M.L. (1968). *Probabilistic Reliability: An Engineering Approach*. New York: McGraw-Hill.
- Singh, C., Billinton, R. (1977). *System Reliability Modeling and Evaluation*. London, England: Hutchinson.
- Singh, C., Billinton, R. (1977). Calculating the frequency of Boolean Expressing Being 1. *IEEE Transactions on Reliability*, R-26, 354-355.
- Singh, C. (1975). Reliability Calculations on Large Systems. *Proceedings of IEEE Annual Reliability and Maintainability Symposium, Washington D.C.*, 188-193.

- Singh, C., Kankam M.D.(1976). Comments on closed form solutions for Delta-star and star-delta conversion of reliability networks. *IEEE transactions on Reliability*, R-25, 336-339.
- Singh C., Billinton R. (1977). *System reliability modeling and evaluation*. London, England: Hutchinson.
- Singh, C. (1977). On the behaviour of failure frequency bounds. *IEEE Transactions on Reliability*, R-26, 63-66.
- Spitsbergen, J.C. (1995). Reliability of electronic devices containing epoxy resins. Electro/95 International Electronics Conference and Exposition, 421-433.
- Swift, K. G., Raines, M., Booker, J. D. (2000). Case studies in probabilistic design. *Engineering Design*, 11-4, 299 – 316.
- Tanase, M.E., & Lie, I. (2005). Frequency exchanger from electronic telemetry equipment of movement features. *IEEE 28th international spring seminar on electronics technology*, 469-472.
- Tencer, M., (1994). Moisture ingress into nonhermetic enclosures and packages: A Quasi-steady model for diffusion and attenuation of ambient humidity variations. *IEEE Transactions*, 196-209.
- Tillman, F.A., Hwang, C.L. (1977). Optimization techniques for system reliability with redundancy: A review. *IEEE Transactions on Reliability*, 26, 148-155.
- Uschitsky, M., & Suhir, E. (2001). Moisture diffusion in epoxy molding compounds filled with particles. *Electronic Packaging*, 123, 47-51.

- Valdastri, P., & Menciassi, A. (2004). An implantable telemetry platform system for In Vivo monitoring of physiological parameters. *IEEE Transactions on Information Technology in Biomedicine*, 8, 271-278.
- Van Der Pol, J.A., & Kuper, F.G. (1996). Relation between yield and reliability of integrated circuits and application to failure rate assessment and reduction in the one digit fit and PPM reliability era. *Microelectronics and Reliability*, 36, 1603-1610.
- Vesley, W.E. (2002). *NASA Fault Tree Handbook with Aerospace Applications*. Washington, D.C.: NASA.
- Wang, W., & Loman, J.M. (2004). Reliability block diagram simulation technique applied to IEEE Std. 493 standard network. *IEEE Transactions on industry applications*, 40, 887-895.
- Wang, L., & Johannessen, A. (2005). A programmable microsystem using system-on-chip for real-time biotelemetry. *IEEE Transactions on Biomedical Engineering*, 52, 1251-1260.
- Wang, W., Loman, J.M. (2004). Reliability Block Diagram Simulation Techniques Applied to the IEEE Std. 493 Standard Network. *IEEE Transactions on industry applications*, 40-3, 1119-1123.
- Wang, W., Loman, J.M. (2002). On reliability modeling and analysis of highly-reliable, large systems. *Reliability and maintainability symposium*, 456-459.
- Weil, L., Pecht, M. (1993). Reliability evaluation of plastic encapsulated parts. *IEEE Transactions on Reliability*, 42, 536-540.
- Weibull, W. (1951). A statistical distribution function of wide applicability. *Applied Mechanics*, 18, 293-297.

- Wilson, R.P., Liebsch, N. (2007). All at sea with animal's tracks; methodological and analytical solution for the resolution of movement. *Deep-Sea Research*, 54, 193-210.
- Wong, E.H., Teo, Y.C., Lim, T.B. (1998). Moisture diffusion and vapour pressure modeling of IC packaging. *Electronic Components and Technology Conference*, 1372-1378.
- Wong, E.H., Koh, S.W., Lee, K.H., Rajoo, R. (2002). Advanced moisture diffusion modeling & characterization for electronic packaging. *Electronic Components and Technology Conference*, 1297-1303.
- Wong, E.H., Rajoo, R. (2003). Moisture absorption and diffusion characterization of packaging materials-advanced treatment. *Microelectronics Reliability*, 43, 2087-2096.
- Wong, K.L. (1995). A new framework for part failure rate prediction model. *IEEE Transactions on Reliability*, 44, 139-146.
- Yang, G. (2007). *Life cycle: Reliability Engineering*. New Jersey: John Wiley & Sons.
- Yoon, S., Han, B., Wang, Z. (2007). On moisture diffusion modeling using thermal-moisture analogy. *Electronic Packaging*, 129, 421-426.
- Zhao, X.J., Caers, J.F.J. (2003). Prediction of moisture induced failures in flip chip on flex interconnections with non-conductive adhesives. *IEEE electronics components and technology conference*.
- Zhao, W., Elsayed, E.A. (2004). An accelerated life testing model involving performance degradation, *Proceedings annual reliability and maintainability symposium, Los Angeles, California, USA, January 25-29*.
- Zhu, T.L. (1993). A reliability-based safety factor for aircraft composite structures. *Computers & Structures*, 48-4, 745-748.

Zou, W., Coffin, J., & Arvelo, A. (2006). Reliability analysis on epoxy based thermal interface subjected to moisture environment. *IEEE Transactions*, 1082-1087.

Appendix 1

Raw failure data:

Tag #	Life Data			Failure Mode				
	Survival Data (Days)	Hours	Status	Battery	Leakage	Communication	Temp	Press
1731	42.7	1024.8	Failed	1				
1446	21.3	511.2	Failed	1				
1303	10.7	256.8	Failed	1				
1254	91	2184	Failed			1		
1124	730	17520	Failed	1				
3487	105	2520	Failed	1	1			
1355	58.6	1406.4	Failed				1	1
1682	84	2016	Failed					1
1132	360.79	8658.96	Failed	1				
1125	238.48	5723.52	Failed	1				
1122	479.5	11508	Failed	1				
1746	320	7680	Failed	1				
1056	480	11520	Failed	1				
1151	1468	35232	Failed			1		
1214	168	4032	Failed			1		
426	336	8064	Failed	1				
949	272	6528	Failed			1		
99	13.35	320.4	Failed				1	
1100	429.16	10299.84	Running			1		
1124	336	8064	Running			1		
62	221	5304	Running				1	
71	164.53	3948.72	Running				1	
1165	402.87	9668.88	Failed			1		
124	223.81	5371.44	Failed				1	
253	406.7	9760.8	Failed	1				
283	402.91	9669.84	Failed	1		1		
101	305.75	7338	Failed	1				
1308	336	8064	Failed			1		
1310	327.32	7855.68	Running			1		
1359	336	8064	Running			1		
851	168	4032	Running			1		
1137	336	8064	Failed	1				
55	261.54	6276.96	Failed					1
73	351.7	8440.8	Failed			1		
94	429.5	10308	Failed			1		
1357	427.325	10255.8	Failed	1				
238	300	7200	Failed				1	
3379	384	9216	Failed	1				

272	293.33	7039.92	Failed	1			
940	202.66	4863.84	Failed	1			
1145	293.33	7039.92	Failed	1			
3450	341.33	8191.92	Failed	1			
1157	261.33	6271.92	Failed	1			
3671	682.66	16383.84	Failed	1			
965	700	16800	Failed	1			
1121	640	15360	Failed	1			
8307	66.66	1599.84	Failed			1	
8615	136	3264	Running			1	
8304	352	8448	Running			1	
1242	266.54	6396.96	Running				1
2001	117.36	2816.64	Running				1
5661	2.6	62.4	Failed				1
5670	93.19	2236.56	Failed				1
446	218.66	5247.84	Failed	1			
1112	336	8064	Failed	1			
1047	490.66	11775.84	Failed	1			
1150	672	16128	Failed	1			
5257	366	8784	Running				1
5650	366	8784	Running				1
5662	366	8784	Running				1
6292	58	1392	Running				1
5236	730	17520	Failed	1			
5291	180	4320	Failed	1			
5284	180	4320	Failed	1			
5268	180	4320	Running			1	
5237	180	4320	Running			1	
5279	180	4320	Running			1	
5312	180	4320	Running			1	
5276	180	4320	Running			1	
5314	180	4320	Running			1	
5246	180	4320	Running			1	
6951	35	840	Failed			1	
6837	42	1008	Failed			1	
6933	37	888	Failed			1	
6946	41	984	Failed			1	
6926	39	936	Failed	1		1	
6922	32	768	Failed	1		1	
6886	40	960	Failed	1		1	
6663	289	6936	Failed	1			
7386	202	4848	Running				1
5178	180	4320	Failed				1
5309	181	4344	Running				1
7375	150	3600	Failed				1
7383	150	3600	Failed				1

5259	60	1440	Failed	1			
6459	42.33	1015.92	Failed	1			
7657	24.67	592.08	Failed				1
7661	31.5	756	Failed		1		1
1319	25	600	Failed		1		
6740	2.6	62.4	Failed		1		
5991	16.1	386.4	Failed		1		
7430	71.01	1704.24	Failed		1		
7480	12.5	300	Failed		1		
7473	153.39	3681.36	Failed		1		
8805	87.31	2095.44	Failed		1		
8813	66.47	1595.28	Failed		1		
8821	87.31	2095.44	Failed		1		
4908	10	240	Failed	1		1	
8188	10	240	Failed	1			
8155	12	288	Failed	1			
8214	12	288	Failed	1			
8283	12	288	Failed	1			
8122	293	7032	Failed	1			
8287	15	360	Failed	1			
8615	136	3264	Failed	1			
8307	66.66	1599.84	Failed	1			
1121	640	15360	Failed	1			
9769	54.16	1299.84	Failed				1
9817	85.83	2059.92	Failed				1
9832	79.21	1901.04	Failed				1
9959	44.93	1078.32	Failed				1
1133	640	15360	Failed	1			
4881	10.6	254.4	Failed	1			
8666	261.33	6271.92	Failed	1			
3198	469.33	11263.92	Failed	1			
10008	2	48	Running		1		
7457	1	24	Running		1		
7484	121.56	2917.44	Running		1		
8101	5	120	Running		1		
9423	83.57	2005.68	Running		1		
8702	400	9600	Failed	1			
1798	586.66	14079.84	Failed	1			
6163	402.97	9671.28	Failed	1			
5518	398.08	9553.92	Failed	1			
4442	244.77	5874.48	Failed	1			
4215	906.66	21759.84	Failed	1			
10355	149.44	3586.56	Failed	1			
10448	89.47	2147.28	Failed			1	
10451	89.5	2148	Failed			1	
10452	63.48	1523.52	Failed			1	

10446	63.48	1523.52	Failed			1		
8802	63.51	1524.24	Failed			1		
8660	63.51	1524.24	Failed			1		
9188	224	5376	Failed	1				
9724	14.33	343.92	Failed	1				
10804	3	72	Failed		1			
10817	4	96	Failed		1			
10864	4	96	Failed		1			
10890	4	96	Failed		1			
10754	3	72	Failed	1				
12053	82	1968	Failed	1				
11516	218.66	5247.84	Failed	1				
11519	27.58	661.92	Failed	1				
11543	2.88	69.12	Failed	1				
11597	320	7680	Failed	1				
11604	277.25	6654	Failed	1				
11670	71.06	1705.44	Failed	1				
11105	99.72	2393.28	Failed	1				
11137	243.72	5849.28	Failed	1				
11163	197.05	4729.2	Failed	1				
8050	42.66	1023.84	Failed		1			
13140	3.08	73.92	Failed		1			

Count =	152	152	72	36	24	13	15
Max =	1468	35232					
Min =	1	24					
Range =	1467	35208					

Appendix 2

Hazard plot data:

		Median Rank	x-axis	y-axis
hours	Order	F(t)	ln(t)	ln(ln(1/(1-F(t))))
24	1	0.006704981	3.178054	-5.001542725
48	2	0.016283525	3.871201	-4.109403876
62.4	3	0.025862069	4.133565	-3.641905323
62.4	4	0.035440613	4.133565	-3.321909169
69.12	5	0.045019157	4.235844	-3.077723578
72	6	0.054597701	4.276666	-2.879822476
72	7	0.064176245	4.276666	-2.713141393
73.92	8	0.073754789	4.302983	-2.568945784
96	9	0.083333333	4.564348	-2.441716399
96	10	0.092911877	4.564348	-2.327742142
96	11	0.102490421	4.564348	-2.224407328
120	12	0.112068966	4.787492	-2.129798829
240	13	0.12164751	5.480639	-2.042474935
240	14	0.131226054	5.480639	-1.961322077
254.4	15	0.140804598	5.538908	-1.88546216
256.8	16	0.150383142	5.548298	-1.814190457
288	17	0.159961686	5.66296	-1.746932714
288	18	0.16954023	5.66296	-1.683214754
288	19	0.179118774	5.66296	-1.622640434
300	20	0.188697318	5.703782	-1.564875368
320.4	21	0.198275862	5.76957	-1.509634669
343.92	22	0.207854406	5.840409	-1.456673593
360	23	0.21743295	5.886104	-1.40578029
386.4	24	0.227011494	5.956873	-1.356770122
511.2	25	0.236590038	6.236761	-1.309481147
592.08	26	0.246168582	6.383642	-1.26377051
600	27	0.255747126	6.39693	-1.219511514
661.92	28	0.26532567	6.495145	-1.176591234
756	29	0.274904215	6.628041	-1.134908555
768	30	0.284482759	6.64379	-1.094372539
840	31	0.294061303	6.733402	-1.054901068
888	32	0.303639847	6.788972	-1.016419703
936	33	0.313218391	6.841615	-0.978860718
960	34	0.322796935	6.866933	-0.942162276
984	35	0.332375479	6.891626	-0.906267736
1008	36	0.341954023	6.915723	-0.871125042
1015.92	37	0.351532567	6.92355	-0.836686207
1023.84	38	0.361111111	6.931316	-0.802906864

1024.8	39	0.370689655	6.932253	-0.769745867
1078.32	40	0.380268199	6.98316	-0.737164955
1299.84	41	0.389846743	7.169996	-0.705128444
1406.4	42	0.399425287	7.248789	-0.673602963
1440	43	0.409003831	7.272398	-0.642557219
1523.52	44	0.418582375	7.328779	-0.611961783
1523.52	45	0.42816092	7.328779	-0.581788908
1524.24	46	0.437739464	7.329251	-0.552012357
1524.24	47	0.447318008	7.329251	-0.522607252
1595.28	48	0.456896552	7.374805	-0.493549937
1599.84	49	0.466475096	7.377659	-0.464817853
1599.84	50	0.47605364	7.377659	-0.436389425
1704.24	51	0.485632184	7.440875	-0.408243955
1705.44	52	0.495210728	7.441578	-0.380361526
1901.04	53	0.504789272	7.550156	-0.352722915
1968	54	0.514367816	7.584773	-0.325309502
2005.68	55	0.52394636	7.603738	-0.298103194
2016	56	0.533524904	7.608871	-0.271086353
2059.92	57	0.543103448	7.630422	-0.244241714
2095.44	58	0.552681992	7.647519	-0.217552323
2095.44	59	0.562260536	7.647519	-0.191001465
2147.28	60	0.57183908	7.671957	-0.164572597
2148	61	0.581417625	7.672292	-0.138249278
2184	62	0.590996169	7.688913	-0.112015103
2236.56	63	0.600574713	7.712694	-0.085853633
2393.28	64	0.610153257	7.78042	-0.059748324
2917.44	65	0.619731801	7.978462	-0.03368245
3264	66	0.629310345	8.090709	-0.007639028
3600	67	0.638888889	8.188689	0.018399271
3600	68	0.648467433	8.188689	0.044450208
3681.36	69	0.658045977	8.211038	0.070532074
4032	70	0.667624521	8.302018	0.096663798
4320	71	0.677203065	8.371011	0.122865067
4729.2	72	0.686781609	8.461511	0.149156456
4863.84	73	0.696360153	8.489584	0.175559575
5247.84	74	0.705938697	8.565572	0.20209724
5371.44	75	0.715517241	8.588851	0.228793663
5376	76	0.725095785	8.5897	0.255674672
5723.52	77	0.73467433	8.652339	0.282767965
6271.92	78	0.744252874	8.743838	0.310103408
6276.96	79	0.753831418	8.744641	0.337713383
6528	80	0.763409962	8.783856	0.365633201
6936	81	0.772988506	8.844481	0.393901592
7039.92	82	0.78256705	8.859352	0.422561299
7039.92	83	0.792145594	8.859352	0.451659789
7200	84	0.801724138	8.881836	0.481250134

7338	85	0.811302682	8.900822	0.511392087
7680	86	0.820881226	8.946375	0.542153434
7680	87	0.83045977	8.946375	0.573611693
8064	88	0.840038314	8.995165	0.605856286
8064	89	0.849616858	8.995165	0.638991353
8191.92	90	0.859195402	9.010904	0.673139445
8440.8	91	0.868773946	9.040832	0.708446469
9216	92	0.87835249	9.128696	0.745088414
9600	93	0.887931034	9.169518	0.783280727
9668.88	94	0.897509579	9.176668	0.82329169
9669.84	95	0.907088123	9.176767	0.865462083
9760.8	96	0.916666667	9.18613	0.910235093
10255.8	97	0.926245211	9.235599	0.95820372
10308	98	0.935823755	9.240676	1.010189789
11520	99	0.945402299	9.35184	1.067384229
15360	100	0.954980843	9.639522	1.131617303
16383.84	101	0.964559387	9.704051	1.205939925
16800	102	0.974137931	9.729134	1.296090047
17520	103	0.983716475	9.771098	1.415270815
35232	104	0.993295019	10.46971	1.610418356



